

Magnetism in solid ^3He

M. Roger*

Institut Laue-Langevin, Ave des Martyrs, 38042 Grenoble Cedex, France

J. H. Hetherington

Physics Department, Michigan State University, East Lansing, Michigan 48824

J. M. Delrieu

S.P.S.R.M., Cea-Cen Saclay, 91191 Gif-sur-Yvette, France

The theory of magnetism in solid ^3He is reviewed with emphasis on the multiple-spin-exchange theory of the magnetic interaction. Critical experiments are discussed briefly, and the most reliable present values for various quantities are chosen. Various theories of ^3He magnetism are considered, with the conclusion that multiple particle exchange is the most likely mechanism. The microscopic theory of exchange is presented mainly from the standpoint of tunneling ducts. The spin Hamiltonian which results from two-, three-, and four-particle ring exchange is derived and studied in the high-temperature limit, in mean-field approximation, and with spin waves. Two reasonable parameter sets are selected which fit the experimental data, with the conclusion that the exchanges are mainly three- and four-particle rings. A discussion is given of remaining problems together with some conjectures.

CONTENTS

I. Introduction	2	5. Optimization of the path $L(t)$	18
II. Experimental Results	4	6. More straightforward approximations for the potential V	19
A. High-temperature data	4	7. Estimation of δV from experimental elastic compressibility of ^3He	19
1. Expansions in powers of $1/T$	4	D. Conclusions about the exchange mechanism	19
2. Pressure versus field measurements	6	V. Exchange Hamiltonian in Terms of Spin Operators	21
B. Ordered phases—phase diagram	6	A. Introduction of the spin coordinates	21
1. At low field $H < 4.1$ kG, an unexpected antiferromagnetic phase	6	B. Dominant exchanges expected in a bcc lattice	22
2. At fields larger than 4.1 kG, a phase with strong ferromagnetic tendencies	7	C. Cyclic permutation operators in terms of Pauli spin operators	22
3. Other phase transitions	8	D. Kind of cycles and sign of the exchange	23
C. Effect of specific volume	9	VI. High-Temperature Series Expansions	23
III. Theoretical Models	9	A. Description of method	23
A. Pre-1975 theories	9	B. Results	24
B. Post-1975 theories	10	VII. Phase Diagram Within the Molecular-Field Approximation	25
C. Ring-exchange models	10	A. Application of the molecular-field approximation to the four-spin exchange Hamiltonian	25
IV. Physical Origin of Multiple Exchange	12	B. Minimization of the free energy—general methods	26
A. Exchange Hamiltonian—main hypothesis for the calculation of the exchange rates	12	1. The method of Luttinger and Tisza	26
B. Approximation to the wave function	14	2. The method of Villain	26
1. Definition of a home-based function	14	3. Computer minimization	28
2. Approximation to the home-based function ψ	14	a. Elementary method	28
a. Definition of a one-dimensional path along the duct	14	b. Method using some “thermal agitation”	28
b. Behavior of the wave function in the duct, along the path $L(t)$	14	C. Systematic search for the high-field phase at zero temperature, assuming it appears from the ferromagnetic phase at some critical field H_c through a second-order transition	28
c. Inadequacy of variational wave functions	15	D. Properties of the high-field naf phase	30
C. Improvement of the wave function in the duct	15	1. Free energy and magnetization as a function of the field H	30
1. The correction factor $f(t)$	15	2. Phase diagram	31
2. Principle of the variational method	16	a. Second-order transition line between the naf phase and the paramagnetic phase	31
3. Calculation of two- and four-spin exchange in bcc solid ^3He	16	b. The transition “pseudoferrromagnetic” \rightarrow naf	32
a. Choice of the path $L(t)$	16	VIII. A Two-Parameter Model	32
b. Calculation of the effective potential $\tilde{V}(t)$	17	A. One-parameter models	32
c. Calculation of the exchange constant	17	1. Triple exchange	32
4. Analysis of the one-dimensional Schrödinger equation in $L(t)$	18	2. Folded four-spin exchange K_F	32
		3. Planar four-spin exchange K_P	32
		a. Low-field phase	32
		b. High-temperature series expansions	33
		B. Two-parameter model (J_t, K_P)	33

*On leave from CEA-CEN SACLAY-91191 Gif-sur-Yvette, France.

1. Low-field phase	33	c. Diagonalization of the Hamiltonian	55
2. Critical temperature of the uudd phase. Adjustment of the two parameters	33	2. The uudd phase	56
3. High-temperature data	34	a. Spin-wave Hamiltonian	56
4. Susceptibility, dipolar anisotropy, resonance properties of the uudd phase	34	b. Diagonalization of the Hamiltonian	58
5. High-field phase	35	3. scf and ssqf phases	59
6. Whole phase diagram	36	a. Hamiltonian	59
7. Main features of the two-parameter model J_t, K_p	36	b. Diagonalization of the Hamiltonian	60
IX. The Spin-Wave Approximation	37	4. pf phase, the spin-flop naf phase	61
A. Spin-wave Hamiltonian	37	a. Spin-wave operators	61
B. Properties of the spin-wave spectrum	38	b. Hamiltonian	61
1. Optical modes	38	c. Diagonalization	62
2. Possible experimental investigations on the optical mode	38	d. Correction to the molecular-field energy at $T=0$	62
3. Experimental evidence of the acoustic mode at low temperature	39	References	62
C. Spin fluctuation at $T=0$. Numerical evaluations	39		
1. Corrections to the molecular-field energy at $T=0$	39		
2. Zero-point spin deviation	40		
X. Refitted Two-Parameter Model, Taking into Account the Spin-Wave Velocity	40		
A. Determination of the parameters	40		
B. Phase diagram	41		
C. Magnetization of the high-field phase	42		
D. Susceptibility of the uudd phase	42		
E. Spin-wave calculations	42		
1. Optical mode	42		
2. Mean spin-wave deviation at zero temperature	42		
3. Nuclear-magnetic-resonance frequency in zero field	42		
4. Variation of the zero-field resonance frequency with the temperature	42		
XI. Three-Parameter Models	43		
A. Three-parameter model including J_t, K_p, K_F	43		
1. High-temperature results	43		
2. Stable phase at $T=0$ and $H=0$	43		
3. Mean spin-wave velocity	43		
4. Choice of a set of parameters	43		
5. Phase diagram	44		
6. Susceptibility and zero-field resonance frequency	44		
B. Three-parameter model including J_{NN}, J_t, K_p	45		
XII. Summary	45		
A. Phase diagram	45		
B. High-temperature series expansions	45		
1. Zero-field expansion of the partition function	45		
2. Susceptibility	47		
XIII. General Perspective	47		
Appendix A: Variational Method For the Tunneling Pseudopotential	47		
Appendix B: Series Expansion Details	48		
Appendix C: Calculation of the Spin-Wave Velocity in the uudd Phase	49		
1. General hydrodynamic equations	49		
2. Mean spin-wave velocity in the molecular-field approximation	49		
a. Susceptibility	49		
b. Calculation of $M_{ }$	53		
c. Calculation of M_{\perp}	54		
Appendix D: Spin-Wave Approximation	54		
1. Generalities on the spin-wave approximation	54		
a. Quantization of the spin fluctuation in the Holstein-Primakoff (1940) formalism (for spin 1/2)	54		
b. Expansion of the Hamiltonian at second order in δS_i	54		

I. INTRODUCTION

A system of helium atoms seems to be particularly simple: The He atoms are practically impenetrable hard spheres, the attractive part of their interaction potential being weak. However, in the condensed state both isotopes ^4He and ^3He present a large variety of interesting properties as a direct consequence of quantum mechanics. Because of this weak attractive interaction and of the light mass of the atoms, the zero-point agitation is large, and helium cannot solidify under atmospheric pressure, even at $T=0$. Nevertheless, a solid can be obtained at high pressure by decreasing the available space for each atom. In the solid the mean-square displacement of the atoms is large (30% of the interatomic distance for ^3He), and in contrast to ordinary solids, atom-atom exchange processes are significant. For spin- $\frac{1}{2}$ ^3He fermions this exchange induces an effective interaction between nuclear spins (as a consequence of the Pauli principle, which couples the spin state with the parity of the orbital wave function). These exchange interactions cause the nuclear spins to order at a temperature around 1 mK. ^3He is the only solid in which nuclear magnetic ordering due to actual whole-atom exchange has been observed. In other solids nuclear exchange interactions are always much smaller than dipolar magnetic nuclear interactions, which lead to magnetic order at extremely low temperatures in the microKelvin range. (See Abragam and Goldman, 1982.)

The most obvious mechanism for magnetism in ^3He is nearest-neighbor exchange. Nearest-neighbor exchange leads to an ordinary Heisenberg model for the spin Hamiltonian. The sign of the exchange constant must be negative, corresponding to antiferromagnetism. It is, therefore, called the Heisenberg nearest-neighbor antiferromagnetic (HNNA) model. The earliest high-temperature magnetic experiments agreed with this model reasonably well. However, the HNNA model soon proved to be inadequate. Almost every prediction it makes at low temperatures is qualitatively wrong. In particular, it predicts a second-order transition at about 2 mK, but experiment has shown a first-order transition at about 1 mK. It predicts a decrease in susceptibility relative to the Curie-Weiss law, while experiment shows that it increases. It predicts a single low-temperature phase in the field-

versus-temperature phase diagram, while experiment finds two phases. It predicts a suppression of the critical temperature with increasing field, and experiment finds that the high-field critical temperature increases with field.

Recent experiments have provided further unexpected results. Most peculiarly the low-temperature, low-field phase is now known not to be cubic (in its magnetic structure), and is probably the antiferromagnetic "uudd" phase. This phase has alternate pairs of ferromagnetic planes of atoms with the planes normal to the 100 direction (or 010 or 001). The spins in these planes are oriented up, up, down, down, thus the abbreviation uudd.

At first it was hard to think of any kind of exchange mechanism that would be more plausible than the nearest-neighbor exchange. That the mechanism is actual atom exchange is almost dictated by the fact that the effect is about three orders of magnitude greater than magnetic dipole interactions and about three orders of magnitude smaller than phonon effects. All theories suggesting an actual mechanism have therefore been exchange theories, but with complications. Some mechanism must always be envisaged to "stir" the atoms in the solid. The method of stirring can be due to vacancies, rings of atoms exchanging, or double pair exchange mediated by phonons. Ordinary pair exchanges interacting via lattice distortion, which has also been proposed as a mechanism, is a case of the last mentioned type where the phonons are virtual. Only the ring-exchange suggestion has been able to explain most of the phenomena observed.

The exchange mechanisms in ^3He are certainly very different from those in electronic magnetic materials: In ^3He , not only the electrons but the whole atoms, electrons and nuclei, exchange places. Exchange corresponds to real permutations of hard spheres. Exchanges involving rings of more than two particles (three or four) are reasonable. To illustrate this, think of the following picture suggested by Willard (1980). Suppose you are traveling at rush hour in the metro—the crowd is so dense that people can hardly move; if you want to trade places with your neighbor, it is practically impossible, but if two or three people agree to move cyclically with you, you can change places. This is exactly the situation we find in a hard-sphere solid at large densities.

A short time after the observation of the magnetic ordering, Hetherington and Willard (1975) showed that large ring-exchange terms can account for the first-order transition at 1 mK and give qualitatively the shape of the phase diagram.

High-temperature series expansion of a Hamiltonian which included multiple exchange terms (Roger and Delrieu, 1977) then showed that large four-spin terms can explain an increase in the susceptibility with respect to the Curie-Weiss law extrapolated to low temperatures, as is experimentally observed. At the same time, new variational approximations of the wave function, taking into account the geometric correlations between hard cores, were proposed by Delrieu and Roger (1978). In contrast to earlier calculations based on Gaussian wave functions (McMahan and Wilkins; 1975; McMahan, 1972b), these

approximations lead to the conclusion that three- and four-spin exchange are at least of the same order of magnitude as two-particle exchange in hard-sphere quantum solids.

The purpose of this paper is to review our knowledge of the microscopic origin of ring-exchange Hamiltonians and their consequences for the magnetic and thermodynamic properties of solid bcc ^3He .

The subject breaks naturally into two parts. First is the question of the microscopic calculation of the exchange rates. The microscopic theory gives only order-of-magnitude estimates of the exchange rates, but it gives support to the ring-exchange model (Roger, 1980; Delrieu *et al.*, 1980a).

Second is the phenomenological analysis of the four-spin exchange Hamiltonian (Roger, Delrieu, and Landesman, 1977; Delrieu and Roger, 1978; Roger, Delrieu, and Hetherington, 1980c). It leads to:

- (i) increased susceptibility with respect to the Curie-Weiss law,
- (ii) a high-field phase with strong ferromagnetic tendencies, having large magnetization even at relatively low field (≈ 5 kG) and a second-order critical temperature of transition to the paramagnetic phase, which increases with the magnetic field H , and
- (iii) an antiferromagnetic phase at low field, appearing through a first-order transition.

All these features are in agreement with the experimental results. In fact quantitative fits of most measured quantities and qualitative fits of the phase diagram are possible with only two or three exchange parameters.

All theorists are not in accord that ring exchange is the complete explanation. We shall mention other theories in Sec. III and return to our own views of the successes and problems in Sec. XII.

Section II summarizes the main experimental data on the nuclear magnetic properties of solid bcc ^3He . Section III gives an outline and a critical analysis of the different theoretical models proposed during the last decade. The microscopic origin of multiple spin exchange in a hard-sphere quantum solid is explained in Sec. IV. Fundamental assumptions based on the ideas first published by Thouless (1965a) are used there to estimate the exchange frequencies. New variational approximations of the wave function, taking into account the hard-core correlations during the exchange process, are considered. After establishing the general form of the Hamiltonian in terms of permutation operators and spin operators (Sec. V), we exhibit the high-temperature series expansion up to third order for zero field and to second order for arbitrary magnetic field H (Sec. IV). As a general result, we show that large four-spin terms can account for the increase of susceptibility with respect to the Curie-Weiss law and the unexpected value of the T^{-3} term in the specific-heat expansion.

In Sec. VII we give general methods for minimizing the free energy within the molecular-field approximation. We

emphasize some general results about the phase diagram. For most physical values of the parameters, the high-field phase has two simple sublattices. With large values of the four-spin exchange parameters this phase presents strong ferromagnetic tendencies as observed experimentally. Its phase diagram agrees qualitatively with the experimental results [the second-order transition temperature $T_{c2}(H)$ increasing with H up to high field].

Section VIII presents a search for the simplest model fitting the available experimental data within the precision of the experiments, and for the phase diagram within the accuracy of the mean-field approximation (which is poor at low field). Most of the experimental data can be fit with a two-parameter model retaining only three-spin exchange J_t and planar four-spin exchange K_p (pair transposition being neglected).

A spin-wave calculation for the uudd phase is discussed in Sec. IX. The spin-wave spectrum of the uudd phase presents an optical branch with a frequency of the order of 150 MHz in zero field. We suggest the experimental investigation of this optical mode by observing the small coupling between spin waves and phonons. Such an experiment could test whether the ordered phase is really the uudd (the Osheroff experiment does not identify this phase with certainty); it could also test the validity of our model. The renormalization of the zero-temperature molecular-field energy by the spin waves is calculated for the uudd and the high-field phase. This allows calculation of a higher approximation to the field of transition between the two phases. We also evaluate the mean spin deviation $\langle \frac{1}{2} - S_z \rangle$ at zero temperature. We calculate the mean spin-wave velocity at low temperatures. The theoretical value obtained with the two-parameter models given in Sec. VIII disagrees by about 30% with the experimental value given by Osheroff and Yu (1979). This leads us to readjust the parameters J_t , K_p of our two-parameter model (Sec. X). We then investigate models with more than two parameters, taking into account pair exchange or folded four-spin exchange in order to obtain a better quantitative agreement with all experimental data (Sec. XI).

Section XII is a summary and Sec. XIII an overview. Appendix D contains a summary of the spin-wave theory as applied to four-spin systems. It is relegated to an appendix because of its rather mathematical character, but it is intended to be readable enough that students could understand the calculations without special knowledge.

II. EXPERIMENTAL RESULTS

A. High-temperature data

1. Expansions in powers of $1/T$

In order to clarify the relationship between various high-temperature measurements it is useful first to develop a "model-independent" expansion of the free energy.

In a magnetic field H , the partition function is

$$Z = \text{tr} e^{-\beta H}; \quad H = H_{\text{ex}} + H_z. \quad (2.1)$$

H_{ex} is the exchange Hamiltonian and $H_z = -\gamma \hbar \sum_i \vec{S}_i \cdot \mathbf{H}$ is the Zeeman Hamiltonian.

Expanding the exponential factor in powers of β and taking the logarithm, we obtain the free energy F :

$$\begin{aligned} F &= -\frac{1}{\beta} \ln Z \\ &= -\frac{N}{\beta} \left[\ln 2 + \tilde{e}_2 \frac{\beta^2}{8} - \tilde{e}_3 \frac{\beta^3}{24} + \dots \right. \\ &\quad \left. + \frac{1}{2} \left[\gamma \frac{\hbar}{2} H \beta \right]^2 \left[1 + \Theta \beta + \alpha_2 \frac{\beta^2}{8} + \dots \right] \right. \\ &\quad \left. - \frac{1}{12} \left[\gamma \frac{\hbar}{2} H \beta \right]^4 (1 + a_{21} \beta + a_{22} \beta^2 + \dots) \right. \\ &\quad \left. + \dots \right]. \quad (2.2) \end{aligned}$$

The reader will note that the coefficients are not consistently named. Values for \tilde{e}_2 , \tilde{e}_3 , and Θ are usually quoted in this form (some drop the tildes). α_2 , a_{21} , and a_{22} have never been measured and cannot be said to have become standardized. It is still necessary to check values quoted in the literature to see how they are defined. (For another notation see Guyer, 1978.)

This expansion is based on the hypothesis that an exchange Hamiltonian describes the spin properties correctly, which it does if solid ^3He is strongly localized. This means more precisely the following:

- (i) There is one atom localized at each site.
- (ii) The rates of exchange are very small compared to the energy of the zero-point motion.
- (iii) The concentration of ground-state vacancies or thermal vacancies is negligible, so that the hypothetical system formed by these vacancies does not modify appreciably the magnetic order due to exchange.

These hypotheses are certainly valid at high densities (in particular, in the hcp or fcc phases), but they are not definitively proved in the bcc phase near melting.

However, if the system were not localized, the expansion (2.4) would contain not only forms in β^n , $n \geq 2$, but possibly a form in T (as in a Fermi liquid), in $1/T$, or $\ln T$. Until now such terms, as predicted by Heritier and Lederer (1978) for example, have never been observed, and we suppose this hypothesis of localization to be valid.

The expansion (2.2) is general and does not make any hypotheses on the structure of the exchange Hamiltonian. From this expansion, we deduce the following:

- (i) The entropy at zero field,

$$\begin{aligned} S &= -\frac{\partial F}{\partial T} \\ &= Nk_B (\ln 2 - \tilde{e}_2 \beta^2 / 8 + \tilde{e}_3 \beta^3 / 12 + \dots). \quad (2.3) \end{aligned}$$

- (ii) The specific heat at zero field,

$$C_v = T \left[\frac{\partial S}{\partial T} \right]_v$$

$$= \frac{Nk_B}{4} (\tilde{e}_2 \beta^2 - \tilde{e}_3 \beta^3 + \dots). \quad (2.4)$$

(iii) The inverse susceptibility at zero field,

$$\chi^{-1} = - \frac{v}{\mu_0 k_B} \left[\frac{\partial^2 F}{\partial H^2} \right]^{-1}$$

$$= C_1^{-1} (T - \Theta + B/T + \dots), \quad (2.5a)$$

$$B = \Theta^2 - \left[\frac{\alpha_2}{8} \right], \quad (2.5b)$$

$$C_1 = \frac{\mu_0 R}{v} \left[\frac{\gamma \hbar}{2k_B} \right]^2, \quad (2.5c)$$

where μ_0 is the permeability of free space, R the gas constant, v the specific volume, and $\gamma \hbar / 2k_B$ the Zeeman splitting in mK per tesla. With this definition of C_1 , χ is in dimensionless mks units.

(iv) The pressure,

$$P = - \frac{\partial F}{\partial v}$$

$$= (\tilde{e}'_2 \beta / 8 - \tilde{e}'_3 \beta^2 / 24 + \dots)$$

$$+ (\gamma \hbar H \beta / 2)^2 (\Theta' / 2 + \alpha'_2 \beta / 16 + \dots), \quad (2.6)$$

where the primes indicate differentiation with respect to molar volume v .

The earliest measurements of magnetic exchange coefficients were made by Reich (1963) and Garwin and Landesman (1964), using NMR techniques. These and other NMR experiments are discussed in a review of NMR effects in quantum solids by Guyer, Richardson, and Zane (1971). Non-NMR experiments were reviewed by Trickey, Kirk, and Adams (1972).

Among the high-temperature coefficients which have been measured ($\tilde{e}_2, \tilde{e}_3, \Theta, B$), \tilde{e}_2 is certainly known with the best accuracy. The pressure measurements of Panczyk and Adams (1970) in zero field in the high-temperature range $13 < T < 100$ mK provide accurate values of $\partial \tilde{e}_2 / \partial v$, in terms of the molar volume, and give, after integration,

$$\tilde{e}_2 = 5.14(v/24)^{36.26} (\text{mK}^2),$$

where v is in cm^3/mole . For the melting curve volume, $v = 24.2 \text{ cm}^3/\text{mole}$, we have

$$\tilde{e}_2 \approx 6.95 \text{ mK}^2.$$

The specific-heat measurements performed in a high-temperature range $20 \lesssim T \lesssim 50$ mK (Greywall, 1977; Hebral *et al.*, 1979),

$$C_v \approx \frac{R}{4} \frac{\tilde{e}_2}{T^2},$$

give values of \tilde{e}_2 in a good agreement with the measurements of Panczyk and Adams.

Greywall (1977) quotes the smallest errors and gives values at $v = 23.785$ and 24.454 , which can be interpolated by

$$\tilde{e}_2 = 4.971(v/24)^{33.85} (\text{mK}^2).$$

This gives $\tilde{e}_2 = 6.58 \text{ mK}^2$ at $v = 24.2 \text{ cm}^3/\text{mole}$.

At low temperatures $2 \leq T \leq 20$ mK the specific-heat measurements show a deviation of $T^2 C_v(T)$ with respect to a constant which is identified with the next term of the series:

$$T^2 C_v(T) = \frac{R}{4} \left[\tilde{e}_2 - \frac{\tilde{e}_3}{T} \right].$$

For the same molar volume $v = 23.8 \text{ cm}^3/\text{mole}$, Dundon and Goodkind (1974; 1975) give $\tilde{e}_3 \approx +11 \text{ mK}^3$, and Hebral *et al.* give $|\tilde{e}_3| < 2 \text{ mK}^3$. Halperin (Halperin, 1979) has suggested that this Hebral *et al.* data should be corrected for a thermometric effect. Our own estimate of \tilde{e}_3 derived from Hebral with the inclusion of this effect is $\tilde{e}_3 \approx 3.5 \text{ mK}^3$. Recent measurements by Mamiya *et al.* (1981) give $\tilde{e}_3 \approx 25 \text{ mK}^3$ at the melting curve and estimate \tilde{e}_3 to vary as $v^{62 \pm 3}$ in terms of molar volume v . Although the measurements of this coefficient do not agree, they seem in contradiction with the Heisenberg model, which predicts large negative \tilde{e}_3 . Along the melting curve, the experimental entropy of Kummer *et al.* (1977) can be remarkably well fit above 1.2 mK by the high-temperature expansion (2.3) with $\tilde{e}_2 = 7 \text{ mK}^2$ and $\tilde{e}_3 = 7.8 \text{ mK}^3$ (Fig. 3 below). We doubt, however, that this expansion, limited to the third order, makes any physical sense at such low temperatures so near the first-order transition.

The Curie-Weiss temperature (generally deduced from susceptibility measurements) is not known accurately. It has been measured either at too high temperatures (Kirk, Osgood, and Garber, 1969), where the deviation with respect to the Curie law is too small to give good precision, or at low-temperature ranges $2 < T < 15$ mK (Prewitt and Goodkind, 1977; Bakalyar *et al.*, 1977), where deviations from the Curie-Weiss law become important. Kirk *et al.* give $\Theta \approx -3 \pm 0.4$ mK, Prewitt and Goodkind give $\Theta \approx -2.6$ mK, and Bakalyar *et al.* give $\Theta = -3.3$ mK. Thus

$$-3.3 \lesssim \Theta \lesssim -2.6 \text{ mK}.$$

Below 10 mK, in contrast to the behavior of an ordinary Heisenberg antiferromagnet, the susceptibility increases with respect to the Curie-Weiss law. This result was first reported by Osheroff (1972) and was based on one experimental point. It was confirmed by the results deduced from multiple echos observed by Bernier and Delrieu (1977). It was also confirmed by Bakalyar *et al.* (1977) using pulsed NMR. A more detailed measurement was then performed by Prewitt and Goodkind (1977), who gave the following values for the coefficients Θ and B in

the high-temperature expansion (2.5):

$$\Theta = -2.6 \text{ mK} \quad \text{and} \quad B = -2.7 \text{ mK}^2.$$

This negative value for B is in contradiction with a Heisenberg model which gives $B = \sum_n (z_n/2)J_n^2$ (z_n is the number of n th neighbors and J_n the interaction between n th neighbors). The large uncertainty on Θ leads to a large uncertainty on B . Moreover, the conventional method of measurement gives only relative values of χ . Fitting the experimental curve by the theoretical expansion (2.5) requires the adjustment of three parameters: Θ , B , and C_1 (the volume of solid being unknown). The precision on B estimated by Prewitt and Goodkind is certainly optimistic. We do not think B is determined to better than 50% accuracy.

A unique method, the investigation of multiple echoes (Bernier and Delrieu, 1977), can give absolute measurements of the local magnetization, eliminating one parameter in the fit of Eq. (2.5). This method might be used to obtain accurate absolute values of the magnetization at any field.

2. Pressure versus field measurements

An important experiment in the history of the theory of magnetism in solid ^3He is that of Kirk and Adams (1971), measuring $P(T, H)$. This experiment measures e'_2 and Θ' [see Eq. (2.6)]. The experiment was interpreted as a breakdown of the Heisenberg (HNNA) model at a time before the phase transition's peculiarities were known. That general conclusion we now know to be correct, but none of the theories introduced to explain this experiment were successful. It seems probable now that there are unrecognized errors in the measurements. The data can be treated as in Panczyk and Adams (1970), that is, by integrating the values of $d\Theta/dv$ to find Θ . The data do not agree well with Eq. (2.6), however, and no complete agreement can be expected unless we go outside the framework of a spin Hamiltonian [see the discussion below Eq. (2.2); see also Guyer, 1978]. Private communication with Adams indicated a possible error might be an undetermined additive constant in P , which could differ from one field to another. Even taking this into account does not resolve all difficulties. By assuming Eq. (2.6) holds, and that an overall unknown field-dependent pressure must be added, our analysis of the $P(H, T)$ data of Kirk and Adams (1971) gives $\Theta = -1.55 \pm 0.25 \text{ mK}$, which is still in substantial disagreement with other measurements.

At the time this manuscript was being revised, an experiment by VanDegrift, Bowers, Pipes, and McQueeney (1982) showed agreement with the main features of the Kirk and Adams experiment. They quote a Θ value of $-1.60 \pm 0.06 \text{ mK}$ for $v = 24.25 \text{ cc/mole}$. We have made preliminary fits and find the results of the later sections of this paper to be surprisingly insensitive to the value of Θ . Therefore, we have not thought it necessary to adjust our fits until an experimentally agreed upon value of Θ is available.

B. Ordered phases—phase diagram

1. At low field $H < 4.1 \text{ kG}$, an unexpected antiferromagnetic phase

The susceptibility measurements performed a long time ago (Kirk, Osgood, and Garber, 1969) at $10 \lesssim T \lesssim 30 \text{ mK}$ showed that solid ^3He had an antiferromagnetic behavior with a negative Curie-Weiss constant $\Theta \simeq -3 \text{ mK}$. With a nearest-neighbor Heisenberg model (HNNA), we would have expected a second-order transition at $T_{c2} \simeq 2 \text{ mK}$ to a two-sublattice antiferromagnetic phase (normal antiferromagnet), the "naf phase." This result is deduced from the high-temperature series expansion (Rushbrooke, Baker, and Wood, 1974) of the HNNA model, which gives $T_{c2} = -0.69\Theta$. A slightly higher transition temperature might be expected because experimentally the second-order transition in a "well-behaved" spin- $\frac{1}{2}$ Heisenberg antiferromagnet like SmGaG (Onn, Meyer, and Remeika, 1967) is observed at $T_{c2} = -0.8\Theta$. This expected transition was briefly thought to be found at 2.7 mK (Osheroff, Richardson, and Lee, 1972). But it soon proved that the 2.7-mK transition was the much anticipated superfluid transition in liquid ^3He . (This confusion arose because of the presence of both the liquid and the solid in the Pomeranchuk refrigerator.) Finally, the observation in 1974 (Halperin *et al.*, 1974; Kummer *et al.*, 1975) of an abrupt drop of entropy at a much lower temperature $T_{c1} = 1 \text{ mK}$, suggesting a first-order transition, demonstrated the inapplicability of the HNNA model. The recent experiments have proved that this transition is actually first order, with a discontinuity in magnetization (Prewitt and Goodkind, 1980) and in entropy ($0.442R \ln 2$; Osheroff and Yu, 1980).

Nothing was known about the magnetic structure of this phase until the magnetic resonance experiments of Osheroff, Cross, and Fisher (1980). The phases occurring within a Heisenberg model, including first- and second-neighbor interactions have two or four sublattices with cubic symmetry (see, for example, Herpin, 1968). As the dipolar interaction energy is zero at lowest order in a cubic lattice, those phases would give a very low resonance frequency (of the order of a few kHz).

The observation by Osheroff *et al.* (1980) of a large zero-field resonance frequency $\Omega_0 = 825 \text{ kHz}$ proved that the actual magnetic structure does not have cubic symmetry. By using monocrystals in a magnetic field they observed three domains having only three possible spin orientations. Consequently the direction of anisotropy is along one of the three axes, (001), (010), (100). Any other symmetry axis would give more than three possible directions.

Investigating simple one-Fourier-component structures described by the plane-wave equation

$$\mathbf{S}_i = \text{Re}(\mathbf{S}_k e^{i\mathbf{k}\cdot\mathbf{R}_i}),$$

they found only one of these structures in agreement with the experiment. Its wave vector is $\mathbf{k} = \pi/a(001)$. It consists of 001 "ferromagnetic" planes (planes of parallel

spins) arranged in the sequence up, up, down, down, . . . , (uudd phase). The structure is illustrated in Fig. 1.

Owing to uniaxial symmetry, the dipolar energy is

$$E_D = \frac{1}{2} \lambda (d^z)^2,$$

where \mathbf{d} is a unit vector indicating the direction of, say, the up spins. The estimation of λ in molecular field gives $\lambda = 7.26 \rho^2 (\frac{1}{2} \gamma \hbar)^2$ where ρ is the number density. As λ is positive, the dipolar energy is minimum for $d^z = 0$. The spins orient in a direction perpendicular to (001), i.e., in the plane of the (001) ferromagnetic planes. Thus the anisotropy is "planar," in agreement with the behavior of the resonance spectrum that they observed. The orientation of the spins is free within (001) planes. Any small magnetic field removes this degeneracy, orienting the spins perpendicular to itself.

The zero-field resonance frequency is

$$\Omega_0 = (\lambda \gamma^2 / \chi_1)^{1/2}.$$

Taking the experimental value of the susceptibility χ_1 (Prewitt and Goodkind, 1977), Osheroff, Cross, and Fisher found $\Omega_0 \approx 875$ kHz in good agreement with the experimental value.

The uudd phase is the simplest structure agreeing with the experimental results, but more complicated phases

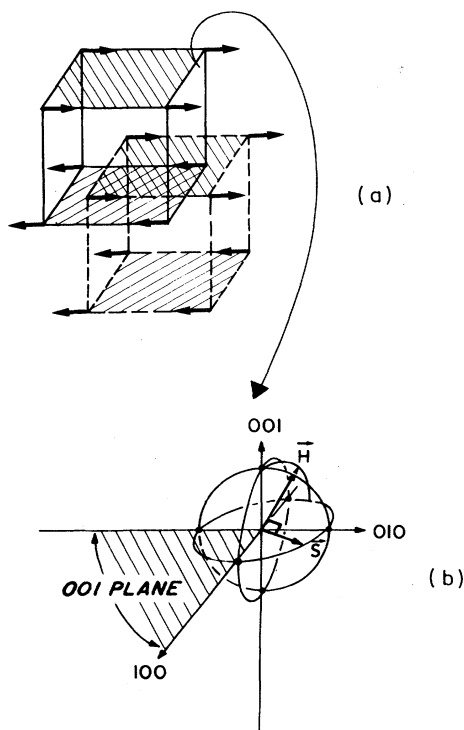


FIG. 1. The uudd phase. The bcc lattice is split into two simple cubic lattices, respectively represented by full and dashed lines. Within a given (001) plane (dashed plane) the spin vectors are identical and lie in the plane. (a) In zero field, the spin orientation is free in the dashed (001) plane. (b) When a small field is applied, the spins remain in the 001 plane but become oriented perpendicular to the field.

with several Fourier components are not excluded. For example, structures consisting of a sequence of n layers of (100) ferromagnetic planes with spins "up" alternating with n layers of (100) ferromagnetic planes with spins "down" give approximately this same resonance spectrum with a zero-field resonance frequency Ω_n differing from the resonance frequency Ω_0 of the uudd phase by less than 10% (Roger, 1980): $(\Omega_n - \Omega_0) / \Omega_0$ is 6% for $n = 4$ and 7.4% for $n \rightarrow \infty$. More experiments are needed to identify this phase with certainty. The uudd phase has four magnetic sublattices. Consequently, for symmetry reasons, the spin-wave spectrum has one acoustic mode and one optical mode (each doubly degenerate). Within the four-spin exchange model (see Sec. IX), the frequency of the optical mode is estimated to be 150 MHz. In Sec. IX we suggest that the coupling between the exchange and the phonons will allow observation of this optical mode and identification of the uudd phase. Neutron diffraction will give a direct classification of the phase, but the large absorption cross section of ^3He for neutrons makes this a very difficult experiment. Nonetheless, preliminary experiments are encouraging (Benoit *et al.*, 1982).

Prewitt and Goodkind (1977) made the first observation of the low-field (uudd) phase off the melting curve, and also give a value for the magnetic susceptibility of that phase:

$$\chi = C_1 / 5.2 \text{ mK}.$$

Recent results by Morii *et al.* (1978) give χ slightly lower,

$$\frac{C_1}{5.9 \text{ mK}} \leq \chi \leq \frac{C_1}{5.2 \text{ mK}}.$$

Osheroff and Yu have measured the shape of the melting curve from about 0.4 to 1 mK and have been able to deduce the entropy as a function of temperature. It fits well with the T^4 behavior expected from spin-wave theory, and they deduce a "mean spin-wave velocity." They obtain $8.4 \pm 0.4 \text{ cm/sec}^{-1}$ for this quantity, making it one of the best measured properties of magnetic ^3He .

2. At fields larger than 4.1 kG, a phase with strong ferromagnetic tendencies

In a magnetic field, the first-order transition to the phase described above is observed up to $H = 4.1$ kG, at a critical temperature $T_{c1}(H)$ which decreases slightly with H . Above 4.1 kG a second-order transition is found with a critical temperature $T_{c2}(H)$ increasing with H . The occurrence of this second-order transition was first suggested on the basis of the entropy curves and confirmed by a careful analysis (Adams, Delrieu, and Landesman, 1978) of the thermodynamical measurements of Kummer, Mueller, and Adams (1977) in a magnetic field H between 4 and 12 kG. The existence of this transition has been confirmed by other experiments (Godfrin *et al.*, 1980; Schuberth, Bakalyar, and Adams, 1979). The second-order transition was recently investigated up to high field, $H = 72$ kG, by Godfrin *et al.* (1980). The measurements

of Godfrin *et al.* do not define exactly the second-order critical temperature, but a temperature somewhat lower at which the entropy becomes negligible ($S \approx 0.2 \ln 2$); nevertheless, their experiments indicate that the critical temperature increases up to $T \approx 3.5$ mK at $H = 72$ kG.

The magnetization of this phase can be estimated from several experiments (Godfrin *et al.*, 1980; Kummer, Mueller, and Adams, 1977; Adams *et al.*, 1980). They all agree with a value of about one-half of the saturation magnetization M_0 at the relatively low value of the magnetic field $H = 4.1$ kG. This is a field such that $\gamma \hbar H / 2k_B \approx \frac{1}{10} |\Theta|$, whereas in ordinary antiferromagnets this quantity needs to be of order $|\Theta|$ for such strong magnetization. Godfrin *et al.* (1980) measured the variation of the limiting pressure $\Delta P(H) = P(H) - P(0)$ in a Pomeranchuk cell in terms of the magnetic field H . Neglecting the entropy at very low temperature, the laws of thermodynamics give

$$\left(\frac{dP}{dH} \right)_{\text{melt}} = \frac{M_s - M_l}{V_s - V_l}, \quad (2.7)$$

where M_s and M_l are, respectively, the magnetizations of the solid and the liquid, while V_s and V_l are the molar volume of the solid and the liquid. [This equation is similar to the Clausius-Clapeyron equation, the conjugate variables (H, M) being substituted for (T, S).] Neglecting the magnetization M_l of the liquid, we deduce the magnetization M_s of the solid by taking the slope of the curve $P(H)$:

$$M_s \sim (V_s - V_l)(dP/dH).$$

The experimental curves of $P(H)$ and $M_s(H)$ deduced from Godfrin *et al.* are shown in Fig. 24 below. The magnetization varies slowly from $0.6M_0$ around 4 kG to $0.7M_0$ at 72 kG. The magnetization at low field agrees with the value measured directly by Prewitt and Goodkind (1980): $0.5M_0$ at 4 kG.

These results are consistent with the magnetic resonance data of Adams *et al.* In this phase, they observed a broadening and shift of the resonance line almost independent of the field between 4.3 and 29 kG, which indicates that the variation of the magnetization is quite low. No precise value of the magnetization can be deduced from their measurement, because the shape of the sample is undetermined. Recent experiments of Osheroff (1982) on monocrystals give $M = 0.57M_0$. Thus this phase has strong ferromagnetic tendencies: high magnetization and a critical temperature, increasing with the field. It differs strongly from a ferromagnetic phase, however, because its magnetization differs from the saturation magnetization. The shape of the whole diagram is shown in Fig. 2. It does not resemble the usual antiferromagnet, which has only one phase with cubic symmetry (the naf phase), bounded by a second-order transition. In the usual antiferromagnet the transition temperature decreases with increasing magnetic field H .

3. Other phase transitions

Some other possible phase transitions or specific-heat anomalies have been suggested. Schuberth, Bakalyar, and Adams (1979) indicated they had discovered a possible phase transition in the solid, more or less coincident with the A transition in the liquid, at fields above 27 kG. (The experiments were carried out in a Pomeranchuk cell, so that both the liquid and the solid were present.) Yu and Anderson (1979) and Delrieu (private communication) suggested that this was a nonequilibrium artifact due to the formation of underpolarized solid from the liquid. This seems to have been confirmed by recent work of Hunt, Morii, and Adams (1981).

The peak in the specific heat at 2 mK (see Fig. 3) has been speculated in the past to be related to a second-order phase transition, although this does not seem to be considered likely now because no coincident effects in other

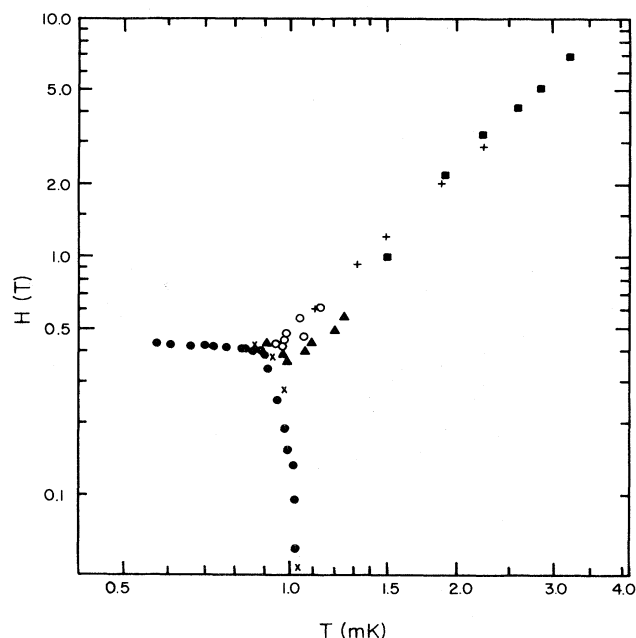


FIG. 2. Experimental phase diagram in the H - T plane for bcc ^3He near melting. Osheroff (1982) observed a first-order transition bounding the low-field phase (\bullet), and another first-order transition (\circ). Adams's group (Kummer *et al.*, 1975) observed a first-order (\times) and a second-order ($+$) line. Godfrin *et al.* (1980) observed a strong entropy anomaly (\blacksquare), presumably an extension of the second-order phase transition of Adams. Prewitt and Goodkind (1980) observed two transitions for fields near 0.4 T which they reported to be second order (\blacktriangle). This figure shows that the situation near 0.4 T and 1 mK is not yet clearly defined by experiment. However, the low-field, low- T phase is almost certainly entirely bounded by a first-order transition, and coming out of the region near 0.4 T and 1 mK a line of some kind clearly extends to the upper right. Osheroff's (1982) recent experiments seems to show definitely that some part of this extension is also a first-order transition. All these results are in strong contradiction to an HNNA model which leads to a second-order transition arcing from $7T$ at $T=0$ to 2 mK at $H=0$.

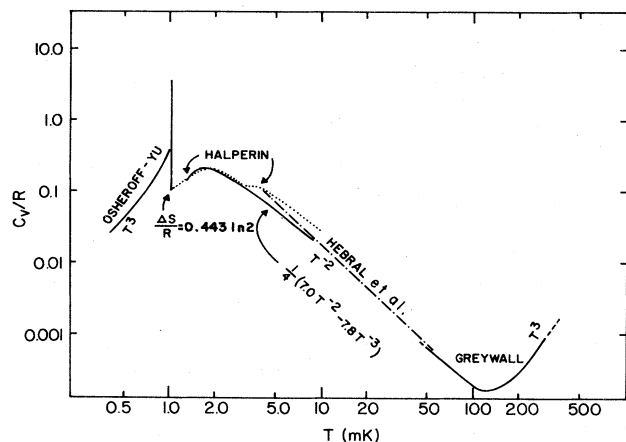


FIG. 3. Specific heat for solid ^3He in the range 0.4–300 mK. The curve labeled Osheroff-Yu (1980) exhibits T^3 behavior characteristic of spin waves. The vertical line at 1.03 mK corresponds to the first-order phase transition, the entropy change being $0.443R \ln 2$ as measured by Osheroff. A somewhat less well-known region above the transition is shown by the older measurements of Halperin *et al.* (1974, 1978). Also shown is the line $\frac{1}{4}(7.0T^{-2} - 7.8T^{-3})$ which fits the data of Kummer *et al.* (1975) in this region rather well. Hebral *et al.* (1979) have measured the T^{-2} region from 5–50 mK. Greywall (1977) has measured above 50 mK, where the phonon (T^3) contribution begins to come in.

parameters have been found and because no indication of the transition seems to have been found in NMR experiments.

Prewitt and Goodkind (1980) find a second transition below the second-order transition studied by Godfrin *et al.* and by Adams *et al.* at about 4.1 kOe. This region is complex both experimentally and in mean-field theory. The recent observations in this region by Osheroff (next paragraph) confirm this complexity, although it is not certain that the second transition observed by Prewitt and Goodkind is one of the transitions observed by Osheroff.

Osheroff (1982) has traced the boundary of the low-field phase down to 0.4 mK. He has reported that the first-order boundary of the low-field phase shows a sharp bend at about 0.89 mK and 4.0 KOe, which indicates that another first-order phase line meets it there. His investigations seem to show a first-order transition between the high-field phase and the paramagnetic phase, which more or less follows the supposed second-order transition found by other workers. His measurements of this first-order phase line extend up to about 6 KOe and 1.15 mK. If our mean-field theory results are meaningful, we would expect this first-order line to end at a critical point.

C. Effect of specific volume

Most of the results so far quoted refer to experiments done on or near the melting curve. It is possible to correlate all results above the melting curve which have been obtained so far by assuming that all quantities of dimen-

sion mK scale as v^γ where $\gamma = 18 \pm 1$ (e.g., $\tilde{\epsilon}_2$, which has dimensions of mK^2 , scales as v^{36} , etc.). (See, for example, Mamiya *et al.*, 1981). If this result holds true in detail (i.e., if the phenomena all scale according to a single function of v), then we shall have to presume that only a single physical mechanism of exchange is important. As the experimental results cannot be interpreted with less than two exchange mechanisms—three-particle exchange J_t and four-particle exchange K_p (see Sec. VIII)—all significant exchange frequencies J_t, K_p, \dots , will have to vary according to a single function of v . At first sight there seems no simple way to link these mechanisms to a single physical process. However, the calculations of Avilov and Iordansky (1982) suggest that J_t and K_p are nearly of the same size and will vary with v in a similar way. We return to this point briefly in Sec. XIII.

III. THEORETICAL MODELS

A. Pre-1975 theories

The earliest work on magnetism in solid ^3He was done by Bernardes and Primakoff (1960) and thereafter by Nosanow and co-workers (Nosanow, 1964; Nosanow and Mullin, 1965; Hetherington, Mullin, and Nosanow, 1967). These workers used a perturbation-theory approach to determine the exchange rate. The sign of the exchange was not understood to be definite.

Even as late as 1972 the question of the sign of the exchange was not universally agreed upon. Trickey, Kirk, and Adams (1972), in their excellent review, said that it might depend on the delicate cancellation of large numbers.

Thouless' paper in 1965 (Thouless, 1965a) marks a turning point in the understanding of exchange in solid ^3He . Thouless settled the question of the sign of the exchange. (It is antiferromagnetic for nearest-neighbor exchange, ferromagnetic for three-particle rings, etc.; see Secs. IV and V.) He also gave the form of the spin exchange operator for four-spin ring exchange.

During this period there were a large number of theoretical papers on the magnetic effects. All of them were based on the assumption that only nearest-neighbor exchanges are important. That idea can now be ruled out. We mention the review by McMahan (1972a) as being very good in that context. A different approach by Brandow (1971, 1972) and by Østgaard (1972) was based on the t -matrix theory taken over from nuclear physics. The effective density in solid ^3He is much higher than in nuclei, so the t -matrix approach becomes very difficult.

More or less beginning with Thouless (1965a), the suggestion that higher exchanges play an important role was an undercurrent. Guyer and his collaborators kept the idea alive with a series of papers using three- and four-spin exchange in various contexts (Guyer and Zane, 1969; Zane, 1972; McMahan and Guyer, 1973; Mullin, 1975; and Guyer, Mullin, and McMahan, 1975).

By 1974 Guyer (Guyer, 1974) was convinced that the

theory which relied on nearest-neighbor exchange was inadequate. He also gave a convincing presentation of the contradictions at a meeting in Aussois, France in 1974.

B. Post-1975 theories

After the experiments of Kummer *et al.* (1975) and of Halperin *et al.* (1974, 1978), the theories changed character to a more speculative form. The review by Guyer (1978) gives an idea of the theoretical situation at that time. The paper of McMahan and Wilkins (1975) was an attempt to calculate the magnitude of four-spin exchanges, perhaps in the older tradition. Beal-Monod (1977) proposed a model based on spin glasses, which must be ruled out now that we know that the low-temperature phase is ordered. Sokoloff and Widom (1975a, 1975b) proposed a ground-state vacancy model. Two more vacancy models were proposed by Andreev, Marchenko, and Meierovich (1977) and by Heritier and Lederer (1977, 1978).

These vacancy models were suggested by the ferromagnetic tendencies of ^3He in the paramagnetic state. The fact that vacancies favor ferromagnetism can be simply shown in the following way: When, after n successive jumps on a closed path, a vacancy returns to its initial position, the net effect is a cyclic permutation of the $n - 1$ atoms involved on this path. If only jumps to nearest-neighbor sites are allowed, all such closed paths in a bcc lattice have an even number of steps (such a lattice is called "alternated"), and correspond to cyclic permutation of an odd number of particles. Such permutations favor ferromagnetism (see Sec. V). Thus, if all allowed permutations are odd, one can prove easily that the ground state for one isolated vacancy is ferromagnetic (Nagaoka, 1965, 1966). Consequently, in an antiferromagnetic lattice, a vacancy can lower its energy by constructing a local ferromagnetic surrounding called a "polaron." The presence of a concentration $x \simeq 5 \times 10^{-4}$ of such (possibly nonequilibrium) polarons could account for the enhancement of the low-field susceptibility at low temperatures (Heritier and Lederer, 1977; Montambaux, Heritier, and Lederer, 1982). Until now no explanation of the first-order transition and of the structure of the low-field phase has been given within this model. On the same basis, but taking into account the variation of the number of vacancies with the magnetic field, Andreev, Marchenko, and Meierovich (1977) reported that ground-state vacancies can induce a ferromagnetic phase above some finite external field H . The first-order transition they predict between this phase and the paramagnetic phase is in contradiction with the experimental results. With a concentration of vacancies of the order of 10^{-4} we expect some anomalies in the high-temperature thermodynamic data in the range $10 \lesssim T < 100$ mK (Heritier and Lederer, 1978). Careful specific-heat measurements revealed no anomaly (Greywall, 1977; Hebral *et al.*, 1979). However, in fairness to the conceivers of the vacancy idea, it should be mentioned that all earlier measurements of specific heat had indicated just such an anomaly (Castles and

Adams, 1973; Pandorf and Edwards, 1968; Sample and Swenson, 1967).

Another approach to the problem was suggested by Papoular (1978). Papoular proposed some kind of lattice distortion which would "freeze in" the antiferromagnetism. More recently Guyer and Kumar (1982) have suggested a similar, more specific model: A phenomenological treatment of the free energy, expanded in powers of the order parameter $p = \langle 2S_z \rangle$, shows the negative p^4 terms can induce a first-order transition (Landau and Lifschitz, 1958b, *Statistical Physics*). A possible physical origin of such fourth-order terms is the coupling between exchange and phonons. As a rough approximation, we can take an HNNA model with an exchange constant J varying isotropically with the molar volume V : $J = J_0[1 + \Gamma_J(\Delta V/V)]$. A free-energy expansion in powers of the order parameter shows that a first-order transition can occur if the critical parameter $\eta = \frac{3}{2} N k_B K T_N \Gamma_J^2$ ($T_N = 4J$ is the Néel temperature and K the compressibility) is larger than one (Bean and Rodbell, 1962). Although $\Gamma_J = d \ln J / d \ln V \simeq 18$ is quite large, η is nevertheless of the order of 1.6×10^{-2} (Landesman, 1978), which is much too small to induce a first-order transition. Guyer and Kumar note that an examination of the χ^{-1} vs T curves shows that they become rather straight at low temperatures and would apparently pass through the origin if extrapolated. They say that this may mean an absence of a temperature scale in the underlying physical exchanges, whatever they may be. They thus assume that some static deformation effect as described above (but involving the proper shear distortion to induce the uudd structure) is needed to obtain the observed first-order transition. Models based on this exchange-phonon coupling each fit only one experimental datum (the critical temperature of the first-order transition) with one adjustable parameter. The value given for this parameter seems to require a very large dependence of J on the molar volume or shear distortion.

The low experimental value of η leads to the conclusion that the coupling of exchange with phonons is likely not essential for the magnetic properties of solid ^3He . Furthermore, with large exchange-phonon coupling we would again expect some anomalies in the high-temperature thermodynamic data (in the range $10 \leq T \leq 300$ mK), for which there is no evidence.

Finally, the multiple exchange model proposed by Hetherington and Willard (1975) was a phenomenological success, but when it was first proposed lacked sufficient theoretical support for general acceptance. Their multiple exchange model incorporated large values for the four-spin exchange terms. Such multiple exchange models with large four-spin ring exchanges are at the present time the only ones which can account for most of the available experimental data.

C. Ring-exchange models

Two main ideas lead us to choose this model. (a) Four-spin exchange gives fourth-order terms in the ex-

pansion of the free energy and can induce a first-order transition. (b) By simple geometrical arguments we are convinced that multiple exchanges (like three- and four-particle cyclic permutations) could be microscopically justified in hard-sphere quantum solids. We view the multiple exchange theories to be in the tradition of earlier calculations of exchange, say those of McMahan and Wilkins (1975). However, unlike them, we refuse to trust the variational wave functions in the exchanging configurations.

The Lennard-Jones interaction potential between the atoms presents an impenetrable hard core of diameter $\sigma_H \cong 2.14 \text{ \AA}$ and a weak attractive part (see Fig. 4). Because of the light mass of ^3He atoms, the kinetic energy term in the Schrödinger equation is more important than the attractive part of the potential energy. Therefore, a simple hard-sphere model can be useful in describing ^3He (Kalos, Levesque, and Verlet, 1974). Thus exchange process in ^3He can be approximated as real permutations of hard spheres.

Let us take now the simple model represented by Fig. 5. Four hard discs, a, b, c, d are free to move in the space limited by eight fixed discs (1–8). The positions of these discs are those of four ^3He atoms and their eight nearest neighbors in a 110 plane of the bcc lattice [Fig. 5(a)].

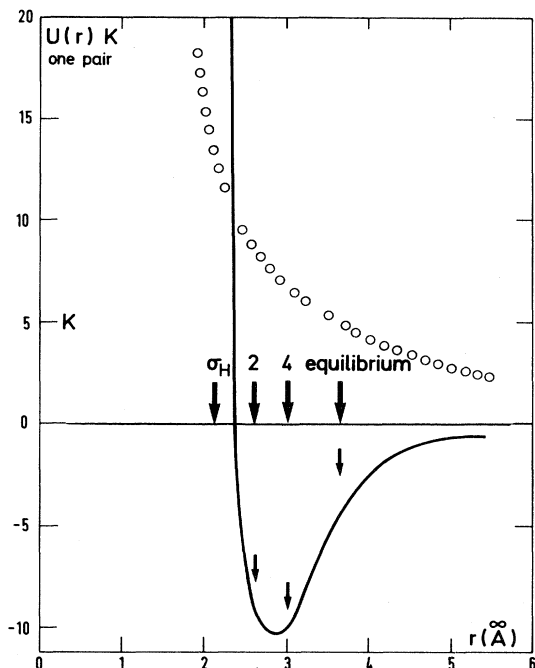


FIG. 4. Lennard-Jones potential. The equilibrium distance R_0 between atoms is larger than the distance r_0 corresponding to the minimum of the Lennard-Jones potential. $\sigma_H = 2.14 \text{ \AA}$ is the equivalent hard-core diameter. The arrows show the distance between atoms during two- or four-atom exchange with fixed surrounding neighbors. The approximate kinetic energy per pair (open circles) in the ^3He ground state as a function of nearest-neighbor distance shows that the kinetic energy is as large as the potential energy is the equilibrium configuration.

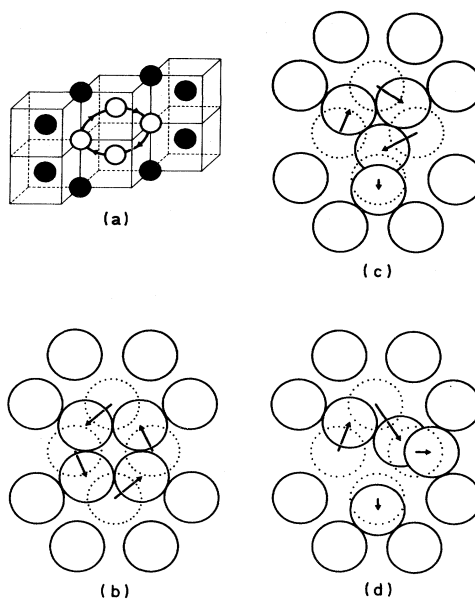


FIG. 5. Ring exchanges in the bcc lattice. (a) Four atoms and their eight first neighbors in a (110) plane of the bcc lattice. (b) As the lattice opens, $\sigma/a \cong r_4$, the first exchange to occur is cyclic four-particle exchange. (c) and (d) show how two- or three-particle exchange requires overlapping of the hard cores at the same density as (b). The eight surrounding atoms are supposed to be fixed.

(i) If the ratio $r = \sigma/a$ between the radius σ of the discs and the parameter a of the unit lattice cell is larger than some critical value r_4 , any permutation of two, three, or four discs is geometrically impossible without overlapping the hard cores.

(ii) With r slightly smaller (corresponding to lower density) than r_4 , the permutation of two or three discs remains impossible, but four atoms can exchange cyclically.

(iii) As r decreases, the lattice becomes more open, and with $r_{234} < r < r_{34}$, three- and four-particle cyclic permutations are allowed but two-particle exchange is forbidden.

(iv) All three kinds of permutations (with 2, 3, or 4 atoms) can only occur if r is smaller than r_{234} .

Thus, as the lattice opens, the last type of exchange to occur is that of the two-particle permutations, and this simple picture suggests that three- and four-particle exchanges could be favored at large densities. However, this model is very crude because it does not take into account the displacements of the surrounding atoms and because it is planar. We need more quantitative arguments.

Estimates of the exchange rates corresponding to different permutations can be carried out only if we are able to find a reliable approximation for the wave function in the exchange configuration. Although it gives a correct value for the ground-state energy, the Gaussian wave function generally used in the literature (i.e., a product of Jastrow functions with independent phonon eigenfunctions; McMahan, 1972b; McMahan and Wilkins, 1975)

does not describe the wave function correctly in the exchange configurations. The Gaussian tails of these wave functions are unreasonably small in the exchanging configurations. Exponential tails, which are longer, are expected to be a better description in these configurations.

IV. PHYSICAL ORIGIN OF MULTIPLE EXCHANGE

A. Exchange Hamiltonian—main hypothesis for the calculation of the exchange rates

In spite of the large zero-point motion, exchange occurs “rarely,” the experimental exchange frequencies $J_p \sim 10^7$ Hz being 10^4 times smaller than the Debye frequency $\omega_D \approx 3.5 \times 10^{11}$ Hz. Thus the ³He atoms can be considered to be strongly localized in the solid. The fact that, at low temperatures $5 \text{ mK} \lesssim T \lesssim 100 \text{ mK}$, the entropy is reduced to the magnetic entropy $\approx R \ln 2$ seems to confirm this hypothesis.

The study of this kind of exchange as it applies to solid ³He was begun by Thouless (1965a). His work is based on the earlier work of Conyers Herring (1962). We review the theory here and derive Thouless’ result that the exchange rate is given by a surface integral over the “home-based” wave function, which we define below.

In this section only identical *distinguishable* particles will be considered. The restriction to totally antisymmetric wave functions will be made in the next section, where the spin pseudo-Hamiltonian will be derived. By restricting our discussion to distinguishable particles for the moment, we need consider only the “orbital” part of the wave function, since there is no spin-spin or spin-orbit interaction.

In the $3N$ -dimensional configuration space, the orbital wave function $\psi(\mathbf{r})$, $\mathbf{r}=(\mathbf{r}_1, \mathbf{r}_2, \dots, \mathbf{r}_N)$, takes appreciable values only when each particle i is near its lattice site \mathbf{R}_i . The ground-state wave function is of constant phase and has no nodes, and therefore we can assume that it is real and positive. Following Thouless (1965a), we give the name “cavity” to a region of configuration space where the probability $\psi^2(\mathbf{r})$ for the wave function is high. For a system of N identical but distinguishable particles, there are $N!$ ways to assign N particles to N lattice sites. Thus we define $N!$ cavities Ω_P , each containing configurations in which each particle i is near the lattice site $\mathbf{R}_{P(i)}$ (P representing any permutation of N numbers). These cavities are connected by regions of small but finite probability for the wave function called “ducts.” The cavity centers can be defined as the points in hyperspace where each particle is exactly located on a lattice site. Therefore, the cavity centers are the points where $\psi^2(\mathbf{r}) = \max$ (i.e., at $\mathbf{r} = \mathbf{R}_{P(i)}$). The idea of the cavity can be visualized if one considers the surfaces of constant probability density, $\psi^2(\mathbf{r}) = \text{const}$, as comprising a $3N$ -dimensional topographic map. For $\psi^2(\mathbf{r})$ just less than the maximum we find hyperspherical surfaces surrounding the cavity centers. As the probability density is decreased the spherical contour surfaces grow and become deformed. (In

fact, certain local maxima in the wave function may exist which would complicate the picture.) At very low probability densities the surfaces of the distinct cavities Ω_i would first touch, then become connected along the paths of the “ducts.” The ducts can therefore be defined as paths along which the probability density of this ground-state wave function is always greater than some value; these paths connect the cavities corresponding to different permutations P . The exchange P of N particles corresponds to the tunneling from one cavity Ω_E ($E \equiv \text{identity}$) to Ω_P .

Figure 6 illustrates the partition of the four-dimensional configuration space into two cavities Ω_1 and Ω_2 and two ducts D_1 and D_2 for the very simple case of two particles in a two-dimensional box. In a $3N$ -dimensional configuration space, the topology of cavities and ducts is very intricate. Nevertheless, the problem can

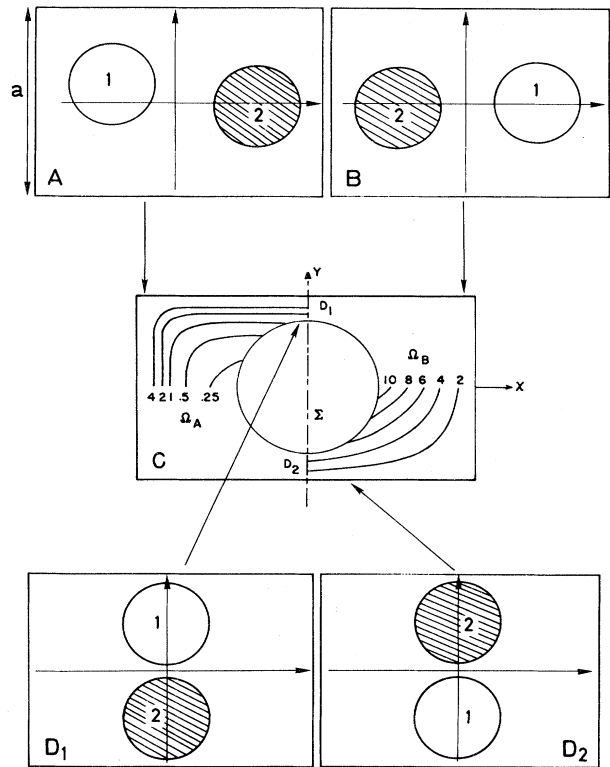


FIG. 6. The exchange of two hard disks in a box of two dimensions. x_1, y_1 and x_2, y_2 are the coordinates of particles 1 and 2, respectively, and $x = x_1 - x_2$; $y = y_1 - y_2$; $X = (x_1 + x_2)/2$, $Y = (y_1 + y_2)/2$ are their relative coordinates. The particles are shown in A and B in positions which correspond to the two “cavities” Ω_A and Ω_B . In D_1 and D_2 the particles are shown in the ducts. In C the four-space is represented by the two-dimensional plane (x, y) . At each point (x, y) the orthogonal X, Y subspace is rectangular (L_1, L_2) although its shape changes from point to point on the x, y plot. Contours in the lower right of C show the area $A = L_1 L_2$ corresponding to each point x, y . Also shown in the upper left of C are transverse “kinetic energies” calculated as $(1/L_1^2) + (1/L_2^2)$, being proportional to the energy of a two-dimensional particle in a box of sides L_1, L_2 .

be simplified by the following physical hypothesis.

Let us imagine a perfectly localized system where there is no exchange at all (all paths or "ducts" between cavities are closed). In this case the ground state of the N identical but distinguishable particles is $N!$ degenerate. The opening of the ducts removes this degeneracy. The number of ducts leading from any one cavity is equal to the number of physically possible exchanges. For example, if only nearest-neighbor exchange is possible then there will be $\frac{1}{2}qN$ ducts leaving each cavity (where q is the number of nearest neighbors). With four-particle rings of nearest neighbors tunneling cyclically, we would still have a number of order- N tunnels from each cavity. Each pair of cavities connected by ducts corresponds to one type of exchange. Some pairs of cavities may be connected by more than one duct, but in this case these parallel "ducts" are simply different orientations of the same particles while tunneling (for example, when nearest neighbors tunnel and are passing each other there are several orientations with equal probability). For convenience we shall refer to all the parallel ducts connecting two cavities as a single duct.

In the limit of low exchange rates (compared to the Debye frequency), the opening of one duct between two cavities Ω_E and Ω_P changes the relative phases of the wave function $\psi(\mathbf{r})$ in Ω_E and Ω_P , but does not appreciably affect the magnitude $|\psi(\mathbf{r})|$ of the wave function in the cavities. Therefore, we can isolate two cavities, Ω_E and Ω_P , and one duct D , connecting both cavities, independently of other ducts and cavities. We calculate the exchange frequency J_P corresponding to the permutation P as the tunneling rate between the cavities Ω_E and Ω_P through the duct D (see Fig. 7). The exchange frequency J_P is defined as one-half of the energy difference $E^S - E^A$ between the ground state ψ^S and the first excited state ψ^A in the region $\Omega_E - D - \Omega_P$.

Writing the Schrödinger equations for both states, and combining these equations in order to eliminate the potential energy $U(\mathbf{r})$, we obtain

$$(E^A - E^S)\psi^A\psi^S = \frac{\hbar^2}{2m}(\psi^A\nabla^2\psi^S - \psi^S\nabla^2\psi^A).$$

Integrating both sides over a part v (e.g., over one cavity) of the $3N$ -dimensional configuration space and applying integration by parts on the right-hand side, we obtain

$$(E^A - E^S) \int_v \psi^A\psi^S dv = \frac{\hbar^2}{2m} \int_{\Sigma_v} (\psi^A\nabla\psi^S - \psi^S\nabla\psi^A) \cdot d\mathbf{S}. \quad (4.1)$$

Σ_v is the hypersurface limiting the hypervolume v . If v is chosen to be the half space of configurations limited by the $(3N-1)$ -dimensional nodal surface Σ_N (where $\psi_A=0$), we obtain the simple formula (Thouless, 1965a)

$$\begin{aligned} -2J_P &\equiv E^A - E^S \\ &= -\frac{\hbar^2}{2m} \int_{\Sigma_N} \psi^S\nabla\psi^A \cdot d\mathbf{S} / \int_v \psi^A\psi^S dv. \end{aligned} \quad (4.2)$$

Note that with this definition J_P will always be negative.

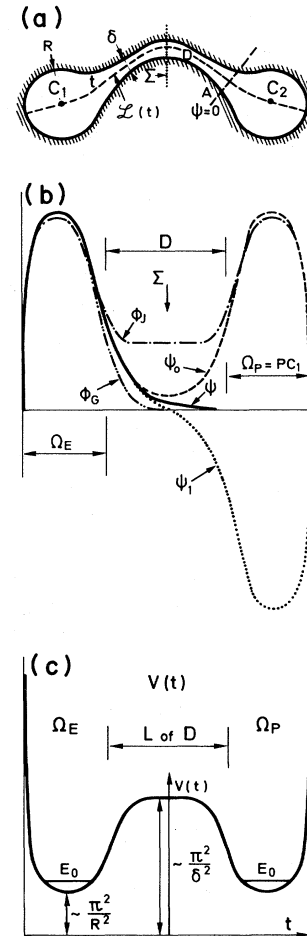


FIG. 7. Schematic representation of exchange: (a) In the configuration space of two cavities Ω_E and Ω_P corresponding to the permutation P and one duct D connecting Ω_E and Ω_P . Ω_E and Ω_P represent the system in permuted configurations at "equilibrium" (i.e., when each atom is near its lattice site). Exchange P occurs through the duct D connecting Ω_E and Ω_P . The duct section is small compared to the dimensions of the cavities because the space for zero-point motion is reduced by hard cores in the exchange configurations. Σ is the $(3N-1)$ -dimensional median plane equidistant from the centers C_1 and C_2 of the two cavities. $\mathcal{L}(t)$ is the fall line along the middle of the duct, where the real ground-state function is maximum. A correct "home-based function" as defined by Herring (1962) is the exact solution of the Schrödinger equation in Ω_E and D , with D closed at A near Ω_P . (b) Behavior of some wave functions along the line $\mathcal{L}(t)$. t is the curvilinear coordinate along the line $\mathcal{L}(t)$. $\Psi_0(t)$: exact symmetric ground-state function. $\Psi_1(t)$: exact antisymmetric first excited state. $\Psi(t)$: Home-based function, solution of the Schrödinger equation in Ω_E and D , with D artificially closed on A at the end of the duct ($\Psi=0$ on A). Ψ decreases exponentially near the center of the duct. $\phi_j(t)$: Jastrow wave function, depending only on distance from the wall. It is approximately constant at the center of the duct and too large compared to Ψ . $\phi_0(t)$: product of Jastrow wave functions and Gaussian-like functions. It decreases too rapidly in the duct compared to Ψ . (c) Structure of the effective potential V defined by Eq. (4.4), representing the localization energy of the system in a given section of the duct.

In order to calculate J_P , Eq. (4.2) makes it clear that the wave function must be determined in the center of the exchange duct. Of course this kind of many-body wave function cannot be calculated except by methods which take full account of the many-dimensional character of the problem.

In principle, the Monte Carlo procedure developed by Kalos and co-worker (Ceperley and Kalos, 1979) can determine exact solutions of the Schrödinger equation.¹ The ground state ψ^S and the first excited state ψ^A could be determined separately by assigning adequate limiting conditions on the surface Σ . An important question still remains: Within a reasonable computing time can we obtain a sufficient number of events in the low-probability region D to deduce accurate values of ψ^S and ψ^A on the exchange surface Σ ? We think this calculation is possible. In any case the method is worth investigating because it seems to be the only one which could give definite values of the exchange frequency J_P .

As a first step, if we want only to compare the relative orders of magnitude of the different kinds of exchange J_P , we can use approximations to the wave function.

B. Approximation to the wave function

1. Definition of a home-based function

If the duct is narrow, the magnitudes $|\psi^S|$ and $|\psi^A|$ of the even and odd modes are practically the same in the cavities Ω_E and Ω_P . Consequently the linear combination

$$\psi_1 = \frac{1}{2}(\psi^S + \psi^A) \quad (4.3)$$

is mainly localized in one of the two cavities, and

$$\psi_2 = \frac{1}{2}(\psi^S - \psi^A)$$

is localized in the other (see Fig. 7).

As defined by Herring (1962) and McMahan (1972a, 1972b), ψ_1 represents a "home-based function" for the system. Thus

$$\psi^S = (\psi_1 + \psi_2) \quad \text{and} \quad \psi^A = (\psi_1 - \psi_2). \quad (4.4)$$

In the half space v limited by the median hyperplane Σ_M , we have

$$|\psi^S| \simeq |\psi^A| \simeq |\psi|$$

and the integral $\int_v \psi^2 dv = \frac{1}{2}$.

Using this fact and Eqs. (4.4) and (4.1), one obtains

$$J_P = -2 \frac{\hbar^2}{2m} \int_{\Sigma} (\psi_1 \nabla \psi_2 - \psi_2 \nabla \psi_1) \cdot d\mathbf{S}. \quad (4.5)$$

¹We note that Thouless (1965b) was the first to suggest that a Monte Carlo method could be used to improve the wave function in the duct. He made a model calculation based on two particles in a box (the three-dimensional equivalent of Fig. 6) and showed that exchanges could be calculated in that six-dimensional problem.

This relation emphasizes that ψ must be known with accuracy inside the duct, in particular in the middle, on the exchange surface Σ .

2. Approximation to the home-based function ψ

We must find reliable approximations to ψ . As pointed out by Thouless (1965a), a good approximation to the home-based function ψ_1 can be obtained by localizing the wave function in one cavity C_1 , artificially closing the duct D at its end A opposite to C_1 (see Fig. 7). The exact home-based function as defined in Eq. (4.3) actually gets smaller as one passes the nodal plane of ψ_A until a point near the second cavity, where it must cross zero and become negative (although small), as can be seen by considering the fact that ψ_1 and ψ_2 are orthogonal. Closing the duct on the nodal plane of ψ_1 would leave it unchanged. If the exchange is small, so the ψ_1 is very small in the neighborhood of its nodal plane and near the end of the duct, then closing the duct arbitrarily at a surface near the end should not affect ψ_1 much near the center of the duct.

If we are able to solve the Schrödinger equation thus obtained, in C_1 and D , the solution ψ_1 is a reliable approximation to the home-based function.

a. Definition of a one-dimensional path along the duct

The topological structure shown schematically in Fig. 7(a) allows us to distinguish the direction along the duct from the directions perpendicular to it.

For this purpose we define new coordinates in configuration space: Let $L(t)$ be a one-dimensional path joining the centers of the two cavities through the midst of the duct D . The parameter t is the distance along the path.

$L(t)$ is given by its trajectory $\mathbf{x}(t) = (x_1(t), x_2(t), \dots, x_{3N}(t))$. We define a new local system of coordinates, including the variable t and $3N - 1$ variables $u_j(t, x_1, \dots, x_{3N})$ orthogonal to t and to each other.

b. Behavior of the wave function in the duct, along the path $L(t)$

Let us consider a path $L(t)$ such that the Schrödinger equation can be separated in the following way:

$$-\frac{\hbar^2}{2m} \frac{\partial^2}{\partial t^2} \psi - \frac{\hbar^2}{2m} \nabla_1^2 \psi + U\psi = E_0 \psi, \quad (4.6)$$

where ∇_1^2 designates the Laplacian operator in the $(3N - 1)$ -dimensional subspace orthogonal to t . This separation is obvious if $L(t)$ is a straight line. It is also true if $L(t)$ is a gradient line of ψ , as shown in Delrieu, Roger, and Hetherington (1980a).

We can define an effective potential V inside the duct D

$$V = -\frac{\hbar^2}{2m} \frac{\nabla_1^2 \psi}{\psi} + U, \quad (4.7)$$

and we can write Eq. (4.6) in the one-dimensional form

$$-\frac{\hbar^2}{2m} \frac{\partial^2}{\partial t^2} \psi + V\psi = E_0\psi. \quad (4.8)$$

V depends mainly on the variable t , and at fixed t is of the order of the localization energy of the system inside the duct. The first term of Eq. (4.7) measures the local curvature of ψ in the subspace orthogonal to t ; it is roughly fixed by the hard-core limiting conditions ($\psi=0$ if two hard cores touch each other). The duct being narrow, V is much larger than E_0 . For this reason, Eq. (4.8) has a simple WKB solution along the line $L(t)$:

$$\psi(t) = C \exp \left[- \int_0^t \left(\frac{2m}{\hbar^2} (V - E) \right)^{1/2} dt \right].$$

In the center of the duct V is roughly constant, that section of duct being by symmetry nearly constant. Thus the decrease of ψ is roughly exponential. A good approximation of ψ must satisfy this condition. The wave functions used in exchange calculations made heretofore do not (McMahan, 1972a, 1972b; McMahan and Wilkins, 1975).

c. Inadequacy of variational wave functions

The essential correlations between hard cores can be described by Jastrow wave functions (Hansen, Levesque, and Schiff, 1971),

$$\prod_{i < j} f(\mathbf{r}_i - \mathbf{r}_j).$$

$f(\mathbf{r}_i - \mathbf{r}_j)$ is a continuous function, depending only on the distance $|\mathbf{r}_i - \mathbf{r}_j|$ between particles, constant at large distance and null if two hard cores overlap:

$$f(\mathbf{r}_i - \mathbf{r}_j) = 0 \text{ if } |\mathbf{r}_i - \mathbf{r}_j| < \sigma. \quad (4.9)$$

The Jastrow function is sometimes used by itself to approximate the ground state of the quantum liquid. It does not directly introduce long-range order, while it does prevent overlapping of hard cores. The advantage of specifying this function over specifying the two-body correlation function is that there are no difficult constraints on the functions. There is, however, the difficulty that exact matrix elements cannot be calculated because integrals over it do not separate and remain $3N$ -dimensional. Feenberg (1969) develops the theory of these functions, which he calls BDJ functions (for Bijl-Dingle-Jastrow).

If the width of the duct is roughly constant near the median surface Σ , the Jastrow function, which depends only on the distance between the particles, is roughly constant (see Fig. 7). In contrast, the exact wave function ψ has a faster exponential decrease. Thus use of the Jastrow function alone would overestimate the exchange frequencies.

The same reasoning explains the fact that in calculations performed on liquid or solid He, using only Jastrow wave functions, the liquid-solid transition is found at much too large a density compared to the experimental result.

A more localized description of the helium atoms can be given by

$$\Phi_G = \prod_{i < j} f(\mathbf{r}_i - \mathbf{r}_j) \prod_i e^{-A(\mathbf{r}_i - \mathbf{R}_i)^2}, \quad (4.10)$$

which is a product of a Jastrow function with independent Gaussian functions, localizing the atoms on their sites, or it can be given by a more complex function:

$$\Phi_{\text{ph}} = \prod_{i < j} f(\mathbf{r}_i - \mathbf{r}_j) \cdot \phi_{\text{ph}}, \quad (4.11)$$

which is a product of a Jastrow function and a phonon wave function.

Variational calculations using Φ_G or Φ_{ph} give a correct value of the ground-state energy E_0 (compared to the exact results obtained by Hansen, Levesque, and Schiff, 1971, using Monte Carlo methods). This indicates that these functions describe correctly the true wave function ψ in the regions where $|\psi|$ is large (i.e., in the cavities). However, exchange being $\sim 10^4$ times smaller than the Debye frequency, the minimization in those calculations is practically independent of the value of ψ inside the duct.

These Gaussian-type functions Φ_G or Φ_{ph} fall off much too rapidly (like e^{-at^2}) along $L(t)$ inside the duct, the decrease of the correct wave function being rather exponential. For this reason they underestimate the exchange frequencies. For four-spin exchange, the exchange duct is longer than for pair exchange, and the Gaussians fall off drastically in the middle of the duct, so that these approximations strongly underestimate four-spin exchange with respect to pair exchange. We believe that is why McMahan and Wilkins (1975) find negligible values for four-spin exchange. It is for this reason that we believe those results are unreliable.

C. Improvement of the wave function in the duct

1. The correction factor $f(t)$

As emphasized in Sec. IV.B, the function Φ_G describes correctly the wave function ψ in the cavities and needs essentially to be corrected along $L(t)$ inside the duct.

We discuss here the possibility of improving the function Φ_G by multiplying it by a one-variable function $f(t)$ and taking the trial wave function

$$\psi(\mathbf{r}) = \phi_G(\mathbf{r}) f(t(\mathbf{r})), \quad (4.12)$$

where for every point P of coordinates \mathbf{r} , $t(\mathbf{r})$ corresponds to the orthogonal projection of P on the trajectory $L(t)$ (i.e., the closest point).

The form of ψ so chosen supposes that Φ_G describes sufficiently well the variations of the wave functions with respect to the variable orthogonal to t , and must only be corrected along $L(t)$.

Two methods have been used to optimize the function f .

- (i) In Sec. IV.C.2 we develop a variational method: $f(t)$

is determined by requiring that $\psi(\mathbf{r})$ satisfy the Schrödinger equation as well as possible for each point of the duct (Delrieu and Roger, 1978).

(ii) A simpler method is outlined in Sec. IV.C.4. If $L(t)$ is a gradient line of the exact wave function ψ [i.e., in each point of $L(t)$ the tangent to $L(t)$ is parallel to the gradient of ψ], ψ satisfies a one-dimensional Schrödinger equation along $L(t)$. For this method an approximate one-dimensional Schrödinger equation is solved on $L(t)$. (See Delrieu, Roger, and Hetherington, 1980a.)

The second approximation may be less satisfying than the variational method, which requires that the Schrödinger equation be approximately verified not only on a one-dimensional path $L(t)$ but for each part of the duct. However, it is much simpler and gives the essential results for calculating exchange. The physics of the exchange process appears more clearly with the second method. It also allows us to consider simple optimizations of the path $L(t)$ (i.e., to determine the structure of the displacement of the surrounding atoms).

2. Principle of the variational method

The solutions of the Schrödinger equation (in this paragraph we take $\hbar^2/2m = 1$ to simplify the formulas),

$$-\nabla^2\psi + U\psi = E\psi,$$

make the quantity

$$I = \langle |\nabla\psi|^2 \rangle - \langle (E - U)|\psi|^2 \rangle$$

stationary.

Here $\langle \rangle$ designates the integration over the $3N$ -dimensional space. The function $f(t)$ is determined variationally by minimizing I .

If $\delta\psi = \phi\delta f$ represents a variation of ψ , the variational principle gives

$$\delta I = \delta f \{ \langle \phi \nabla^2(\phi f) \rangle_1 + \langle (E - U)\phi^2 f \rangle_1 \} = 0, \quad (4.13)$$

where $\langle \rangle_1$ represents the integration over the $(3N - 1)$ variables u_j , orthogonal to t .

The calculation can be carried out for any trajectory $L(t)$, but is very intricate for a general curved path. It becomes much simpler if we take $L(t)$ as the straight line joining the centers of the cavities. [This approximation is valid if the radius of $L(t)$ is very large compared to the width of the duct.] In this case the condition (4.13) leads, after some algebra (see the details in Appendix A), to the following one-dimensional Schrödinger equation:

$$-\frac{\partial^2}{\partial t^2}\tilde{f}(t) + V(t)\tilde{f}(t) = E\tilde{f}(t), \quad (4.14a)$$

with

$$V(t) = \frac{\langle U\phi^2 \rangle_1}{\langle \phi^2 \rangle_1} - \frac{1}{2} \frac{\langle \phi^2 \nabla^2 \ln \phi \rangle_1}{\langle \phi^2 \rangle_1} + \frac{1}{4} \frac{\partial^2}{\partial t^2} \ln \langle \phi^2 \rangle_1, \quad (4.14b)$$

where $\tilde{f}(t) = f(t)\langle \phi^2 \rangle_1^{1/2}$. The exchange parameter J is $\frac{1}{2}(E_S - E_A)$, where E_S and E_A can now be interpreted as

the energy of the lowest two states of the Schrödinger equation (4.14).

For each value of t , $\tilde{f}(t)$ gives the mean-square value of ψ in the subspace orthogonal to t , t being fixed. Physically the effective potential $\tilde{V}(t)$ can be interpreted as the localization energy of the system inside the duct for a given value of t . Thus exchange appears as the tunneling of the system through an effective potential barrier, which for ^3He is essentially the kinetic energy of the particles [second term in Eq. (4.14b)]. In the lattice positions, the particles are away from the minimum of the potential energy U ; during exchange U actually decreases as the hard cores come close together, but the kinetic energy term $\phi^2 \nabla^2 \ln \phi$ increases.

3. Calculation of two- and four-spin exchange in bcc solid ^3He

a. Choice of the path $L(t)$

Consider the straight line joining the center C_1 of Ω_E of coordinates $(\mathbf{R}_1, \mathbf{R}_2, \dots, \mathbf{R}_N)$ to the center C_2 of Ω_P of coordinates $(\mathbf{R}_{v_1}, \mathbf{R}_{v_2}, \dots, \mathbf{R}_{v_i})$, with $v_i = P(i)$.

The projection t of a point \mathbf{r} in configuration space onto C_1C_2 is defined by the simple relation

$$t(\mathbf{r}) = \sum_i \frac{\mathbf{r}_i \cdot (\mathbf{R}_i - \mathbf{R}_{v_i})}{\|C_1C_2\|} + C$$

with

$$\|C_1C_2\| = \left[\sum_i |\mathbf{R}_i - \mathbf{R}_{v_i}|^2 \right]^{1/2}.$$

The arbitrary constant C can be chosen such that $t = 0$ at the center of one cavity. Figure 8 illustrates this projection t in the case of two- and four-particle exchange.

The choice of this path means that we consider only the movement of the exchanging particles, the mean positions of the surrounding particles being unchanged. This approximation is correct for four-atom exchange because this exchange can occur easily without a large displacement of the surrounding atoms (see Fig. 5) and the straight line C_1C_2 follows approximately the middle of the duct. The choice of a straight line is not valid for two-particle exchange, which requires a large displacement of the surrounding atoms in order to prevent hard-core overlap. In this case the straight line C_1C_2 is outside the duct. A better choice for $L(t)$ would be the straight line joining the center of the cavity to the middle of the duct. This choice is better physically because it takes into account the increase of the length t_Σ of the exchange path due to hard-core repulsion [cf. Fig. 9(a)]. The numerical value of the effective potential barrier does not change appreciably between this choice and the first one (V is essentially fixed by the "free space" δ between hard cores during exchange).

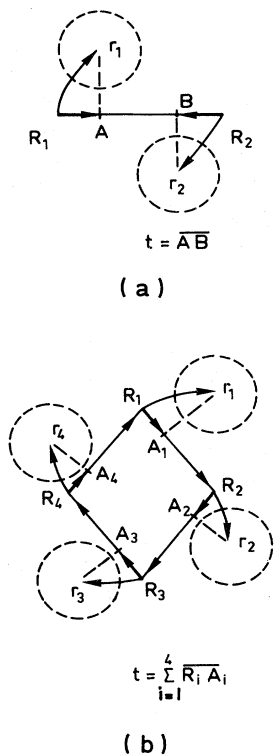


FIG. 8. Definition of the exchange variable t , $\mathcal{L}(t)$ being chosen as the straight line joining the centers C_1, C_2 of the two cavities (a) for two-particle exchange, (b) for four-particle exchange.

b. Calculation of the effective potential $\tilde{V}(t)$

The potential $\tilde{V}(t)$ is given by Eq. (4.14b). The integration $\langle \rangle_{\perp}$ was performed by Monte Carlo–Metropolis techniques (Hammersley and Handscomb, 1964) on 16 particles surrounding the exchanging atoms with periodic boundary conditions. To simplify $U(r)$ the hard-sphere model was chosen: $U = \infty$ if for any pair $|r_i - r_j| < \sigma$ ($\sigma = 2.14A$).

For two-spin exchange, the value of \tilde{V} is sensitive to the variational parameter A of the Gaussian wave function Φ_G . The parameter A is chosen to minimize the ground-state energy E_0 with $\psi = \Phi_G$. It is not determined with good accuracy; from Hansen, Levesque, and Schiff (1971) we take $4 < A < 5$.

Figure 9 shows $V(t)$ for two-particle exchange, with $A = 4$, $A = 5$.

The potential corresponding to four-particle exchange is less sensitive to A because the displacement of the surrounding particles is less important.

c. Calculation of the exchange constant

The exchange frequency is determined by the one-dimensional Schrödinger equation (4.14a) with effective potential $\tilde{V}(t)$ [Eq. (4.14b)]. Although this equation can

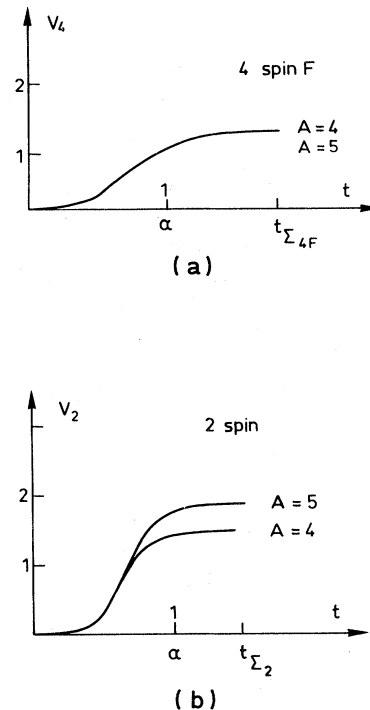


FIG. 9. Effective potential $V(t)$ of the one-dimensional Schrödinger equation (4.10) obtained in the variational method by Monte Carlo integration: (a) four-particle exchange, (b) two-particle exchange; for two-particle exchange this potential is function of the value of the parameter $A \sim 4$ or 5 of the Gaussian trial wave function ϕ_G [Eq. (4.8)].

be solved numerically, we find it more convenient to approximate $V(t)$ by its first Fourier component:

$$V(t) = \frac{\delta V}{2} \sin \frac{\pi t}{2 t_{\Sigma}}$$

In this case, the solutions of the Schrödinger equation are Mathieu functions, and the exchange frequency is given by (Erdelyi *et al.*, 1953)

$$2J_P = \left[\frac{\pi}{2L} \right]^2 (b_1 - a_0) = 8 \left[\frac{\pi}{L} \right]^2 \left[\frac{2}{\pi} \right]^{1/2} q^{3/4} e^{-4\sqrt{q}},$$

with $q = (L^2/\pi^2)\delta V$, L representing the length of the path $L(t)$ from the center C_1 of one cavity to the exchange surface Σ , and δV being the difference of potential between these extreme positions. Thus

$$J_P = -4 \left[\frac{2}{L} \right]^{1/2} (\delta V)^{3/4} \exp \left[-\frac{4L}{\pi} \sqrt{\delta V} \right]. \quad (4.15)$$

(It should be noted that $(4/\pi)\sqrt{\delta V} \cdot L$ corresponds to the term $\int [V(t) - E_0]^{1/2} dt$ given by the WKB approximation to Eq. (4.14b).)

(i) Two-spin exchange. The length of the path joining the center C_1 of Ω_E to the middle of the duct is $L = 1.49\sigma$; with $A = 4$ we obtain $\delta V \simeq 96/\sigma^2$ and $J_{\text{NN}} = -1.2 \times 10^{-6}/\sigma^2 = -2.1 \times 10^{-3}$ mK; with $A = 5$

we have $\delta V = 118.4/\sigma^2$ and $J_{\text{NN}} = -1.8 \times 10^{-6}/\sigma^2 = -3.1 \times 10^{-3}$ mK.

(ii) Folded four-spin exchange K_F . The length of the path is twice the distance between nearest neighbors. The potential δV does not depend on A ; $\delta V \simeq 65.2/\delta^2$. We obtain $K_F = -1.8 \times 10^{-6}/\sigma^2 = -3.1 \times 10^{-3}$ mK.

This result indicates that four-spin exchange is of the same order of magnitude as two-spin exchange, but the calculation is too rough to determine whether folded (F) or planar (P) four-spin exchange is larger. (See next section.) We chose to study K_F because at the time this calculation was performed there was no experimental evidence for predominant planar exchange K_P . The results are not satisfying because they are about 3 orders of magnitude too small. In Sec. IV.C.5 we discuss a variant of this approach which should lead to more realistic values of the exchange, as it has for hcp ^3He .

4. Analysis of the one-dimensional Schrödinger equation in $L(t)$

For the exact function ψ , we define a gradient as a path $L_g(t)$ such that at each point the tangent to $L(t)$ is parallel to the gradient of ψ :

$$\frac{\partial \psi_i}{\partial x_i} = \lambda(t) \frac{\partial x_i(t)}{\partial t}.$$

(In particular, the ridge fall line of ψ is a gradient line.) It can be shown easily (Delrieu, Roger, and Hetherington, 1980a) that if $L_g(t)$ is a gradient line, the exact wave function ψ obeys along $L_g(t)$ the one-dimensional Schrödinger equation

$$-\frac{\hbar^2}{2m} \frac{\partial^2}{\partial t^2} \psi(t) + V(t)\psi(t) = E\psi(t) \quad (4.16a)$$

with effective potential

$$V(t) = U - \frac{\hbar^2}{2m} \nabla_1^2 \ln \psi, \quad (4.16b)$$

where ∇_1 is the gradient in the configuration space orthogonal to the tangent to the line $L(t)$. $V(t)$ is essentially the energy of the system in the exchange configuration for a given value of t .

Equation (4.16b) is exact if we know the exact wave function ψ . However, if we have some approximation ϕ of ψ , we can obtain a simple estimate V^e of V by replacing ψ by ϕ in Eq. (4.16b):

$$V^e(t) = U - \frac{\hbar^2}{2m} \nabla_1^2 \ln \phi.$$

We can then solve (numerically) the one-dimensional Schrödinger equation (4.16a) with potential $V^e(t)$. If the solution $\psi^e(t)$ thus obtained is close to the function ϕ along $L(t)$, ϕ is certainly a good approximation to the exact wave function. If $\psi^e(t)$ is very different from ϕ , ϕ cannot give a reliable approximation to the exchange frequency, but we can take ψ^e instead of ϕ .

This method gives a very simple way (i) to test the validity of a given variational wave function ϕ (up to now

no published calculations of exchange, based on variational wave function ϕ , have given estimates of their accuracy); (ii) to improve a given trial function ϕ .

Application of this method to the variational wave functions [Eqs. (4.10) and (4.11)] shows that V^e is close to the variational potential \bar{V} calculated in Sec. IV.C.3, but that ψ^e deviates strongly from ϕ_G , the Gaussian-type function ϕ_G having too rapid a decrease in the duct.

5. Optimization of the path $L(t)$

In the WKB approximation, the exchange frequency corresponding to the one-dimensional Schrödinger equation (4.16) is

$$J_P \sim \exp \left[- \int_0^{t_\Sigma} \left[\frac{2m}{\hbar^2} [V(t) - E] \right]^{1/2} dt \right]$$

(t_Σ is the value of t on the exchange surface Σ). The optimum path $L(t)$ is that which gives the maximum value for J_P . It thus minimizes the integral

$$I = \int_0^{t_\Sigma} \{ m [V(t) - E] \}^{1/2} dt.$$

This integral is similar to the "action" S defined for a classical system,

$$S = \int_{L'} [m(E' - U)]^{1/2} d\tau.$$

As pointed out by Gervais and Sakita (1977), the path which minimizes I satisfies the equations

$$m \cdot \frac{d^2 \mathbf{r}}{dt^2} = \frac{\partial V}{\partial \mathbf{r}},$$

$$\frac{1}{2} m \cdot \left[\frac{d\mathbf{r}}{dt} \right]^2 = -E + V(t),$$

which are equations of classical mechanics if t is imaginary time.

Hence if the effective potential (4.16b) is known (i.e., if the exact wave function is known), the optimum path is the classical trajectory with potential $-V(r)$ and energy $-E$ passing through two given points in configuration space: the centers of the two cavities. [This path is analogous to the "most probable escape path" (MPEP) defined in Banks, Bender, and Wu (1973)].

In practice, this path is very difficult to determine because, first, we do not know the exact wave function ψ giving the effective potential $V(t)$ [we can, however, replace ψ in Eq. (4.16b) by an approximation ϕ ; see Sec. IV.C.4], and, second, the problem of finding the classical trajectory in a many-dimensional space is a huge task!

Let us now proceed to crude approximations: As seen in Sec. IV.C.3, it is reasonable to approximate the potential $V(t)$ by its first Fourier component. In this case,

$$I \sim \sqrt{V_0} L,$$

where V_0 represents the maximum value of the potential, and $L = t_\Sigma$, the length of the path $L(t)$.

We can now discuss the physical meaning of two limits

of the path we consider in this paper.

(i) The straight line we choose in Sec. IV.C.3 minimizes the length L of the path without attention to V_0 . It corresponds to the physical limit where the neighboring particles do not move. We expect this approximation to be better at lower densities.

(ii) An opposite limit can be obtained by minimizing V for each value of t , without taking L into account. In this "adiabatic" limit, for each value of t the surrounding medium deforms elastically in order to make V minimum. This approximation has been used for hcp ^3He at high densities by Delrieu and Sullivan (1981); it leads to an elastic deformation in $1/R^3$ at large distances.

In fact the optimum path is generally between these two limits. It minimizes the product $\sqrt{V_0} \cdot L$ and not L or V_0 separately, as was done in (i) and (ii), respectively. Roger has shown (1980) that it corresponds to an exponential falloff of the atomic displacements at large distances.

6. More straightforward approximations for the potential V

A very simple method of estimating δV proposed by London (1954) gives the same result as the variational method described above.

The particles are considered to be independent. The kinetic energy of one particle is taken as that of a point mass in a spherical potential of radius δ_i . The radius δ_i corresponds to the largest sphere allowed by the hard cores when the neighbors are fixed in their equilibrium position:

$$E = \sum_i \left(\frac{\pi}{\delta_i} \right)^2.$$

The difference of potential $\delta\tilde{V}$ between the equilibrium position (center of the cavity: $t=0$) and the exchange configurations (exchange surface Σ : $t=t_\Sigma$) is

$$\delta\tilde{V} = \pi^2 \sum_i \left(\frac{1}{\delta_i^2(t_\Sigma)} - \frac{1}{\delta_i^2(0)} \right). \quad (4.17)$$

We assume equal spacing between the exchanging particles in the exchange configuration Σ . For four-spin exchange, the available space δ is restricted in only two dimensions for each particle (i.e., the neighborhood has a roughly cylindrical shape). For this reason

$$\delta\tilde{V} \simeq \frac{2}{3} \pi^2 \sum_i \left(\frac{1}{\delta_i^2(t_\Sigma)} - \frac{1}{\delta_i^2(0)} \right),$$

where δ_i is the spacing between particles in the plane perpendicular to this cylindrical box. With this approximation we obtain

$$\delta\tilde{V} = 69/\sigma^2.$$

(The variational method gives $\delta\tilde{V} = 65/\sigma^2$.) This method has been used by Delrieu, Roger, and Hetherington (1980a, 1980b) to compare the rates of two-, three-, and four-atom exchange in triangular lattices.

7. Estimation of δV from experimental elastic compressibility of ^3He

The absolute values of the exchange constant given by the variational method for bcc ^3He or by the London method (Delrieu, Roger, and Hetherington, 1980a, 1980b) in triangular or hcp lattices are several orders of magnitude lower than the experimental results. For example, in bcc ^3He we found (Sec. IV.C.3)

$$K_F \simeq -3 \times 10^{-3} \text{ mK}.$$

These methods overestimate the potential barrier for two reasons:

(a) They neglect the attractive part of the Lennard-Jones potential. This part can play an important role in the evaluation of the effective potential barrier δV . As pointed out before, due to the large kinetic energy of the atoms, the equilibrium distance ($R_0 = 3.65 \text{ \AA}$ for bcc ^3He at melting) between the atoms is larger than the distance $R_m = 2.9 \text{ \AA}$, corresponding to the minimum of the Lennard-Jones potential. During exchange, the distance between the moving particles is reduced. For example, in bcc ^3He , in the critical exchange configuration the distances between exchanging particles and their nearest neighbors is reduced to 3.1 \AA for planar four-spin exchange and 2.85 \AA for two-body exchange, as shown by the arrows on Fig. 4 (we assume the neighboring particles to be fixed). These distances are near the minimum of the Lennard-Jones potential, hence the potential energy decrease of about 5 K per pair of atoms. Rough estimation leads to a net decrease of the effective potential barrier of about 10–15%, due to this effect.

(b) We take limit (i) of Sec. V.C.5. The opposite limit (ii) is certainly more realistic, in particular at high densities; hence Delrieu and Sullivan (1981) applied it for hcp ^3He . They take the effective potential barrier δV as the elastic compression energy due to the local increase in volume $\Delta v = v - v_0$ required for exchanging the particles. They estimate the exchange length

$$L = [\sum_i (\delta x_i)^2]^{1/2}$$

by finding the approximate displacements of all atoms in the exchange configuration, including those in the surrounding medium. The geometry of the three-particle exchange in the hcp solid is shown in Fig. 10.

The results, in terms of the molar volume are shown in Fig. 11 and compared with the experimental values given by Guyer, Richardson, and Zane (1971). The agreement is satisfactory.

D. Conclusions about the exchange mechanism

The calculation of exchange from first principles is a huge problem. A lot of work remains to be done to improve the rough approximations used in the calculations which have been presented here.

Through the approach presented, exchange in a quantum crystal appears as tunneling through a barrier of essentially kinetic energy. The hierarchy among the dif-

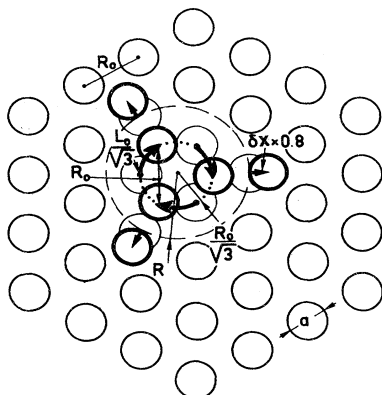


FIG. 10. Geometry of the exchange of ^3He atoms in the hcp solid. The atoms that move are shown in bold lines in their displaced position. Only six atoms are treated as moving, as far as a determination of the length of the exchange path is concerned. The three atoms involved in the cyclic motion are assumed to maintain their original distances from each other, while the distance to near neighbors is allowed to be slightly less (see text) (from Delrieu and Sullivan, 1981).

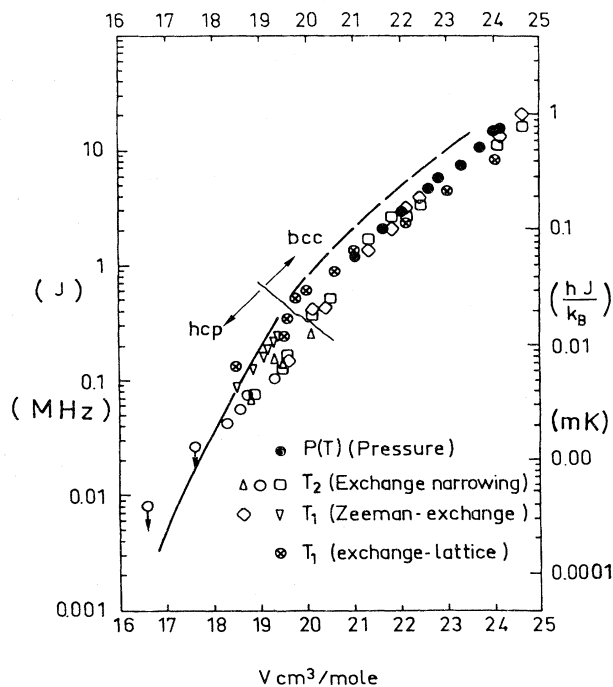


FIG. 11. Comparison of the calculated and measured exchange constant for hcp ^3He . The solid line is the calculation of Delrieu and Sullivan (1981), while the measured points are various NMR measurements (as compiled by Guyer, Richardson, and Zane, 1971). Also included for comparison is the result of the same calculation extended into the bcc regime, where it is not expected to be correct because of the differing geometry and expected four-spin exchange effects (from Delrieu and Sullivan, 1981).

ferent types of exchange is determined by two competitive effects:

(i) Exchange increases when the height V of the potential barrier decreases (V is roughly the kinetic energy of the atoms in the exchange configuration).

(ii) Exchange decreases when the length L of the path $L(t)$ leading from one equilibrium position to the exchanged position increases.

Multiple three- or four-spin exchanges have a longer path L than do pair exchanges, but a much smaller energy barrier V because the hard cores are farther away. For higher-order multiple exchanges of n atoms ($n > 4$), the kinetic energy barrier is not much lower than the barrier corresponding to three- or four-spin exchange, but the increasing L disfavors these exchanges. We expect that this competition between the effects of these two characteristic parameters favors one or two types of multiple exchange which, depending on the geometry of the lattice, could be three- and/or four-spin exchange. We do not expect multiple exchanges of a large number of atoms to be of the same order of magnitude because the exchange frequencies are exponential functions of these parameters. In a bcc lattice, four-spin exchange is probably preponderant. (Phenomenological analysis based on the experimental results leads us to consider also three-spin exchange, smaller than four-spin exchange but not negligible. See Secs. VII and VIII.) In a triangular geometry, three-spin exchange disturbs the surrounding atoms less than other types of exchanges and is probably preponderant. This result is particularly important because *even* permutations (e.g., three-spin exchange) favor ferromagnetism (see Thouless, 1965a, and Sec. V); thus the model predicts ferromagnetism in hcp ^3He . The ordering temperature estimated from nuclear-magnetic-resonance experiments is about $50 \mu\text{K}$. The sign of the Curie-Weiss constant could be determined by susceptibility measurements at, say, 0.2 – 1 mK . Such temperatures are attainable by nuclear adiabatic demagnetization.

We also predict ferromagnetism for one (or two) layers of ^3He atoms adsorbed on surfaces. Ferromagnetism has been observed for ^3He adsorbed on graphite. Actually it is not clear whether this effect is related to the first solid layer, the second layer, or the liquid (Godfrin *et al.*, 1980). Three-spin exchange is negligible in the first layer, which is too dense. However, if the arrangement of atoms in the second layer is approximately triangular, three-spin exchange could provide a reasonable interpretation for the observed effect. Other models suggest that this ferromagnetism comes from the liquid (Beal-Monod and Mills, 1978). Further experiments are needed.

This approach can be applied to other quantum solids, for example to solid hydrogen (Delrieu and Sullivan, 1981). The frequency of cyclic three-molecule exchange is estimated to be in the range of 1 kHz , or 10^4 times larger than previous calculations in solid H_2 , which were based on Gaussian wave functions. This exchange frequency could explain the motional narrowing of the resonance line observed for HD impurities in hcp parahydrogen (Delrieu and Sullivan, 1981). The method can be ex-

tended to understanding tunneling effects in other many-body systems: bandwidth of vacancies in He, effects at the surface of solid He, and H in metals.

Our viewpoint also offers a qualitative explanation for a surprising theoretical result recently obtained. Theoretical calculations (Levesque, 1980) using Jastrow functions find that in *liquid* ^3He the polarized state is energetically more favorable than the unpolarized state. We put forward the following interpretation: As shown in Sec. IV.B, the Jastrow functions alone overestimate dramatically the exchange frequencies; Jastrow functions give, at very large density, an hcp solid so that the fluctuations in the hypothetical liquid described by this kind of variational function correspond to those of the hcp phase, i.e., to three-particle exchange as shown above. This may explain the corresponding ferromagnetism found by Levesque. However, in true liquid ^3He , the tunneling and exchange frequencies are much smaller, near solidification, and the fluctuations correspond to the bcc solid phase (not found with Jastrow alone), i.e., to four-atom ring exchange, which is antiferromagnetic. We might conjecture that the liquid would be ferromagnetic for the same reason near a graphite surface (i.e., because the atomic arrangement is triangular there).

V. EXCHANGE HAMILTONIAN IN TERMS OF SPIN OPERATORS

A. Introduction of the spin coordinates

In Sec. IV we showed that a two-cavity wave function for distinguishable particles would have two almost degenerate states of energy $\pm J$ (relative to their average energy). The two-cavity Hamiltonian equations can be written

$$E\psi(\mathbf{R}_1) = J\psi(\mathbf{R}_2),$$

$$E\psi(\mathbf{R}_2) = J\psi(\mathbf{R}_1),$$

where \mathbf{R}_1 and \mathbf{R}_2 are the $3N$ -dimensional coordinates of the centers of the two cavities² (i.e., $\mathbf{R}_1, \mathbf{R}_2$ correspond to all of the atoms being on lattice sites, the difference being the permutation of a few atoms.) Assuming, as we have, that the ducts are independent, we may write the effective many-cavity Hamiltonian as $E\psi(\mathbf{R}) = \sum_{\alpha} J_{\alpha} P_{\alpha}^{(R)} \psi(\mathbf{R})$,

²We have chosen here to express the effective exchange Hamiltonian in terms of $\psi(\mathbf{R}_i)$, which are the values of the many-dimensional wave function at the cavity centers. The $\psi(\mathbf{R}_i)$ might just as well be thought of as the expansion coefficients in an expansion for ψ in terms of home-based wave functions, because the wave function in the neighborhood of the cavity centers will always be proportional to the home-based wave function in that cavity. The reader should take care to distinguish between these concepts of localization in many dimensions and the idea of Wannier functions, which are single-particle functions. One could approximate the home-based wave function as a product of Wannier functions, but this has not proved useful.

where \mathbf{R} runs over all permutations of the atoms and where $P_{\alpha}^{(R)}$ is a coordinate permutation corresponding to the α th duct.

We may antisymmetrize by introducing fermion creation operators which place particles on the lattice sites, e.g., $A_{jm_j}^+$ creates a particle at site j with spin m_j . A basis set of antisymmetric functions can be introduced. These functions have spin projection m_j associated with each site j ,

$$|\{m\}\rangle \equiv |m_1 \cdots m_N\rangle \equiv A_{1m_1}^+ A_{2m_2}^+ \cdots A_{Nm_N}^+ |0\rangle.$$

Then the combined spin and the space wave function (valid if all particles are on lattice sites) is

$$|\psi\rangle = \sum_{m_1 \cdots m_N} \chi(m_1 \cdots m_N) A_{1m_1}^+ \cdots A_{Nm_N}^+ |0\rangle. \quad (5.1)$$

$|\psi\rangle$ is guaranteed to be antisymmetric under exchange of spin and space together, because each of its components is antisymmetric:

$$P_{\alpha}^{(R)} P_{\alpha}^{(\sigma)} |\{m\}\rangle = (-1)^{P_{\alpha}} |\{m\}\rangle.$$

The Hamiltonian depends on spatial permutations only,

$$\begin{aligned} E|\Psi\rangle &= \sum_{\alpha} J_{\alpha} P_{\alpha}^{(R)} |\Psi\rangle \\ &= \sum_{\alpha} J_{\alpha} \sum_{\{m\}} \chi(\{m\}) P_{\alpha}^{(R)} |\{m\}\rangle. \end{aligned}$$

But by rearranging the antisymmetry condition,

$$P_{\alpha}^{(R)} |\{m\}\rangle = (-1)^{P_{\alpha}} (P_{\alpha}^{(\sigma)})^{-1} |\{m\}\rangle.$$

we can express the Hamiltonian in terms of spin permutation operators only,

$$E|\Psi\rangle = \sum_{\alpha} J_{\alpha} (-1)^{P_{\alpha}} \sum_{\{m\}} \chi(\{m\}) (P_{\alpha}^{(\sigma)})^{-1} |\{m\}\rangle.$$

Therefore,

$$E|\Psi\rangle = \sum_{\alpha} J_{\alpha} (-1)^{P_{\alpha}} \sum_{\{m\}} \chi(\{m\}) (P_{\alpha}^{(\sigma)})^{-1} |\{m\}\rangle,$$

where we have recognized that $(P_{\alpha}^{(\sigma)})^{-1} |\{m\}\rangle$ is simply $|m'_1 m'_2 \cdots m'_N\rangle$ where the m'_i are the permuted m_i . Since the $\{m'_i\}$ run over all 2^N states as the $\{m_i\}$ do, we may change the summation variable to $\{m'\}$:

$$E|\Psi\rangle = \sum_{\alpha} J_{\alpha} (-1)^{P_{\alpha}} \sum_{\{m'\}} \chi(P_{\alpha}^{(\sigma)} \{m'\}) |\{m'\}\rangle.$$

Projecting onto states $\langle \{m''\} |$, we have

$$E\chi(\{m''\}) = \sum_{\alpha} J_{\alpha} (-1)^{P_{\alpha}} \chi(P_{\alpha}^{(\sigma)} \{m''\}),$$

or more conventionally

$$E\chi = \sum_{\alpha} J_{\alpha} (-1)^{P_{\alpha}} [P_{\alpha}^{(\sigma)}]^{-1} \chi.$$

For some kinds of exchange (e.g., two-body exchange) $[P_{\alpha}^{(\sigma)}]^{-1} = P_{\alpha}^{(\sigma)}$; for others this is not true (e.g., three- or four-atom ring exchange). When $[P_{\alpha}^{(\sigma)}]^{-1}$ and $P_{\alpha}^{(\sigma)}$ are

not equal, the sum over α always includes both of them because both ducts must be considered and in fact must have equal exchange constant J_α . Therefore, we may drop the inverse to obtain finally

$$E\chi = \sum_{\alpha} J_{\alpha} (-1)^{P_{\alpha}} P_{\alpha}^{(\sigma)} \chi. \quad (5.2)$$

The totally antisymmetric wave function valid at cavity centers is obtained from Eq. (5.1). The quantity $\chi(m_1, m_2, \dots, m_N)$ represents the amplitude for the spin projection m_1 at site 1, m_2 at site 2, etc.

For the energy spectrum and statistical mechanics of this system, therefore, the pseudo-Hamiltonian (5.2) is all we need to consider, and there is a one-to-one correspondence between its eigenstates and those of the whole system.

Any spin permutation operator can be written in terms of the familiar two-particle exchange operators. The operators we shall need for solid ^3He are the three- and four-body cyclic permutations; they are developed in Sec. V.C.

B. Dominant exchanges expected in a bcc lattice

We restrict our attention to cyclic exchanges involving the most compact cycles of two, three, and four atoms. For two-atom transposition, we retain only nearest neighbors, and we call J_{NN} the corresponding frequency. The most compact cycles of three atoms in a bcc lattice have two first-neighbor and one second-neighbor link; let J_t be the corresponding exchange frequency. There are two kinds of four-spin cycles involving four first neighbors. One is planar, K_P , and such that one of the diagonals corresponds to second neighbors and the other to third neighbors; the other is folded, K_F , and both diagonals are second neighbors (see Fig. 12). Some authors (Zane, Krantz, and Sites, 1977) have taken the following notation:

$$J_{\text{NN}} = J_{11}, \quad J_t = J_{112}, \quad K_P = J_{1111,23} \quad \text{and} \quad K_F = J_{1111,22}.$$

Noticing that a cyclic permutation of an even (odd) number of particles is odd (even), the Hamiltonian is written

$$\begin{aligned} H_{\text{ex}} = & -J_{\text{NN}} \sum_{\langle i,j \rangle}^{(1)} P_{ij}^{\sigma} + J_t \sum_{\langle i,j,k \rangle}^{(T)} [P_{ijk}^{\sigma} + (P_{ij}^{\sigma})^{-1}] \\ & - K_P \sum_{\langle i,j,k,l \rangle}^{(P)} [P_{ijkl}^{\sigma} + (P_{ijkl}^{\sigma})^{-1}] \\ & - K_F \sum_{\langle i,j,k,l \rangle}^{(F)} [P_{ijkl}^{\sigma} + (P_{ijkl}^{\sigma})^{-1}]. \end{aligned} \quad (5.3)$$

$P_{ij}^{\sigma}, P_{ijk}^{\sigma}, P_{ijkl}^{\sigma}$ represent, respectively, the two-, three-, and four-spin cyclic permutation operators. The sums are taken over all distinct two-, three-, or four-spin cycles.

C. Cyclic permutation operators in terms of Pauli spin operators

For two-spin permutations we have the familiar expression

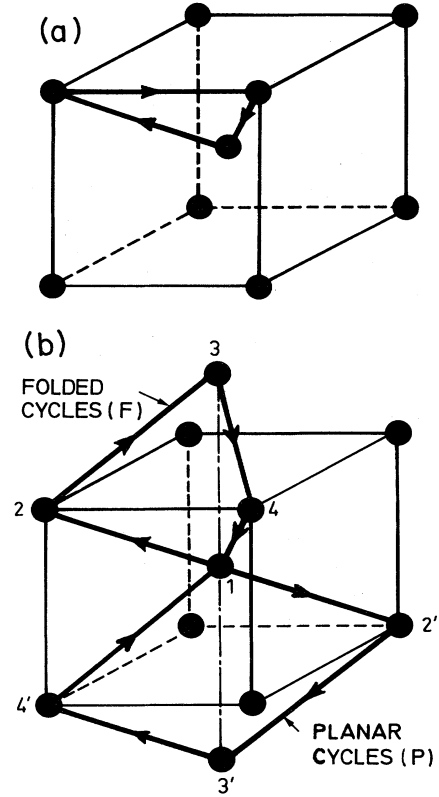


FIG. 12. Compact cycles in a bcc lattice. (a) The most compact three-particle cycle; one leg of the triangle is a second neighbor, and two legs are first neighbors. (b) Most compact four-particle cycles; there are two quadrilaterals with nearest-neighbor sides in the bcc lattice, one planar, the other folded.

$$P_{ij}^{\sigma} = (1 + \sigma_i \cdot \sigma_j) / 2. \quad (5.4)$$

A three-spin permutation operator can be written as the product of two transposition operators,

$$P_{ijk}^{\sigma} = P_{ij}^{\sigma} P_{ik}^{\sigma} = \frac{1}{4} (1 + \sigma_i \cdot \sigma_j) (1 + \sigma_i \cdot \sigma_k).$$

Expanding the right-hand side and using the identity

$$(\sigma_i \cdot \sigma_j)(\sigma_i \cdot \sigma_k) = \sigma_j \cdot \sigma_k + i \sigma_i \cdot (\sigma_j \times \sigma_k), \quad (5.5)$$

we obtain

$$\begin{aligned} P_{ijk}^{\sigma} = & \frac{1}{4} [1 + \sigma_i \cdot \sigma_j + \sigma_j \cdot \sigma_k \\ & + \sigma_k \cdot \sigma_i + i \sigma_i \cdot (\sigma_j \times \sigma_k)]. \end{aligned} \quad (5.6)$$

The imaginary terms cancel in the summation:

$$P_{ijk}^{\sigma} + (P_{ijk}^{\sigma})^{-1} = \frac{1}{2} (1 + \sigma_i \cdot \sigma_j + \sigma_j \cdot \sigma_k + \sigma_k \cdot \sigma_i).$$

A four-spin cyclic permutation operator can be written

$$P_{ijkl}^{\sigma} = P_{ijk}^{\sigma} P_{il}^{\sigma}.$$

Using relations (5.4)–(5.6) we find, after some algebra,

$$P_{ijkl}^{\sigma} + (P_{ijkl}^{\sigma})^{-1} = \frac{1}{4} \left[1 + \sum_{\mu < \nu} \sigma_{\mu} \cdot \sigma_{\nu} + G_{ijkl} \right], \quad (5.8)$$

where the sum $\sum_{\mu < \nu}$ is taken over the six distinct couples (μ, ν) among the four particles $\{ijkl\}$, and

$$G_{ijkl} = (\sigma_i \cdot \sigma_j)(\sigma_k \cdot \sigma_l) + (\sigma_i \cdot \sigma_l)(\sigma_j \cdot \sigma_k) - (\sigma_i \cdot \sigma_k)(\sigma_j \cdot \sigma_l). \quad (5.9)$$

In terms of Pauli spin operators, the Hamiltonian is

$$H_{\text{ex}} = -\frac{J_1}{2} \sum_{i < j}^{(1)} \sigma_i \cdot \sigma_j - \frac{J_2}{2} \sum_{i < j}^{(2)} \sigma_i \cdot \sigma_j - \frac{J_3}{2} \sum_{i < j < k < l}^{(3)} \sigma_i \cdot \sigma_j - \frac{K_P}{4} \sum_{i < j < k < l}^{(P)} G_{ijkl} - \frac{K_F}{4} \sum_{i < j < k < l}^{(F)} G_{ijkl}. \quad (5.10)$$

The sum $\sum_{i < j}^{(n)}$ is taken over all distinct n th neighbors; the sum $\sum_{i < j < k < l}^{(\lambda)}$ with $\lambda = P$ or $\lambda = F$ is taken over all distinct four-spin planar or folded cycles. The coefficients of the two-spin Heisenberg terms are

$$\begin{aligned} J_1 &= J_{\text{NN}} + 3(-2J_t + K_P + K_F), \\ J_2 &= 2(-2J_t + K_F) + K_P, \\ J_3 &= K_P/2. \end{aligned} \quad (5.11)$$

D. Kind of cycles and sign of the exchange

In Sec. IV [Eq. (4.2)] we mentioned that J is always negative. Therefore, J_{NN} , J_t , K_P , and K_F are always negative as we have defined them. It is clear from Eqs. (5.10) and (5.11) that two-body exchanges always lead to an ordinary Heisenberg Hamiltonian with antiferromagnetic exchange. Furthermore, three-body ring exchange leads to a Heisenberg Hamiltonian with ferromagnetic exchange. It can be shown that a system with only even exchanges (e.g., 3, 5, 7, etc. rings) will always yield a ferromagnetic ground state.

Suppose that only even permutations P_e are allowed. Then

$$P_e \Psi = +\Psi.$$

In the configuration space the regions which correspond to one another by a forbidden odd permutation are disconnected. We thus have a partition of the configura-

tion space into disconnected domains. We know from a general theorem about the Schrödinger equation (Courant and Hilbert, 1937) that the ground-state orbital wave function for N distinguishable particles in one of those domains has no nodes. Hence ψ'_0 is symmetric with respect to all allowed permutations

$$P_e^r \psi'_0 = +\psi'_0.$$

Thus we must take a symmetric (ferromagnetic) spin-wave function χ_0^σ such that $P_e \chi_0^\sigma = +\chi_0^\sigma$ and $\Psi = \Psi_0^\sigma \chi_0^\sigma$ to obtain

$$P_e \Psi = P_e^r \psi'_0 \cdot P_e^\sigma \chi_0^\sigma = +\Psi.$$

The ferromagnetic spin-wave function verifies $P_e^\sigma \chi_0^\sigma = +\chi_0^\sigma$ for any set of even permutations.

Thus, as shown by Thouless (1965a), *even* permutations favor *ferromagnetism* and *odd* permutations *anti-ferromagnetism*, and all constants J_α in Eq. (5.2) are negative.

VI. HIGH-TEMPERATURE SERIES EXPANSIONS

A. Description of method

In this section we take for the exchange Hamiltonian a form slightly more general than Eq. (5.10). We include the possibility of noncyclic four-spin permutations such as the rigid rotation of a four-spin cluster like $P_{ij} \cdot P_{kl} \rightarrow (\sigma_i \cdot \sigma_j)(\sigma_k \cdot \sigma_l)$, as shown in Fig. 13. The fourth-order terms in the Hamiltonian are written in a more general way:

$$K [(\sigma_i \cdot \sigma_j)(\sigma_k \cdot \sigma_l) + (\sigma_i \cdot \sigma_l)(\sigma_j \cdot \sigma_k) + \lambda(\sigma_i \cdot \sigma_k)(\sigma_j \cdot \sigma_l)].$$

This expression takes into account all four-spin permutations, cyclic or not (Roger, 1980; Utsumi and Izuyama, 1977). If only cyclic permutations occur, λ is reduced to -1 [see Eq. (5.9)].

The total Hamiltonian $H = H_{\text{ex}} + H_z$ is the sum of the exchange Hamiltonian

$$H_{\text{ex}} = -\sum_{n=1}^{n=3} \left[\frac{J_n}{2} \sum_{i < j}^{(n)} \sigma_i \cdot \sigma_j \right] - \sum_{\alpha=\{P,F\}} \sum_{i < j < k < l}^{(\alpha)} \frac{K_\alpha}{4} [(\sigma_i \cdot \sigma_j)(\sigma_k \cdot \sigma_l) + (\sigma_i \cdot \sigma_l)(\sigma_j \cdot \sigma_k) + \lambda_\alpha(\sigma_i \cdot \sigma_k)(\sigma_j \cdot \sigma_l)] \quad (6.1)$$

and of the Zeeman Hamiltonian

$$H_z = -\sum_j \gamma \frac{\hbar}{2} \mathbf{H} \cdot \sigma_j, \quad (6.2)$$

\mathbf{H} being the applied external field. Here P and F stand for planar and folded four-atom cycles.

Since H_z commutes with H_{ex} , the partition function $Z = \text{tr}\{e^{-\beta H}\}$ can be written

$$Z = \text{tr}\{e^{-\beta H_{\text{ex}}} e^{-\beta H_z}\}. \quad (6.3)$$

The identities $(\sigma_i^z)^{2n} = I$ and $(\sigma_i^z)^{2n+1} = \sigma^z$ imply

$$e^{-\beta H_z} = \prod_i [(\cosh y)I + (\sinh y)\sigma_i^z] \quad (6.4)$$

with $y = (\gamma \hbar / 2) \beta H$. We now expand the first factor

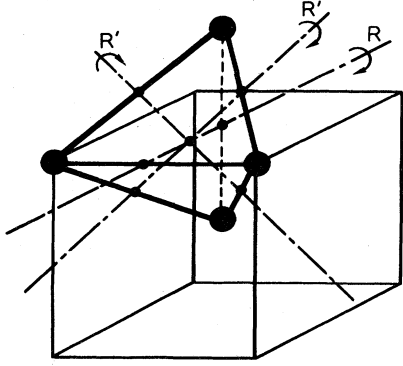


FIG. 13. Rigid rotations of the four-spin tetrahedrons.

$e^{-\beta H_{\text{ex}}}$ in powers of β , but keep the exact form (6.4) for the second term (the series expansion thus obtained is valid only for $T > \Theta \sim \langle H_{\text{ex}} \rangle$, but at any value of the magnetic field H):

$$Z = \text{tr} \left[\sum_{n=0}^{\infty} \frac{(-\beta)^n}{n!} (H_{\text{ex}})^n e^{-\beta H_z} \right]. \quad (6.5)$$

With the following notations:

$$Z_0 = \text{tr} e^{-\beta H_z} = (2 \cosh \beta)^N$$

and for any operator O_p ,

$$\langle O_p \rangle = \frac{\text{tr}(O_p e^{-\beta H_z})}{Z_0} = \text{tr} \left[O_p \prod_{i=1}^N \left(\frac{I + \tilde{p} \sigma_i^z}{2} \right) \right] \quad (6.6)$$

with $\tilde{p} = \tanh \beta$, we write

$$Z = Z_0 \sum_{n=0}^{\infty} \frac{(-\beta)^n}{n!} \langle H_{\text{ex}}^n \rangle.$$

The free energy is

$$F = -\beta^{-1} \ln Z = -\beta^{-1} \left[\ln Z_0 + \sum_{n=0}^{\infty} \frac{(-\beta)^n}{n!} K_n \right], \quad (6.7)$$

where K_n is the n th-order cumulant

$$K_n = \left[\frac{\partial^n}{\partial \lambda^n} \ln \langle e^{\lambda H_{\text{ex}}} \rangle \right]_{\lambda=0}. \quad (6.8)$$

$$\begin{aligned} \bar{e}_2(\tilde{p}) = & 4(1 - \tilde{p}^2) \left\{ (3 + 15\tilde{p}^2)J_1^2 + \frac{3}{4}(3 + 11\tilde{p}^2)J_2^2 + \frac{3}{2}(3 + 23\tilde{p}^2)J_3^2 + (24J_1J_2 + 48J_1J_3 + 36J_2J_3)\tilde{p}^2 \right. \\ & + 6\tilde{p}^2[4 + \lambda_F + 7(2 + \lambda_F)\tilde{p}^2]J_1K_F + 6\tilde{p}^2[4 + \lambda_P + 7(2 + \lambda_P)\tilde{p}^2]J_1K_P \\ & + 3\tilde{p}^2[2 + 3\lambda_F + 11(2 + \lambda_F)\tilde{p}^2]J_2K_F + \frac{3}{2}\tilde{p}^2[2 + 3\lambda_P + 23(2 + \lambda_P)\tilde{p}^2]J_2K_P \\ & + 72(2 + \lambda_F)\tilde{p}^4J_3K_F + \frac{3}{2}\tilde{p}^2[2 + 3\lambda_P + 47(2 + \lambda_P)\tilde{p}^2]J_3K_P \\ & + \frac{3}{8}[3(8 + 4\lambda_F + 3\lambda_F^2) + 3(8 + 4\lambda_F + 3\lambda_F^2)\tilde{p}^2 + (100 + 76\lambda_F + 23\lambda_F^2)\tilde{p}^4 + 71(2 + \lambda_F)^2\tilde{p}^6]K_F^2 \\ & + \frac{3}{8}[3(8 + 4\lambda_P + 3\lambda_P^2) - (8 + 4\lambda_P + 3\lambda_P^2)\tilde{p}^2 + 8(16 + 11\lambda_P + 3\lambda_P^2)\tilde{p}^4 + 72(2 + \lambda_P)^2\tilde{p}^6]K_P^2 \\ & \left. + \frac{3}{8}[8(8 + 2\lambda_F + 2\lambda_P + 3\lambda_F\lambda_P)\tilde{p}^2 + 8(28 + 10\lambda_F + 10\lambda_P + 5\lambda_F\lambda_P)\tilde{p}^4 + 144(2 + \lambda_F)(2 + \lambda_P)\tilde{p}^6]K_FK_P \right\}, \quad (6.13) \end{aligned}$$

The first terms are

$$\begin{aligned} K_1 &= \langle H_{\text{ex}} \rangle, \\ K_2 &= \langle H_{\text{ex}}^2 \rangle - \langle H_{\text{ex}} \rangle^2, \\ K_3 &= \langle H_{\text{ex}}^3 \rangle - 3\langle H_{\text{ex}}^2 \rangle \langle H_{\text{ex}} \rangle + 2\langle H_{\text{ex}} \rangle^3. \end{aligned} \quad (6.9)$$

Within the Ising and Heisenberg models, some diagrammatic methods have been developed to evaluate directly each cumulant K_i (Rushbrooke, Baker, and Wood, 1974). These methods can be generalized to the multiple exchange Hamiltonian. They are very efficient for calculating high-order terms on computers.

As we are, however, only interested here in calculating by hand the first few terms of the series (up to order three), it makes no difference if we apply those diagrammatic methods or if we evaluate each term of each cumulant in a straightforward way.

At order three, we restrict our attention to the zero-field term ($H=0$); in this case $\langle H_{\text{ex}} \rangle$ cancels and K_3 reduces to $\langle H_{\text{ex}}^3 \rangle$.

Thus we only need to calculate $\langle H^n \rangle$ for $n \leq 3$. The traces involved can be generally written

$$\text{tr}[(\sigma_i \sigma_j) \cdot (\sigma_k \sigma_l) \cdot \cdots (\sigma_\mu \sigma_\nu) \cdot \sigma_m^z \sigma_n^z \cdot \cdots \sigma_g^z].$$

Such traces can be evaluated and summed by a simple diagrammatic method.

Some details about this calculation are given in Appendix B.

B. Results

The results have been published in Roger and Delrieu (1977) and Roger, Delrieu, and Landesman (1977).

(a) The partition function is given by

$$N^{-1} \ln Z = \ln Z_0 - \bar{e}_1(\tilde{p})\beta + \bar{e}_2(\tilde{p})\frac{\beta^2}{8} - \bar{e}_3(\tilde{p})\frac{\beta^3}{24}, \quad (6.10)$$

where $\ln Z_0 = \ln 2 - \frac{1}{2}(1 - \tilde{p}^2)$,

$$\bar{e}_1(\tilde{p}) = -\Theta \frac{\tilde{p}^2}{2} - 3[(2 + \lambda_F)K_F + (2 + \lambda_P)K_P] \frac{\tilde{p}^4}{2}, \quad (6.11)$$

and where

$$\Theta = 4J_1 + 3J_2 + 6J_3 \quad (6.12)$$

is the Curie-Weiss constant.

$$\begin{aligned}
\tilde{e}_3(\tilde{p}) = & 12J_1^3 + 9J_2^3 - 54J_3^3 - 108J_1^2(J_2 + J_3) - 108J_2^2J_3 - 54J_1^2[(4 + \lambda_F)K_F + (4 + \lambda_P)K_P] \\
& - 27[J_2^2K_F(2 + 3\lambda_F) + J_2J_3K_P(2 + 3\lambda_P)] + 270(K_F^2 + K_P^2)J_1 \\
& - 27[2J_2K_F^2(1 - 2\lambda_F - \frac{3}{2}\lambda_F^2) + (J_2 + J_3)K_P^2(1 - 2\lambda_P - \frac{3}{2}\lambda_P^2)] \\
& - 54J_2K_FK_P(8 + 2\lambda_F + 2\lambda_P + 3\lambda_F\lambda_P) - 27J_3K_F^2(8 + 4\lambda_F + 3\lambda_F^2) - \frac{27}{2}K_F^3(4 + 3\lambda_F + 2\lambda_F^2 + \lambda_F^3) \\
& - \frac{27}{2}K_P^3(4 + 3\lambda_P + 2\lambda_P^2 + \lambda_P^3) + 27K_F^2K_P(2 - 4\lambda_F - 2\lambda_P + 2\lambda_F^2 + 4\lambda_F\lambda_P + 3\lambda_F^2\lambda_P) \\
& + \text{terms in } \tilde{p}^2, \tilde{p}^4, \dots, \tilde{p}^{12}.
\end{aligned} \tag{6.14}$$

(b) The specific heat in zero field is

$$C_V(H=0) = -T \left[\frac{\partial^2 F}{\partial T^2} \right] = \frac{R}{4} [\tilde{e}_2(0)\beta^2 - \tilde{e}_3(0)\beta^3].$$

(c) The inverse susceptibility is

$$\chi^{-1}(T) = \beta \left[\frac{\partial^2 \ln Z}{\partial H^2} \right]^{-1}.$$

From the p^2 terms in Eq. (6.13) we obtain the zero-field susceptibility

$$\chi_{H \rightarrow 0}^{-1}(T) = C_1^{-1} \left[T - \Theta + \frac{B}{T} + \dots \right],$$

with

$$\begin{aligned}
B = & 4J_1^2 + 3J_2^2 + 6J_3^2 - 6J_1[(4 + \lambda_F)K_F + (4 + \lambda_P)K_P] \\
& - \frac{3}{2}J_2[2(2 + 3\lambda_F)K_F + (2 + 3\lambda_P)K_P] \\
& - \frac{3}{2}J_3(2 + 3\lambda_P)K_P - 3(8 + 2\lambda_F + 2\lambda_P + 3\lambda_F\lambda_P)K_FK_P \\
& + \frac{3}{2}(8 + 4\lambda_P + 3\lambda_P^2)K_P^2.
\end{aligned}$$

As first shown in Roger and Delrieu (1977), large four-spin terms (K_P or K_F) can account for the increase of the susceptibility with respect to the Curie-Weiss law and for the unexpected sign of the T^{-3} term in the specific-heat expansion. This result is shown in Fig. 14 where we retain only cyclic exchanges ($\lambda_F = \lambda_P = -1$) and take the Hamiltonians (5.10) with four adjustable parameters J_1, J_2, K_F, K_P [$J_3 = \frac{1}{2}K_P$; see Eq. (5.11)].

The experimental values of $\tilde{e}_2(0)$ and Θ give two relations between these four parameters, reducing the number of independent variables to two.

Figure 14 represents a two-dimensional plot of $B^* = B/|\Theta|^2$ and $e_3^* = \tilde{e}_3/|\Theta|^3$ in terms of the reduced parameters $K_F^* = K_F/|\Theta|$ and $K_P^* = K_P/|\Theta|$ for a ratio $e_2^* = \tilde{e}_2/|\Theta|^2 = 0.95$. The experimental values (see Sec. II) give $0.62 < e_2^* < 1.17$.

J_1 and J_2 are obtained by solving the system

$$\begin{aligned}
\Theta = & 4J_1 + 3J_2 + 6J_3, \\
\tilde{e}_2 = & 12J_1^2 + 9J_2^2 + 18J_3^2 + 31.5(K_F^2 + K_P^2),
\end{aligned}$$

deduced from Eqs. (6.12) and (6.13).

Of the two solutions, we retain only that which has some physical meaning (the other giving $J_1 > 0$ or $|J_2| > |J_1|$). With $|K_F + K_P| \geq 0.07\Theta$, B is negative and \tilde{e}_3 positive, in agreement with the experimental results. The experimental values of $\tilde{e}_2, \tilde{e}_3, \Theta, B$, although they are not known with sufficient accuracy, put stringent con-

straints on the choice of parameters of the phenomenological Hamiltonian. A careful analysis of these constraints is given in Sec. XI.

VII. PHASE DIAGRAM WITHIN THE MOLECULAR-FIELD APPROXIMATION

A. Application of the molecular-field approximation to the four-spin exchange Hamiltonian

The molecular-field approximation (MFA) replaces the interaction of one atom i with the rest of the crystal by an effective mean field \mathbf{H}_i^m .

The mean-field theory for spin- $\frac{1}{2}$ particles can be derived from a variational principle. In that case one shows that the free energy is bounded by a free energy determined from a trial density matrix. Since the results are identical and the physical motivation somewhat clearer, we proceed to derive the mean-field equations for four-

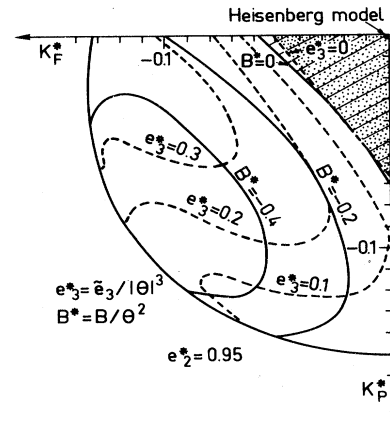


FIG. 14. Four-parameter model J_1, J_2, K_F, K_P . We retain only cyclic exchange ($\lambda_F = \lambda_P = -1$) and also take $J_3 = K_P/2$ [cf. Eq. (5.11)]. The experimental data give (see Sec. II) $0.6 \leq e_2^* = \tilde{e}_2/\Theta^2 \leq 1.2$. One relation among the parameters is obtained by fixing e_2^* . By defining the reduced parameters $J_1^* = J_1/|\Theta|$; $J_2^* = J_2/|\Theta|$; $K_F^* = K_F/|\Theta|$; $K_P^* = K_P/|\Theta|$, we have only two independent variables, K_F^* and K_P^* . This figure represents the variations of $B^* = B/|\Theta|^2$ and $e_3^* = \tilde{e}_3/|\Theta|^3$ in terms of K_F^* and K_P^* for $e_2^* = 0.95$. The hatched area corresponds to $B > 0$ and the dotted area to $\tilde{e}_3 < 0$. We note that outside these areas (i.e., roughly for $|K_F| + |K_P| \geq 0.07|\Theta|$) B is negative and \tilde{e}_3 positive, in agreement with the experimental results.

spin interaction from the effective-field viewpoint.

The mean value of the energy $E_0 = \langle \mathcal{H} \rangle$ is calculated by neglecting the fluctuations of the spins σ_i around their mean value $\langle \sigma_i \rangle$. Within this approximation,

$$\langle \sigma_i \cdot \sigma_j \rangle \sim \langle \sigma_i \rangle \cdot \langle \sigma_j \rangle \quad (7.1a)$$

and

$$\langle (\sigma_i \cdot \sigma_j)(\sigma_k \cdot \sigma_l) \rangle \sim (\langle \sigma_i \rangle \cdot \langle \sigma_j \rangle)(\langle \sigma_k \rangle \cdot \langle \sigma_l \rangle). \quad (7.1b)$$

The Hamiltonian (5.10), or one of similar type, may be separated into two parts, one which contains the quadratic terms E_2 [of type (7.1a)], and one which contains the quartic terms [of type (7.1b)]: $E_0 = E_2 + E_4$. We write

$$E_0 = \sum_i \left[\frac{1}{2} \frac{\partial E_2}{\partial \langle \sigma_i \rangle} + \frac{1}{4} \frac{\partial E_4}{\partial \langle \sigma_i \rangle} \right] \cdot \langle \sigma_i \rangle.$$

Defining the mean field \mathbf{H}_i^m as

$$\mathbf{H}_i^m = - \left[\frac{2}{\gamma \hbar} \right] \left[\frac{1}{2} \frac{\partial E_2}{\partial \langle \sigma_i \rangle} + \frac{1}{4} \frac{\partial E_4}{\partial \langle \sigma_i \rangle} \right], \quad (7.2)$$

we have

$$E_0 = - \frac{\gamma \hbar}{2} \sum_i \mathbf{H}_i^m \cdot \langle \sigma_i \rangle. \quad (7.3)$$

With an external magnetic field \mathbf{H} , we obtain more generally

$$E(H) = - \frac{\gamma \hbar}{2} \sum_i \mathbf{H}_i^{\text{eff}} \cdot \langle \sigma_i \rangle, \quad (7.4)$$

where the effective field $\mathbf{H}_i^{\text{eff}} = \mathbf{H}_i^m + \mathbf{H}$ is the sum of the mean field \mathbf{H}_i^m and the external field \mathbf{H} .

For spin $\frac{1}{2}$, the entropy can be written

$$S = k_B \left\{ N \ln 2 - \frac{1}{2} \sum_i [(1+p_i) \ln(1+p_i) + (1-p_i) \ln(1-p_i)] \right\}. \quad (7.5)$$

$p_i = |\langle \sigma_i \rangle|$ is the sublattice polarization.

The minimization of the free energy $F = E - TS$ with respect to p_i leads to the following equation:

$$\langle \sigma_i \rangle = \frac{1}{2} \tanh \left[\beta \frac{\gamma \hbar}{2} \mathbf{H}_i^{\text{eff}} \right]. \quad (7.6)$$

In all that follows we omit the symbol $\langle \rangle$ and write σ_i for $\langle \sigma_i \rangle$.

B. Minimization of the free energy—general methods

Some systematic methods have been worked out to minimize the molecular-field free energy, using a quadratic Hamiltonian.

1. The method of Luttinger and Tisza

The method of Luttinger and Tisza (1946) is applicable to a system of classical spins \mathbf{S}_i of the same magnitude

$\mathbf{S}_i^2 = S^2$. Its principle is to replace the minimization condition of the free energy,

$$(A) \begin{cases} \frac{\partial F}{\partial \mathbf{S}_i} = 0 \\ \mathbf{S}_i^2 = S^2, \end{cases}$$

by the "weak condition"

$$(B) \begin{cases} \frac{\partial F}{\partial \mathbf{S}_i} = 0 \\ \sum_i \mathbf{S}_i^2 = NS^2. \end{cases}$$

By introducing one Lagrange multiplier λ , the "weak condition" (B) leads to a system of N coupled equations:

$$\frac{\partial F}{\partial \mathbf{S}_i} - \lambda \mathbf{S}_i = 0 \quad \text{with} \quad \sum_i \mathbf{S}_i^2 = NS^2.$$

With a quadratic Hamiltonian, these equations are linear and can be solved easily by Fourier transforms. If the solution of (B) also satisfies (A) the problem is solved, otherwise the method fails.

Unfortunately, with a four-spin interaction Hamiltonian, these N equations are of the third order and cannot be solved algebraically.

2. The method of Villain

The method of Villain (1959) determines the ordered structures which can appear from the paramagnetic phase through a second-order transition. At a second-order transition, the order parameters can be supposed to be arbitrarily small, and the molecular-field equation (7.6) can be linearized. Thus we can apply this method, but phases which occur through a first-order transition may be missed.

If σ_i on each site is arbitrarily small, the third-order terms in \mathbf{H}_i^m coming from four-spin exchange are negligible with respect to the linear terms in σ_i . Thus \mathbf{H}_i^m can be written

$$\mathbf{H}_i^m = - \frac{2}{\gamma \hbar} \sum_j J_{ij} \sigma_j$$

[J_{ij} is the exchange frequency corresponding to the transposition (ij)].

In zero magnetic field, the linearization of Eq. (7.6) gives

$$\sigma_i = \frac{1}{2k_B T} \sum_j J_{ij} \sigma_j. \quad (7.7)$$

Defining the Fourier transform

$$\sigma(\mathbf{k}) = \sum_i \sigma_i e^{i\mathbf{k} \cdot \mathbf{R}_i},$$

we reduce the system of N coupled equations (7.7) to

$$\sigma(\mathbf{k}) = \frac{\mathcal{F}(\mathbf{k})}{2k_B T} \cdot \sigma(\mathbf{k})$$

with

$$\mathcal{F}(\mathbf{k}) = \sum_j J_{ij} e^{i\mathbf{k}\cdot(\mathbf{R}_i - \mathbf{R}_j)}. \quad (7.8)$$

The molecular-field equation (7.6) has a nonzero solution only if the temperature is smaller than the critical value $T_c = \mathcal{F}(\mathbf{k})/(2k_B)$ given by Eq. (7.8).

The stable phase corresponds to the solution that gives the highest critical temperature. Thus we assume that the stable structure has only one Fourier component \mathbf{k}_0 , giving $\mathcal{F}(\mathbf{k}_0)$ maximum. This wave vector \mathbf{k}_0 verifies the equation

$$\frac{\partial \mathcal{F}(\mathbf{k}_0)}{\partial \mathbf{k}_0} = 0.$$

The structure is thus described by the plane-wave equations with one Fourier component,

$$\begin{aligned} \sigma_i &= \sigma_{\mathbf{k}_0} e^{i\mathbf{k}_0 \cdot \mathbf{R}_i} + \sigma_{\mathbf{k}_0}^* e^{-i\mathbf{k}_0 \cdot \mathbf{R}_i} \\ &= \text{Re}(\sigma_{\mathbf{k}_0} e^{i\mathbf{k}_0 \cdot \mathbf{R}_i}). \end{aligned} \quad (7.9)$$

Thus the nature of the phases which can appear from the paramagnetic phase through a second-order transition and their critical temperatures in zero magnetic field do not depend on the fourth-order term in the Hamiltonians (5.10). They depend only on the effective quadratic interactions J_1, J_2, J_3 , (5.11) between first, second, and third neighbors.

For the structures described by Eq. (7.9), all the spin vectors σ_i are parallel to the same plane:

$$\sigma_i \times \sigma_j = (\sigma_{\mathbf{k}} \times \sigma_{\mathbf{k}}^*) (e^{i\mathbf{k}\cdot(\mathbf{R}_i - \mathbf{R}_j)} - e^{-i\mathbf{k}\cdot(\mathbf{R}_i - \mathbf{R}_j)}).$$

The difference of exponentials is a pure imaginary number, thus $\mathbf{D} = i(\sigma_{\mathbf{k}} \times \sigma_{\mathbf{k}}^*)$ is a real vector, and the above relation proves that all the spin vectors are perpendicular to \mathbf{D} .

The condition $\sigma_i^2 = \text{const}$, true at zero temperature, is assumed to remain valid at finite temperature. This condition restricts the ensemble of structures to the two following types (Roger, 1980; Villain, 1959):

(a) Helicoidal phase ($\mathbf{k} \neq \mathbf{Q}/4$; \mathbf{Q} being any vector of the reciprocal lattice). All the spin vectors are parallel to a same plane. From one site i to another j , σ rotates in this plane by an angle $\mathbf{k}\cdot(\mathbf{R}_i - \mathbf{R}_j)$ [see Fig. 15(a)].

(b) Structure ($A, B, -A, -B$; $\mathbf{k} = \mathbf{Q}/4$; \mathbf{Q} being a vector of the reciprocal lattice). The planes perpendicular to \mathbf{k} are ferromagnetic (all vectors σ_i are identical). σ_i can take only four values, $A, B, -A, -B$. Successive planes perpendicular to \mathbf{k} have respective spins $A, B, -A, -B, \dots$ [see Fig. 15(b)]. The uudd phase belongs to this category, with $\mathbf{k} \parallel (100)$.

With effective pair interactions J_1, J_2, J_3 (5.11),

$$\mathcal{F}(\mathbf{k}) = J_1 g_1(\mathbf{k}) + J_2 g_2(\mathbf{k}) + J_3 g_3(\mathbf{k}), \quad (7.10a)$$

where

$$g_n(\mathbf{k}) = \sum_j^{(n)} e^{i\mathbf{k}\cdot(\mathbf{R}_i - \mathbf{R}_j)}, \quad (7.10b)$$

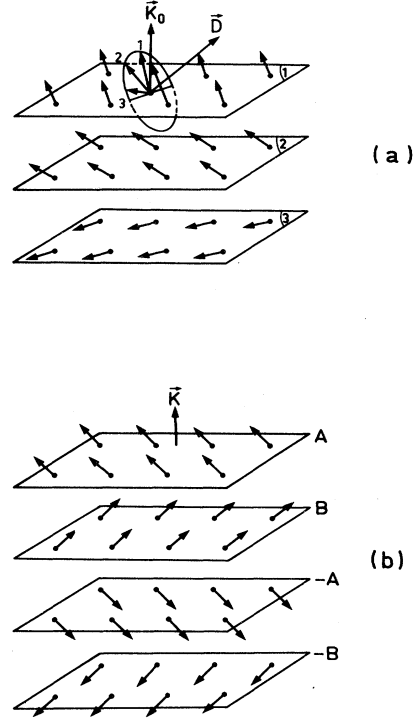


FIG. 15. One-Fourier-component phases. The condition $\sigma_i = \text{const}$ restricts these phases to two types of structures: (a) Helicoidal, (b) Ferromagnetic planes in a sequence $A, B, -A, -B, \dots$.

$\sum^{(n)}$ describing the sum over the n th neighbors of site i .

The minimization of $\mathcal{F}(\mathbf{k})$ for the bcc lattice has been performed in Cooper (1960). For $J_1 < 0$, the result is summarized by Fig. 16. Depending on the value of the parameters $\xi = J_2/J_1$ and $\zeta = 4J_3/J_1$, six phases can appear through a second-order transition:

(p1) The “normal antiferromagnetic phase” (naf): $\mathbf{k} = 2\pi/a(1,0,0)$ with two simple cubic ferromagnetic sublattices with opposite magnetization.

(p2) The “simple cubic antiferromagnetic phase” (scaf): $\mathbf{k} = \pi/a(1,1,1)$ with two simple cubic antiferromagnetic sublattices with orthogonal magnetizations.

(p3) “AF 100” phase: $\mathbf{k} = \pi/a(1,1,0)$: alternate (110) ferromagnetic planes with opposite magnetization.

(p4) “H 100”: helicoidal phase with axis parallel to 100

$$\mathbf{k} = 2/a(\phi_x, 0, 0) \text{ with } \phi_x = \arccos(-1/(\xi + \zeta)). \quad (7.11)$$

(p5) “H 111”: helicoidal phase with axis parallel to (111)

$$\mathbf{k} = 2\phi/a(1,1,1)$$

$$\text{with } \phi = \arccos(\{-1 - [1 - 8\xi(\xi - \zeta)]^{1/2}\}/4\xi).$$

(p6) Helicoidal phase H 110 with

$$\mathbf{k} = 2/a(\phi, \phi, 0); \phi = \arccos[(-1 + \xi)/\xi]^{1/2}.$$

With a quadratic Hamiltonian with no anisotropy, it can be proved that in mean field the phase transitions are al-

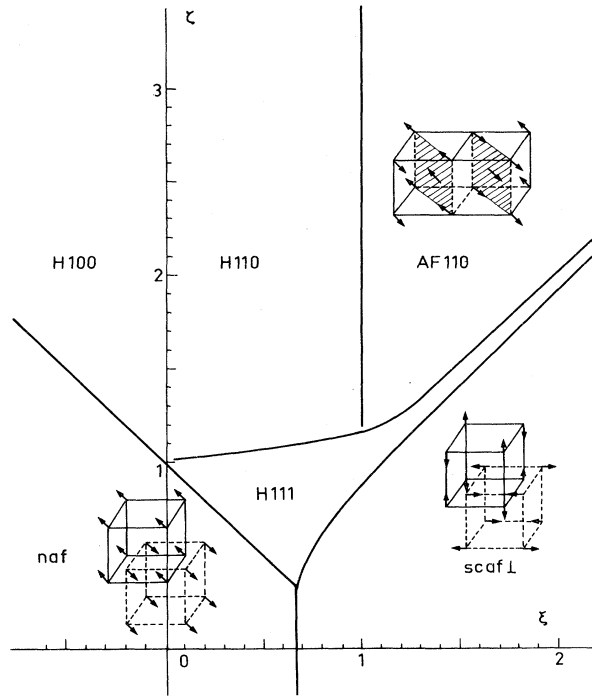


FIG. 16. One-Fourier-component structure having the highest second-order critical temperature in terms of $\xi=(J_2/J_1)$ and $\zeta=4J_3/J_1$, assuming $J_1 < 0$.

ways second order and that the phase appearing at T_c remains stable at a lower temperature. This is not true with a four-spin exchange Hamiltonian:

(i) Other structures with one or more than one Fourier component can appear from the paramagnetic phase with a first-order transition.

(ii) If one of the structures described above appears at T_{C2} with a second-order transition, another phase can appear at $T_{C1} < T_{C2}$ through a first-order transition.

3. Computer minimization

There is no simple algebraic method by which to find systematically the stable phase; thus we need a computer minimization of the free energy. We take a finite number $2n^3$ of spins ($n=2, 3$, or 4) with periodic boundary conditions, and minimize their free energy at zero temperature:

a. Elementary method

The form of the Hamiltonian shows that the molecular-field energy is linear with respect to each isolated spin σ_i . The Hamiltonian is therefore minimum with σ_i parallel to

$$\mathbf{H}_i = - \frac{\partial E}{\partial \sigma_i} . \quad (7.12)$$

For a given configuration C_n of the system, we isolate one spin σ_i , calculate the field $\mathbf{H}_i = -\partial E / \partial \sigma_i$, and put σ_i

parallel to \mathbf{H}_i , which gives a maximum decrease of E with respect to σ_i . We thus obtain a new configuration C_{n+1} .

Starting from a configuration C_0 where the spins are distributed at random, this process converges very rapidly to a structure such that, for each site, σ_i is parallel to \mathbf{H}_i . We thus obtain a local minimum of the energy; however, it can be different from the absolute minimum we seek.

b. Method using some "thermal agitation"

For this kind of problem, the Metropolis method (Hammersley and Handscomb, 1964) is usually applied. This method simulates thermal agitation by generating configurations with probability $e^{-E/kT}$, E being the corresponding energy. The advantage of this method is that it "explores" the configuration space; as the temperature is slowly decreased, we find the configuration with minimum energy. However, at low temperature the convergence is very slow. A greater efficiency can be obtained by combining this method with the preceding one. That is, we superpose a Brownian type agitation and a force tending to align the spins in the direction of the molecular field \mathbf{H}_i .

Starting from a configuration C_n , we choose (either at random or following some order—this does not affect the result) a site i . We add to σ_i a random fluctuation of maximum amplitude δ (δ is analogous to some "temperature"). Then we move σ_i , with an angular ratio α of the order of 0.1, toward the direction of the molecular field \mathbf{H}_i . By decreasing δ slowly, this process converges to the structure of minimum energy.

This method has been applied with some sets of parameters chosen to fit as well as possible the high temperature results or other experimental data, in order to find the stable phase at low field and low temperature. The results are described in Secs. VIII, X, and XI. In some cases (large K_p) we found a new phase with more than one Fourier component which cannot be described by Eq. (7.9).

C. Systematic search for the high-field phase at zero temperature, assuming it appears from the ferromagnetic phase at some critical field H_c through a second-order transition

Although the method of Villain fails at low field because the transition is experimentally shown to be first order, it can be successfully applied at high field where a second-order transition is expected.

At very high field and $T=0$, the system is ferromagnetic with all spins aligned in the direction of the magnetic field. In the ferromagnetic phase, using Hamiltonian (5.10) and the approximation (7.1), the free energy per particle is

$$E(H) = -\frac{1}{2} [4J_1 + 3J_2 + 6J_3 + 3(K_F + K_p)] - \frac{\gamma \hbar}{2} H . \quad (7.13)$$

When H is decreased, the ferromagnetic phase becomes

unstable below some critical value H_c : i.e., the appearance of components of the spin vectors perpendicular to H lowers the energy. An example of this is the occurrence of the naf spin-flop phase in an ordinary Heisenberg antiferromagnet. We thus write

$$\boldsymbol{\sigma}_i = \boldsymbol{\sigma}_i^\perp + \boldsymbol{\sigma}_i^\parallel,$$

$\boldsymbol{\sigma}_i^\perp$ and $\boldsymbol{\sigma}_i^\parallel$ being the components of $\boldsymbol{\sigma}_i$, respectively, perpendicular and parallel to \mathbf{H} for each site i .

We have

$$\boldsymbol{\sigma}_i^2 = \boldsymbol{\sigma}_i^{\perp 2} + \boldsymbol{\sigma}_i^{\parallel 2} = 1. \quad (7.14)$$

We suppose that the transition is second order ($\boldsymbol{\sigma}_i^\perp$ can be arbitrarily small). At lowest order in $\boldsymbol{\sigma}_i^\perp$, the variation of the energy with respect to the ferromagnetic phase takes the form

$$\delta E = \sum_{i,j} \Lambda_{ij} \boldsymbol{\sigma}_i^\perp \cdot \boldsymbol{\sigma}_j^\perp + \frac{\gamma \hbar}{2} H \sum_i \boldsymbol{\sigma}_i^{\perp 2}. \quad (7.15)$$

The condition $\partial E / \partial \boldsymbol{\sigma}_i = 0$ gives the following system of equations:

$$\frac{\gamma \hbar}{2} H \boldsymbol{\sigma}_i^\perp = - \sum_{i,j} \Lambda_{ij} \boldsymbol{\sigma}_j^\perp. \quad (7.16)$$

Defining the Fourier transform

$$\boldsymbol{\sigma}_i^\perp = \sum \boldsymbol{\sigma}_k^\perp e^{i\mathbf{k} \cdot \mathbf{R}_i}, \quad (7.17)$$

we can write Eq. (7.16) as

$$\frac{\gamma \hbar}{2} H \boldsymbol{\sigma}_k = J(\mathbf{k}) \boldsymbol{\sigma}_k,$$

with

$$J(\mathbf{k}) = \sum_j \Lambda_{ij} e^{i\mathbf{k}(\mathbf{R}_i - \mathbf{R}_j)}. \quad (7.18)$$

From this equation we deduce that the stable phase corresponds to the wave vector \mathbf{k}_0 which maximizes the critical field

$$H_c = \left[\frac{\gamma \hbar}{2} \right]^{-1} J(\mathbf{k}),$$

but

$$\left[\frac{\partial J(\mathbf{k})}{\partial \mathbf{k}} \right]_{\mathbf{k}=\mathbf{k}_0} = 0.$$

The corresponding structure has only one Fourier component \mathbf{k}_0 ,

$$\boldsymbol{\sigma}_i^\perp = \text{Re} \boldsymbol{\sigma}_{\mathbf{k}_0} e^{i\mathbf{k}_0 \cdot \mathbf{R}_i}.$$

We take

$$|\boldsymbol{\sigma}_i^\perp| = \text{const} = x.$$

This condition is similar to what we have at $T=0$, $H=0$: $|\boldsymbol{\sigma}_i| = \text{const}$, and thus the same kind of formulas are obtained; the possible structures are restricted to those described in Sec. VII.B.2 and in Fig. 15.

We can write, using Eq. (7.14),

$$|\boldsymbol{\sigma}_i^\parallel|^2 = 1 - x^2 \quad \text{and} \quad |\boldsymbol{\sigma}_i^\parallel| \simeq 1 - \frac{x^2}{2}.$$

(a) For the helicoidal structures at high field

$$\boldsymbol{\sigma}_i^\perp = \begin{pmatrix} x \cos \mathbf{k} \cdot \mathbf{R}_i \\ x \sin \mathbf{k} \cdot \mathbf{R}_i \\ 0 \end{pmatrix}, \quad (7.19)$$

$$\boldsymbol{\sigma}_i^\perp \cdot \boldsymbol{\sigma}_j^\perp = x^2 \cos[\mathbf{k} \cdot (\mathbf{R}_i - \mathbf{R}_j)].$$

δE [Eq. (7.15)] becomes, to second order in x ,

$$\begin{aligned} \delta E = & - \frac{Nx^2}{4} \{ [J_1 + 3(K_F + K_P)] g_1(\mathbf{k}) \\ & + (J_2 - 2K_F - K_P) g_2(\mathbf{k}) \\ & + (J_3 - \frac{1}{2} K_P) g_3(\mathbf{k}) - 8J_1 - 6J_2 - 12J_3 \\ & - 12(K_F + K_P) - \gamma \hbar H \}. \end{aligned} \quad (7.20)$$

The condition $\delta E = 0$ gives the critical field

$$\begin{aligned} \gamma \hbar H_c = & [J_1 + 3(K_F + K_P)] g_1(\mathbf{k}) + (J_2 - 2K_F - K_P) g_2(\mathbf{k}) \\ & + (J_3 - \frac{1}{2} K_P) g_3(\mathbf{k}) - 8J_1 \\ & - 6J_2 - 12J_3 - 12(K_F + K_P). \end{aligned} \quad (7.21)$$

[The functions

$$g_n(\mathbf{k}) = \sum_j^{(n)} e^{i\mathbf{k} \cdot (\mathbf{R}_i - \mathbf{R}_j)}$$

have been defined in Eq. (7.10).] It has been proved recently that this MFA value of the critical field is exact, at least if only one kind of four-spin exchange, K_F or K_P , is present (Hetherington, 1981). With Hamiltonian (5.3), $J_3 = K_P/2$ [see Eq. (5.11)], and H_c reduces to

$$\gamma \hbar H_c = A g_1(\mathbf{k}) + B g_2(\mathbf{k}) + C,$$

with

$$A = J_1 + 3(K_F + K_P) = J_{\text{NN}} + 6(K_F + K_P - J_t)$$

and

$$B = J_2 - 2K_F - K_P = -4J_t.$$

This relation is similar to Eq. (7.10), with the g_3 term eliminated. For all physical values of the parameters giving a negative Curie-Weiss temperature, A is negative. In this case the structure minimizing H_c is found along the horizontal axis ($\zeta=0$) of Fig. 16 with $\xi = B/A$. B is positive, thus ξ is negative, and we always obtain the structures with $\mathbf{k} = (2\pi/a)(1,0,0)$ (naf spin-flop phase), represented on Fig. 17. There are two simple cubic sublattices A, B with respective magnetization $\mathbf{M}_A, \mathbf{M}_B$ at equal angles to the field H , and on opposite sides of it:

$$\angle(\mathbf{M}_A, \mathbf{H}) = \angle(\mathbf{H}, \mathbf{M}_B) = \phi \quad \text{and} \quad |\mathbf{M}_A| = |\mathbf{M}_B|.$$

Its critical field is

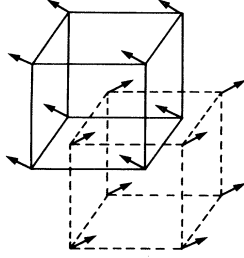


FIG. 17. Structure of the naf phase or the pf phase (both have the same symmetry, the only difference being that the magnetization of the pf phase is not zero at $H=0$). There are two simple cubic sublattices with respective magnetization \mathbf{M}_A and \mathbf{M}_B ; the angle between \mathbf{M}_A and \mathbf{M}_B is 2ϕ .

$$\begin{aligned} H_c &= -\frac{16}{\gamma\hbar}[J_1 + 3(K_F + K_P)] \\ &= -\frac{16}{\gamma\hbar}[J_{\text{NN}} + 6(K_F + K_P - J_t)]. \end{aligned} \quad (7.22)$$

(b) Structures of the second type ($A, B, -A, -B$) can be eliminated at high field. Such structures can only be energetically more favorable than a helicoidal phase with the same \mathbf{k} if $A = B$ (see Roger, 1980, for details). In this particular case the structure can be noted $(+, +, -, -)$. In a bcc lattice, there are three $(+, +, -, -)$ phases depending on the orientation of \mathbf{k} , which must be a symmetry axis.

(i) $\mathbf{k} \parallel 100$ (uudd) phase

$$H_c = -\frac{8}{\gamma\hbar}[J_{\text{NN}} - 8J_t + 6(K_F + K_P)].$$

(ii) $\mathbf{k} \parallel 111$ scf|| phase, which can also be described by two simple cubic antiferromagnetic lattices with parallel spins,

$$H_c = -\frac{8}{\gamma\hbar}[J_{\text{NN}} - 12J_t + 6(K_F + K_P)].$$

(iii) $\mathbf{k} \parallel 110$

$$H_c = -\frac{4}{\gamma\hbar}[J_{\text{NN}} - 10J_t + 6K_F + 5.5K_P].$$

It is easily verified that for physical values of the parameters ($J_t < 0$), these three critical fields are always smaller than the critical field of the naf phase. Therefore, we expect the naf phase to be present at low temperature and at fields near the ferromagnetic transition.

D. Properties of the high-field naf phase

1. Free energy and magnetization as a function of the field H

We define $u = \cos\phi$, ϕ being the angle between the magnetization of one sublattice and the field \mathbf{H} :

$$\phi = \angle(\mathbf{M}_A, \mathbf{H}) = \angle(\mathbf{H}, \mathbf{M}_B).$$

At finite temperature T and magnetic field H , the free en-

ergy is $F(T, H, p, u) = E(H, p, u) - T \cdot S(p)$, with

$$\begin{aligned} E(H, p, u) &= -\frac{N}{2} \{ (-4J_1 + 3J_2 + 6J_3)p^2 \\ &\quad + 3(K_F + K_P)p^4 + 24(K_F + K_P)p^4u^4 \\ &\quad + 8[J_1 - 3(K_F + K_P)p^2]p^2u^2 \\ &\quad + \gamma\hbar Hpu \}. \end{aligned}$$

$S(p)$ is the entropy given by Eq. (7.5); $p = \langle \sigma_i^z \rangle$.

For this phase all four-spin cycles (i, j, k, l) planar or folded, have the same spin configurations $(\sigma_A, \sigma_B, \sigma_A, \sigma_B)$; thus the free energy depends only on $\mathcal{X} = K_F + K_P$. The coefficient of the p^2 term

$$T_{c2} = -4J_1 + 3J_2 + 6J_3,$$

represents the critical temperature of the second-order transition in zero field.

With the above notations,

$$\begin{aligned} E(H, p, u) &= -\frac{N}{2} [T_{c2}p^2 + 3\mathcal{X}p^4 + 24\mathcal{X}p^4u^4 \\ &\quad + 8(J_1 - 3\mathcal{X}p^2)p^2u^2 + \gamma\hbar Hpu], \end{aligned} \quad (7.23)$$

p and u are obtained by minimizing the free energy.

The condition $(\partial E / \partial u) = 0$ gives

$$96\mathcal{X}p^4u^3 + 16(J_1 - 3\mathcal{X}p^2)p^2u + \gamma\hbar Hp = 0. \quad (7.24)$$

We obtained $u(H)$ and the magnetization $M(H) = M_0 u$ (M_0 being the saturation magnetization) by solving this third-order equation.

It is important to notice that, when H is decreased from H_c to zero, $M(H)$ decreases from M_0 to a finite value generally different from zero. If $J_1 / (3\mathcal{X}) - p^2$ is negative, Eq. (7.24) gives at $H=0$ the two solutions, $u=0$ and

$$u = \left[\frac{1}{2} \left[1 - \frac{J_1}{3\mathcal{X}p^2} \right] \right]^{1/2}. \quad (7.25)$$

The second equation gives a lower energy at zero field:

$$E(p) = -\frac{N}{2} [T_{c2}p^2 + 3\mathcal{X}p^4 - 2(J_1 - 3\mathcal{X}p^2)^2 / 3\mathcal{X}]. \quad (7.26)$$

At zero temperature ($p=1$) the magnetization $M(0)$ extrapolated to zero field is thus

$$M(0) = M_0 u = M_0 \left[\frac{1}{2} \left[1 - \frac{J_1}{3\mathcal{X}} \right] \right]^{1/2}.$$

With Hamiltonian (5.3) we have [see Eq. (5.11)]

$$J_1 = J_{\text{NN}} - 6J_t + 3\mathcal{X}$$

and

$$M(0) = M_0 \left[\frac{-J_{\text{NN}}/6 + J_t}{\mathcal{X}} \right]^{1/2}. \quad (7.27)$$

With four-spin exchange \mathcal{K} and with three-spin exchange J_t large enough in magnitude that ($|J_t| > |J_{NN}|/6$), the extrapolation of the curve $M(H)$ in zero field gives a finite value, $M(0) \neq 0$. This phase presents a spontaneous magnetization in zero field. Its symmetry is the same as for a "weak ferromagnetic" phase. However, its magnetization can reach a large value and cannot be considered as "weak." We denote this phase in zero magnetic field as "pseudoferrromagnetic."

Three different experiments agree with a value of the magnetization of the order of $0.5M_0$ at a relatively low field of 4 kG (Sec. II). As $M(H)$ does not vary very much between 0 and 4 kG, this can be achieved by a ratio

$$\frac{-J_{NN}/6 + J_t}{\mathcal{K}} \approx 0.25.$$

Thus we need both four-spin and three-spin exchange with comparable order of magnitude to explain this unusually high magnetization experimentally observed at 4 kG.

2. Phase diagram

a. Second-order transition line between the naf phase and the paramagnetic phase

In the paramagnetic phase, the energy is

$$E(p, u=1) = -\frac{N}{2} [\Theta p^2 + 3\mathcal{K}p^4 + \gamma\hbar Hp],$$

where $\Theta = 4J_1 + 3J_2 + 6J_3$ is the Curie-Weiss temperature.

The value of p is obtained by minimizing the free energy,

$$F(p) = E(p) - TS(p).$$

Using the relation $\partial S(p)/\partial p = -N(\tanh)^{-1}p$, we write the condition $\partial F(p)/\partial p = 0$

$$p = \tanh \left[\beta \left[\Theta p + 6\mathcal{K}p^3 + \frac{\gamma\hbar H}{2} \right] \right]. \quad (7.28)$$

The magnetic field H being fixed, the naf phase appears at some critical temperature $T_{c2}(H)$, when the energy is lowered by adding an infinitesimal component $\sigma_A^{\perp} = -\sigma_B^{\perp}$ of the spin vectors of each sublattice A, B , perpendicular to the field.

This condition can be written

$$\left[\frac{\partial E(p, u)}{\partial u} \right]_{u=1} = 0,$$

so that, using Eq. (7.23), one obtains

$$24\mathcal{K}p^4 + 8J_1p^2 + \frac{\gamma\hbar}{2}Hp = 0. \quad (7.29)$$

The phase diagram is obtained by solving Eqs. (7.28) and (7.29) numerically.

Figure 18 compares the phase diagrams in reduced coordinates [$T/|\Theta|$ and $(\gamma\hbar/2)H/|\Theta|$] for several values of $J_{NN}/|\Theta|$ and J_t/\mathcal{K} , and Fig. 19 compares the

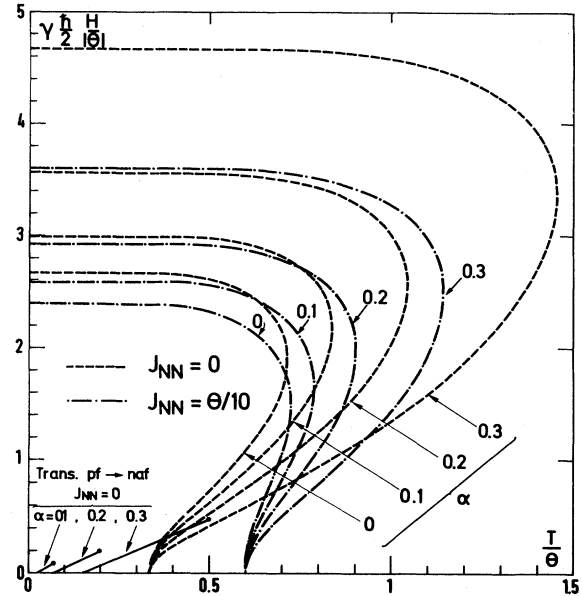


FIG. 18. Molecular-field phase diagram of the naf phase: solid lines, first-order transition from the pf phase to the naf phase; dashed and dotted lines, second-order transition to the paramagnetic phase for different values of the ratio $\alpha = J_t/(K_P + K_F)$, with $J_{NN} = 0$ and $J_{NN} = \Theta/10$, respectively. (All variables are normalized to the Curie-Weiss constant $|\Theta|$.)

magnetization curves. The critical temperature $T_{c2}(H)$ increases with magnetic field up to some limiting field H_l ; it then decreases and reaches zero at the critical field H_c given by Eq. (7.22). The ferromagnetic tendencies (large magnetization in zero field, H_l, H_c) increase with the ratio $\alpha = J_t/\mathcal{K}$. Nevertheless, even with $\alpha = 0$, without ferromagnetic triple exchange, the phase diagram already has a large ferromagnetic tendency: $T_{c2}(H)$ increasing with H , with only four-spin exchange. This ferromagnet-

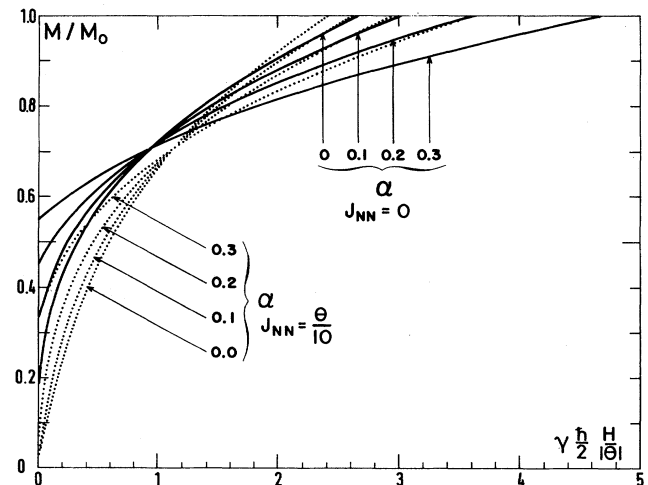


FIG. 19. Magnetization of the naf phase vs the reduced magnetic field, $(\frac{1}{2}\gamma\hbar H/|\Theta|)$, and the ratio $\alpha = J_t/(K_P + K_F)$. Solid lines, $J_{NN} = 0$; dashed lines, $J_{NN} = \Theta/10$.

ic behavior is in qualitative agreement with the experimental results.

b. The transition "pseudoferrromagnetic" \rightarrow naf

For each p , we minimize the energy $E(p, u)$ [Eq. (7.23)] with respect to u :

$$\left[\frac{\partial E(H, p, u)}{\partial u} \right]_{u=u_{\min}} = 0. \quad (7.30)$$

We thus obtain an expression of the free energy in terms of H, T, p :

$$F(H, T, p) = E(H, p, u_{\min}) - TS(p). \quad (7.31)$$

At fixed field H and temperature T , with both sufficiently low, and with $|J_t| > |J_{\text{NN}}|/6$ [see Eq. (7.27)], the curve $F(p)$ has two local minima p_1 and p_2 . At zero field, p_1 corresponds to some finite value u_1 of u (pseudoferrromagnetic phase with finite magnetization) and p_2 corresponds to $u_2=0$ (naf phase). At low temperature, the first local minimum (pf phase) has a lower energy, but as the temperature is increased, both minima approach and cross for some critical temperature T_{c1} . We thus obtain a first-order transition between the pf and naf phase, with discontinuity in angles ϕ and polarization p .

The transition line obtained by varying the field H ends at some critical point (H, T) . This transition line is shown in Fig. 18.

VIII. A TWO-PARAMETER MODEL

As shown in Sec. IV, the exchange frequencies are exponential functions of some characteristic parameters (effective potential V , length L in the configuration space). Thus we do not expect a large number of them to be of the same order of magnitude. However, a one-parameter model (four-spin exchange only) cannot explain all the experimental data. As emphasized in the preceding section, we need both three- and four-spin exchange to explain the large observed magnetization at 4 kG.

Nevertheless, it is interesting to first study the properties of the simplest one-parameter models.

A. One-parameter models

1. Triple exchange

J_t alone leads to ferromagnetism and is excluded by all the experimental results, primarily by the sign of the Curie-Weiss constant.

2. Folded four-spin exchange K_F

With only folded four-spin exchange, the minimization of the free energy at zero temperature is quite easy. The contribution to the mean-field free energy of one isolated cycle (1,2,3,4),

$$E = \langle P_{1234} + P_{1234}^{-1} \rangle,$$

in the notation of Sec. V is minimum for the spin configuration $(\uparrow, \rightarrow, \downarrow, \leftarrow)$. The four-spin vectors are in the same plane, from one site to the nearest neighbor. The spin vectors rotate by $\pi/2$. In a bcc lattice it is possible to make up a structure with *all* folded cycles having the configuration $(\uparrow, \rightarrow, \downarrow, \leftarrow)$ of lowest energy. This phase (denoted scsf) minimizes the total free energy. It has (see Fig. 16) four fcc sublattices with orthogonal magnetizations. It can be described by two interpenetrating simple cubic antiferromagnetic lattices with orthogonal magnetization. As this magnetic structure has cubic symmetry, the magnetic dipolar interactions are null to lowest order because of cancellations in the cubic lattice. The zero-field magnetic resonance frequency expected for such a structure is of the order of one gauss and thus is in fundamental disagreement with the results of Osheroff *et al.* (1980), who measured a frequency of several hundred gauss.

The high-temperature data also cannot be correctly fit within this model. The expansion gives

$$B = 0; \quad e_2 = 175.5K_F^2; \quad \Theta = 18K_F.$$

Fitting $e_2 = 7 \text{ mK}^2$ gives $K_F = -0.2 \text{ mK}$ and leads to $\Theta = -3.6 \text{ mK}$, too negative compared to the experimental results. More details on this simple model have been given in Roger, Delrieu, and Hetherington (1980a).

3. Planar four-spin exchange K_P

a. Low-field phase

In contrast to the preceding case, it is not possible to obtain all planar cycles with the configuration $(\uparrow, \rightarrow, \downarrow, \leftarrow)$ of lowest energy. The system is "frustrated" in some way. Finding the stable structure is not straightforward. We used the computer minimization explained in Sec. VII and found the unusual phase shown in Fig. 20. This structure has ferromagnetic lines (aligned spins) along the 0X direction, parallel to one of the three axes, (100), (010), (001). Perpendicular to 0X, these lines define a planar structure with two interpenetrating simple square

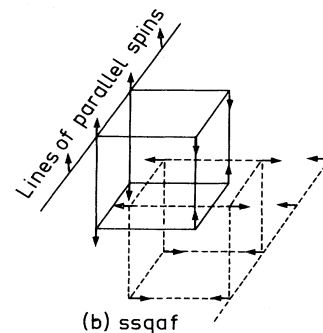


FIG. 20. "Simple square antiferromagnetic phase" (ssqaf) $|K_P| > |J_t|/4$. The lines (100) are ferromagnetic. Perpendicular to (100) we have a planar structure with two interpenetrating simple square antiferromagnetic lattices.

antiferromagnetic lattices with orthogonal magnetization. We denote this phase ssqf. It has two Fourier components and cannot be described by the plane-wave equation (7.9). The four magnetic sublattices are not cubic, and therefore we expect a large dipolar anisotropy. However, the structure of this anisotropy does not agree with the experimental results.

The order parameter is a trihedral given by two orthogonal directors (\hat{d}_1, \hat{d}_2) corresponding to the direction of the spins in each antiferromagnetic sublattice.

Using the symmetry of the magnetic lattice, the anisotropic part of the dipolar energy can be written

$$E_D = -(1/2)V\rho^2 \left[\frac{\gamma\hbar}{2} \right]^2 \{ C_0[(d_1^x)^2 + (d_2^x)^2] + C_1(d_1^y d_2^z + d_1^z d_2^y) \}, \quad (8.1)$$

where $\rho = N/V$ is the number density and where the ferromagnetic lines are along the 100 direction. By numerical summation within the molecular-field approximation (Roger, 1980) we have determined C_0 and C_1 to be

$$C_0 = 2.16 \text{ and } C_1 = 5.31.$$

The equilibrium configuration is determined by the sign of $C_2 = (C_1)/2 - C_0$. With C_2 positive, \hat{d}_1 and \hat{d}_2 are parallel to (010) and (001), respectively.

The second derivative $\partial^2 E_D / \partial \theta^2$ with respect to the rotations of (\hat{d}_1, \hat{d}_2) around (010) or (001) gives two degenerate zero-field resonances:

$$\Omega_2 = \left[\frac{\gamma^2}{\chi_{\parallel}} \rho^2 \left[\frac{\gamma\hbar}{2} \right]^2 \left[\frac{C_1}{2} - C_0 \right] \right]^{1/2} \simeq 0.3 \text{ MHz}. \quad (8.2)$$

The second derivative $\partial^2 E_D / \partial \theta^2$ with respect to the rotation of (\hat{d}_1, \hat{d}_2) around the anisotropy axis OX parallel to 100 gives the resonance

$$\Omega_1 = \left[\frac{\gamma^2}{\chi_{\perp}} \rho^2 \left[\frac{\gamma\hbar}{2} \right]^2 2C_1 \right]^{1/2} \simeq 1.4 \text{ MHz}. \quad (8.3)$$

$[\chi_{\perp}$ and χ_{\parallel} are the susceptibilities for \mathbf{H} , respectively, perpendicular and parallel to the plane (\hat{d}_1, \hat{d}_2) .]

Even taking into account the renormalization due to the zero-point motion (Sec. VIII.B) $\simeq 0.95$ and the spin waves (Secs. VIII.B and IX) $\simeq 0.8$, Ω_1 is too high compared to Osheroff's results. In a magnetic field, the degenerate frequency Ω_2 splits into two modes, giving a more complicated spectrum than that observed by Osheroff *et al.* (1980).

b. High-temperature series expansions

We have $\Theta = 18K_F$, $e_2 = 153K_F^2$; fitting $e_2 \simeq 7 \text{ mK}^2$ would lead to $\Theta = -3.8 \text{ mK}$ (the experiments give $-2.5 \gtrsim \Theta \gtrsim -3.3 \text{ mK}$).

B. Two-parameter model (J_t, K_P)

The high-temperature data can be fit either with a two-parameter model, including triple-exchange J_t and *folded* four-spin exchange K_F (Roger, Delrieu, and Hetherington, 1980a), or with a two-parameter model including J_t and *planar* four-spin exchange K_P (Roger, Delrieu, and Hetherington, 1980b, 1980c). Both models fit the ferromagnetic tendencies of the high-field phase equally well. Because the planar and folded cycles have the same spin configuration in the naf phase, they are equivalent whenever that phase is stable. Only the nature of the low-field phase allows us to choose between the two models: (i) The (J_t, K_F) model has been studied by Roger *et al.*, (1980a). It leads to the scf phase at low field with cubic symmetry and small dipolar anisotropy and is now excluded by the experiment of Osheroff *et al.* (1980). (ii) We retain here only the (J_t, K_P) model, i.e., three-spin exchange and planar four-spin exchange, all other exchanges being neglected.

1. Low-field phase

We used the computer method described in Sec. VII.B to find the configuration of lowest energy for different values of the ratio $\alpha = J_t/K_P$. The ssqf phase remains stable for $\alpha < 0.25$. For $\alpha > 0.25$ our computer process converged to the uudd phase proposed by Osheroff.

The energies are

$$\begin{aligned} \text{ssqf: } E(p) &= \frac{N}{2} p^2 [-4J_t + (2 + 3p^2)K_P], \\ \text{uudd: } E(p) &= \frac{N}{2} p^2 (4J_t + 3K_P p^2). \end{aligned}$$

They are equal at $T=0$ for $J_t = K_P/4$. The contribution to the energy of one isolated three-spin cycle J_t is minimum for a ferromagnetic configuration $(i, j, k) = (\uparrow, \uparrow, \uparrow)$; in the ssqf phase all three-spin cycles have a "frustrated" configuration $(\uparrow, \uparrow, \downarrow)$; in the uudd phase one-half of the three-spin cycles are ferromagnetic, the others are frustrated with $(\uparrow, \uparrow, \downarrow)$. For this reason the uudd phase is favored by large J_t .

2. Critical temperature of the uudd phase.

Adjustment of the two parameters

The free energy of the uudd phase is (within the MFA)

$$F^{\text{uudd}}(p) = N \left[\frac{p^2}{2} (4J_t + 3K_P p^2) - TS(p) \right]. \quad (8.4)$$

For the parameters we are led to choose, the ratio of the p^4 term to the p^2 term is quite large. For this reason, we obtain a strong first-order transition to the paramagnetic phase at a temperature T_{C1} , with a large drop of entropy ($\sim 0.8 \ln 2$).

The first-order transition is extremely abrupt, so the value of p obtained by minimizing Eq. (8.4) is almost 1 up

to T_{C1} . Thus

$$F^{\text{uudd}}(p) \simeq \frac{N}{2}(4J_t + 3K_P).$$

A good approximation to the critical temperature T_{C1} can be obtained by equating this approximate energy of the uudd phase to the energy of the paramagnetic phase $-NT \ln 2$:

$$-T_{C1} \ln 2 = \frac{1}{2}(4J_t + 3K_P). \quad (8.5)$$

This reasoning is valid only if no other phase occurs with a critical temperature larger than T_{C1} .

With $J_t < K_P/4$, in Fig. 16 we have

$$\xi = \frac{J_2}{J_1} = \frac{-4J_t + K_P}{3(-2J_t + K_P)} < 0$$

and

$$\zeta = \frac{4J_3}{J_1} = \frac{2K_P}{3(-2J_t + K_P)} > \frac{4}{3}.$$

The highest second-order critical temperature is obtained for the helicoidal $H100$ phase with wave vector

$$\mathbf{k} = \frac{2}{a}(0, 0, k_z); \quad k_z = \arccos \left[-\frac{3(K_P - 2J_t)}{3K_P - 4J_t} \right].$$

Its critical temperature is

$$T_{C2} = -2 \frac{[3(K_P - 2J_t)]^2}{3K_P - 4J_t} - 4J_t. \quad (8.6)$$

The Curie-Weiss temperature is

$$\Theta = 18(-2J_t + K_P). \quad (8.7)$$

Equations (8.5) and (8.7) give a very simple way to adjust the two parameters J_t, K_P according to the experimental values

$$T_{C1} = 1 \text{ mK}$$

and

$$-3.3 < \Theta < -2.5 \text{ mK}.$$

The large uncertainty in Θ allows us to adjust J_t, K_P such that $T_{C2} < T_{C1}$. With

$$J_t = -0.1 \text{ mK},$$

$$K_P = -0.355 \text{ mK},$$

we obtain, $T_{C1} = 1.06 \text{ mK}$ and $\Theta = -2.79 \text{ mK}$ (with $T_{C2} = 1.05 \text{ mK} < T_{C1}$).

3. High-temperature data

The set of parameters $J_t = -0.1 \text{ mK}$ and $K_P = -0.355 \text{ mK}$ is in quantitative agreement with the experimental data within their accuracy. We obtain

$$\tilde{e}_2 = \frac{17}{36} \Theta^2 + 6\Theta J_t + 180J_t^2 \simeq 7.15 \text{ mK}^2 \quad (8.8)$$

in perfect agreement with the results of Panzyck and Adams (1970). $e_3 \simeq +0.8 \text{ mK}^3$ is positive, as observed experimentally (Hebral *et al.*, 1979; Dundon and Goodkind, 1975, Mamiya *et al.*, 1981), but probably too small. The second coefficient in the inverse susceptibility series,

$$B = -\frac{\Theta^2}{432} - \frac{23}{6} \Theta J_t + 57J_t^2 \simeq -0.5 \text{ mK} \quad (8.9)$$

is negative but rather small compared to the value given by Prewitt and Goodkind (1977). However, we think the experimental error they estimated is rather optimistic, given the low precision on Θ . We believe this partly because the measurements are made at low enough temperature that higher-order terms in the series expansion can lead to an "apparent" value of B different from the real value.

4. Susceptibility, dipolar anisotropy, resonance properties of the uudd phase

The symmetry of the uudd phase being uniaxial, the dipolar energy can be written

$$E_D = \frac{1}{2} \rho^2 \left[\frac{\gamma \hbar}{2} \right]^2 C_0 (d^z)^2. \quad (8.10)$$

OZ is the direction perpendicular to the ferromagnetic planes, and \vec{d} is the direction of the spin vectors. The constant $C_0 \simeq +7.263$ can be obtained from Cohen and Keffer (1955). (See also, Osheroff *et al.*, 1980, and Roger, 1980). As C_0 is positive, the spins orient themselves perpendicular to OZ , i.e., parallel to the ferromagnetic planes (see Fig. 1). The orientation of the spin vectors in these ferromagnetic planes is free in zero field. (This is a "planar anisotropy.") Any external field H orients the spins perpendicular to itself, removing this degeneracy, and the spins flop slightly toward H . The corresponding susceptibility is, within the MFA,

$$\chi_{\perp} = -C_1 / (-32J_t + 24K_P), \quad (8.11)$$

where C_1 is given in Eq. (2.5c). With $J_t = -0.1 \text{ mK}$ and $K_P = -0.355 \text{ mK}$, we obtain

$$\chi_{\perp} \simeq +C_1 / (5.32 \text{ mK}).$$

Prewitt and Goodkind (1977) give $\chi_{\perp} \simeq +C_1 / (5.2 \text{ mK})$. Recent measurements by Morii *et al.* (1978) give

$$C_1 / 5.9 \text{ mK} \lesssim \chi_{\perp} \lesssim C_1 / 5.2 \text{ mK}. \quad (8.12)$$

Even in arbitrarily small field H , the "spin-flop" phase described above is obtained, and there is no simple means to measure the parallel susceptibility χ_{\parallel} .

There is only one resonance frequency in zero field,

$$\Omega_0 = \left[\frac{\gamma^2}{\chi_{\perp}} \rho^2 \left[\frac{\gamma \hbar}{2} \right]^2 \cdot C_0 \right]^{1/2}.$$

With the theoretical value of the susceptibility calculated in the MFA with a two-parameter model $J_t = -0.1 \text{ mK}$,

$K_p = -0.355$, we obtain

$$\Omega_0 \simeq 1163 \text{ kHz} .$$

With the experimental values (8.12) of the susceptibility we conclude that

$$1150 \lesssim \Omega_0 \lesssim 1225 \text{ kHz} . \quad (8.13)$$

These MFA values must be corrected by two renormalization factors:

(i) The first is due to the fact that the MFA does not give the correct ground state.

A better value of the dipolar anisotropy can be evaluated within the spin-wave theory. In principle we have to calculate the mean value

$$\sum_{ij} \left\langle \frac{(\sigma_i \cdot \mathbf{r}_{ij})(\sigma_j \cdot \mathbf{r}_{ij})}{r_{ij}^3} \right\rangle \quad (8.14)$$

taken on the spin-wave ground state. As the main contribution comes from the diagonal part $\sigma_i^z \sigma_j^z$, we roughly estimate the normalization factor to be proportional to $p = 1 - \langle \Delta S_z \rangle$ at zero temperature.

For the uudd phase, the spin-wave calculation gives (Sec. IX) $p \simeq 0.64$. Taking this factor into account, we obtain

$$736 \lesssim \Omega_0 \lesssim 784 \text{ kHz} . \quad (8.15)$$

The fluctuations of the uudd phase with respect to the molecular field ($p \simeq 0.64$) are much larger than those obtained with an ordinary antiferromagnet ($p \simeq 0.85$). Consequently the value (8.15) of Ω_0' is lower than that given by Osheroff *et al.*, who took arbitrarily $p = 0.85$.

(ii) The second renormalization factor is due to the large zero-point motion of the atoms.

We have calculated the correction of the dipolar energy due to the zero-point motion by a Monte Carlo integration based on the variational wave function ϕ_G [Eq. (4.10)] generally used for the calculation of the ground-state energy. For all except this uudd phase, this renormalization factor is on the order of $\sqrt{0.9} \simeq 0.95$.

Although mathematically quite different, this renormalization factor is of the same order as that of the dipolar renormalization in the paramagnetic phase calculated by Harris (1971) and Landesman (1973).

In the uudd phase, the contribution of the first neighbors is zero,³ hence the renormalization factor coming essentially from the contribution of the second neighbors is smaller (around $\sqrt{0.95}$). Taking into account both renormalization factors, we obtain

$$720 \lesssim \Omega_0 \lesssim 760 \text{ kHz} .$$

This result is below the experimental value $\Omega_0 \simeq 825 \text{ kHz}$, but the renormalizations are very rough and, as pointed

³We are indebted to D. S. Fisher for illuminating discussions about this point.

out in (i), the complete calculation of Eq. (8.14) in the spin-wave approximation is needed.

5. High-field phase

According to the general results established in Sec. VII, the high-field phase is the naf phase represented in Fig. 17. It has two simple cubic sublattices with respective magnetization $\mathbf{M}_A, \mathbf{M}_B$, such that $\angle(\mathbf{M}_A, \mathbf{H}) = \angle(\mathbf{H}, \mathbf{M}_B) = \phi$ and $|\mathbf{M}_A| = |\mathbf{M}_B|$. The extrapolation to zero field of the angle $\phi(H)$ gives the finite value

$$\phi(H \rightarrow 0) = \arccos \sqrt{J_t / K_p}$$

(pseudoferrromagnetic phase) .

The corresponding value of the magnetization is

$$M(H \rightarrow 0) = \sqrt{J_t / K_p} M_0 ,$$

M_0 being the saturation magnetization $M_0 = N\gamma\hbar/2$. With our parameters, we obtain $M(H \rightarrow 0) = 0.53M_0$. Osheroff (1982) measured $0.57M_0$ at 4 kG.

At zero temperature, the critical field of transition between the uudd and pseudoferrromagnetic phases is

$$H_{C1} \simeq 12.1 \text{ kG} .$$

This value is too high compared to the value given by Osheroff (1982). However, phase diagrams in molecular field usually give only qualitative agreement with the experiment (even with a Heisenberg model!).

In our model, the second-order critical field between the naf phase and the ferromagnetic phase at $T = 0$ is [see Eq. (7.22)]

$$H_{C2} = -\frac{96}{\gamma\hbar} (K_p - J_t) \simeq 157 \text{ kG} . \quad (8.16)$$

This theoretical value of the transition field is exact (Hetherington, 1981). This is more than twice the value obtained with an HNNA model for the same value of Θ . It correlates well with the extrapolation of the magnetization curve of Godfrin *et al.* (1980) to saturation (Frosatti, private communication). The magnetization of this phase varies slowly from $0.6M_0$ at 12 kG to $1.0M_0$ at the critical field H_{C2} (see Fig. 21), in perfect agreement with the experimental results described in Sec. II.

Figure 21 compares theoretical results for $M(H)$ and for the limiting pressure $P(H)$ in a Pomeranchuk cell to the experimental curves deduced from Adams, Delrieu, and Landesman (1978). The theoretical limiting pressure $P(H)$ is related thermodynamically to the magnetization. Equation (2.1),

$$\left. \frac{dP}{dH} \right|_{\text{melt}} = \frac{M_s - M_l}{V_s - V_l} , \quad (8.17)$$

gives after integration

$$\Delta P(H) = P(H) - P(0) = \frac{1}{V_s - V_l} \int_0^H M_s(H) dH ,$$

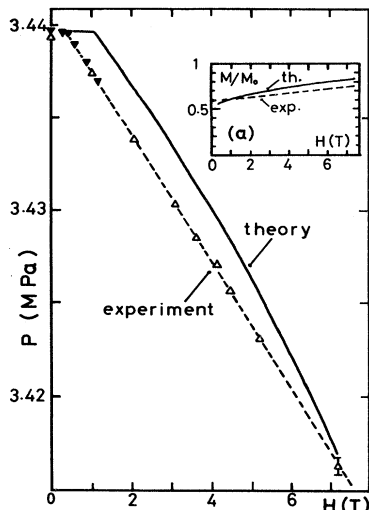


FIG. 21. The limiting pressure $\Delta P = P(H) - P(0)$ measured in a Pomeranchuk cell (dashed line) compared with the theoretical curve (solid line) obtained from the two-parameter model $J_t = -0.1; K_p = -0.355$. The experiments points (Δ), are from Godfrin *et al.* (1980) and (∇) from Kummer, Mueller, and Adams (1977). The inset compares the magnetization deduced from the experiments by a thermodynamic relation [Eq. (8.17)] with that derived from mean-field theory in the same model.

where we have neglected the magnetization of the liquid. The right-hand side represents, in fact, the magnetic energy density $E(H)$.

Experimental and theoretical curves agree quite well. The shift between the two curves representing ΔP comes mainly from the disagreement between the experimental critical field $H_{C1} \approx 4$ kG and the value calculated within the MFA $H_{C1} \approx 12$ kG.

The critical temperature of transition to the paramagnetic phase increases with magnetic field up to $H_L \approx 120$ kG, where $T_{C2}(H_L) = 3.8$ mK. $T_{C2}(H)$ then decreases and reaches zero at the critical field $H_{C2} \approx 157$ kG.

6. Whole phase diagram

The whole phase diagram is represented by Fig. 22. At high field, it is in quantitative agreement with the experimental results. At low field, it gives the essential experimental features, particularly a first-order transition at 1 mK to the uudd phase. However, the field of transition between the uudd and pf phase is too high.

There is a first-order transition between the naf and pf phase (see Sec. VII), ending at a critical point which parallels the second-order transition between the naf and paramagnetic phases. We initially assumed this was perhaps an artifact of the mean-field calculation. However, a recent measurement by Osheroff (1982) indicates a first-order transition in this vicinity, and we expect that it is related to the one we find in mean field. We still have no way of deciding if an exact calculation would cause the parallel first- and second-order transitions to merge, although it would not surprise us. The experimental situa-

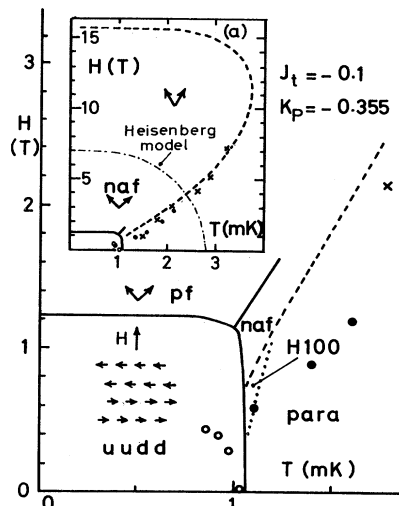


FIG. 22. The phase diagram obtained from the mean-field approximation in our two-parameter model (J_t, K_p): solid curve, first-order transition; dashed curve, second-order transition; \circ first-order data points of Kummer *et al.* (1975); \bullet , second-order data points of Kummer *et al.* (1975); \times , approximate second-order transition temperature given by Godfrin *et al.* (1980); dot-dash line in the inset, the single second-order transition of the HNNA model.

tion at this interesting triple point is not clear enough to make any definitive statement about the details of the phase diagram.

The mean-field theory also yields a helicoidal phase H 100 in a narrow domain near the same triple point. Exact calculation could easily modify this phase or cause it to disappear. Experiment has not excluded it.

7. Main features of the two-parameter model J_t, K_p

This simple two-parameter model accounts for the following data:

- (i) *High-temperature coefficients*
 - * quantitative agreement with $\Theta, \tilde{\epsilon}_2$,
 - * qualitative agreement with the signs of $\tilde{\epsilon}_3$ and B .
- (ii) *Low-field phase*
 - * gives the uudd phase in agreement with the Osheroff measurements,
 - * gives a first-order transition with large drop of entropy at $T = 1$ mK,
 - * gives the susceptibility and resonance frequency in agreement with the experiment.
- (iii) *High-field phase*
 - * quantitative agreement with the observed phase diagram between 10 and 70 kG,
 - * quantitative agreement with the unexpectedly high and slowly varying magnetization.

The molecular-field phase diagram is only in qualitative agreement with the experimental results for $H \lesssim 10$ kG. However, we cannot expect very accurate results from the molecular-field approximation, in particular

with a slightly frustrated system like the uudd phase.

Some criticism could be formulated about our method of determining the parameters. We chose to fit the temperature of the first-order transition $T_{C1}=1$ mK within the MFA. This provided an easy way to determine the parameters, but we do not know how accurate the calculation of this temperature is within the MFA. This will be discussed in more detail in the following sections.

IX. THE SPIN-WAVE APPROXIMATION

At low temperature it is possible to make the harmonic approximation about the mean-field solution. This leads to spin waves and to some lowering of the energy of the system. Appendix D gives an exposition of the technique, which is mathematically tedious, and then applies it to the spin structures and Hamiltonians of interest to us, i.e., naf, scaf, and ssqf phases. We summarize here the main results obtained in Appendix D and analyze their physical consequences.

A. Spin-wave Hamiltonian

The quantization axis OZ is chosen along the common direction of the spins (see Fig. 34 in Appendix D). We quantify the spin deviations with respect to the molecular-field approximation in the usual Holstein-Primakoff (1940) formalism. We introduce the spin-deviation boson operators $\alpha_{l,i}$ by

$$\begin{aligned} S_i^+ &\simeq \alpha_{l,i} , \\ S_i^- &\simeq \alpha_{l,i}^+ , \\ S_i^z &\simeq \frac{1}{2} - \alpha_{l,i}^+ \alpha_{l,i} , \end{aligned}$$

for the two sublattices $l=1, l=2$ with up-spins and

$$\begin{aligned} S_j^+ &\simeq \alpha_{l,i}^+ , \\ S_j^- &\simeq \alpha_{l,i} , \\ S_j^z &\simeq -\frac{1}{2} + \alpha_{l,i}^+ \alpha_{l,i} , \end{aligned}$$

for the sublattices $l=3$ and $l=4$ with opposite spins. We define the Fourier transforms

$$\begin{aligned} \alpha_l(k) &= \frac{2}{\sqrt{N}} \sum_{i \in \varphi_l} \alpha_{l,i} e^{-ikR_i} , \\ \alpha_l^+(k) &= \frac{2}{\sqrt{N}} \sum_{i \in \varphi_l} \alpha_{l,i}^+ e^{+ikR_i} , \end{aligned}$$

where the sum is extended over one sublattice φ_l . The Hamiltonian can be written in the quadratic form.

$$\mathcal{H} = E_0 + \sum_k [\alpha_1^+(k), \alpha_2^+(k), \alpha_3(-k), \alpha_4(-k)] \times \begin{pmatrix} \Omega & \Gamma \\ \Gamma & \Omega \end{pmatrix} \begin{pmatrix} \alpha_1(k) \\ \alpha_2(k) \\ \alpha_3^+(-k) \\ \alpha_4^+(-k) \end{pmatrix} - \text{tr} \Omega . \quad (9.1)$$

Ω, Γ are 2×2 matrices,

$$\Omega = \begin{pmatrix} \omega & \eta \\ \eta^* & \omega \end{pmatrix} \quad \text{and} \quad \Gamma = \begin{pmatrix} \gamma & v^* \\ v & \gamma \end{pmatrix} ,$$

with

$$\begin{aligned} \omega(k) &= +2J_2 - 4J_3 - 4K_F - 12K_P - 2(J_2 + K_P)(\cos ak_x + \cos ak_y) - 4 \left[J_3 + \frac{K_P}{2} \right] \cos ak_x \cos ak_y , \\ \gamma(k) &= 2 \cos ak_z [-J_2 + 2K_F + K_P + (-2J_3 + K_P)(\cos ak_x + \cos ak_y)] , \\ \nu(k) &= |v| e^{i\varphi} = (-J_1 - K_F - 3K_P) 4 \cos \frac{ak_x}{2} \cos \frac{ak_y}{2} e^{i(ak_z/2)} , \\ \eta(k) &= |\eta| e^{i\varphi} = (-J_1 + K_F + 3K_P) 4 \cos \frac{ak_x}{2} \cos \frac{ak_y}{2} e^{i(ak_z/2)} . \end{aligned} \quad (9.2)$$

Note that ν and η have the same complex phase, $\varphi = ak_z/2$. E_0 is the molecular-field energy. The Hamiltonian \mathcal{H} is put into diagonal form

$$\mathcal{H} = E_0 + \sum_k \{ \lambda_+ [e_1^+(k)e_1(k) + e_3^+(k)e_3(k)] + \lambda_- [e_2^+(k)e_2(k) + e_4^+(k)e_4(k)] + [\lambda_+ + \lambda_- - 2\omega(k)] \} \quad (9.3)$$

by using the linear transformation $T(k)$,

$$\begin{pmatrix} e_1(k) \\ e_2(k) \\ e_3^+(-k) \\ e_4^+(-k) \end{pmatrix} = T(k) \begin{pmatrix} \alpha_1(k) \\ \alpha_2(k) \\ \alpha_3^+(-k) \\ \alpha_4^+(-k) \end{pmatrix} . \quad (9.4)$$

The 4×4 matrix $T(k)$ satisfies the identity

$$T^{-1}(k) = \tilde{T} T + \tilde{I} , \quad (9.5)$$

$$\tilde{I} = \begin{pmatrix} I & 0 \\ 0 & -I \end{pmatrix} ,$$

I being the 2×2 identity matrix. This preserves the boson commutation rules for the new operators $e_i(k)$.

There are two doubly degenerate eigenmodes λ_+ and λ_- corresponding, respectively, to one acoustic and one optical mode,

$$\lambda_{\pm} = [u \pm (|v|^2 - c^2)^{1/2}]^{1/2},$$

with

$$\begin{aligned} c &= 2|\eta||v|\sin 2\varphi, \\ u &= \omega^2 - \gamma^2 + |\eta|^2 - |v|^2, \\ v &= 2(\omega\eta^* - \gamma v) = 2(\omega|\eta|e^{-i\varphi} - \gamma|v|e^{i\varphi}). \end{aligned} \quad (9.6)$$

The eigenvectors $e_i(k)$ are given by Eq. (9.4) with

$$T(K) = \begin{pmatrix} R^+ & R^- \\ R^- & R^+ \end{pmatrix}. \quad (9.7)$$

The 2×2 matrices R^{\pm} are defined by,

$$R^{\varepsilon} = \begin{pmatrix} r_{\varepsilon}^* & r_{\varepsilon} \\ s_{\varepsilon}^* & -s_{\varepsilon} \end{pmatrix}$$

with

$$\begin{aligned} r_{\varepsilon} &= \frac{1}{2}e^{i\phi}[\mu_+^*e^{-it} + \varepsilon\mu_+^*e^{it}], \\ s_{\varepsilon} &= \frac{1}{2}e^{i\phi}[\mu_-^*e^{it} + \varepsilon\mu_-^*e^{-it}], \end{aligned} \quad (9.8)$$

where $\mu_{\varepsilon}^{\prime\prime}$ is given by

$$\mu_{\varepsilon}^{\prime\prime} = \left\{ \left[\omega + \varepsilon'\gamma + \frac{\varepsilon''\text{Re}[v(\eta + \varepsilon v^*)]}{(|v|^2 - c^2)^{1/2}} \right] (2\lambda_{\varepsilon}^{\prime\prime})^{-1} \right\}^{1/2}. \quad (9.9)$$

The phases ϕ and t are defined by

$$\begin{aligned} e^{2i\phi} &= v^*/|v|, \\ e^{2it} &= [(|v|^2 - c^2)^{1/2} + ic]/|v|. \end{aligned} \quad (9.10)$$

B. Properties of the spin-wave spectrum

1. Optical modes

At $k=0$, we have $c=0$, and the coefficients η, v are real; thus

$$\lambda_{\varepsilon} = u + \varepsilon v = (\omega + \varepsilon\eta + \gamma + \varepsilon v)(\omega + \varepsilon\eta - \gamma - \varepsilon v). \quad (9.11)$$

We obtain an acoustic mode and one optical mode with frequency

$$\lambda_{-}(k=0) = 16(K_F + 3K_P)(-8J_1 + 4J_2 + 16J_3 + 12K_P). \quad (9.12)$$

In the particular case of a two-parameter model (J_i, K_P) [see Eq. (5.11)], this relation reduces simply to

$$\lambda_{-} = 16\sqrt{6K_P J_i}. \quad (9.13)$$

With $J_i = -0.1$ mK and $K_P = -0.355$ mK, we obtain

$$\lambda_{-} \simeq 150 \text{ MHz}.$$

The spin-wave spectrum is shown in Fig. 23.

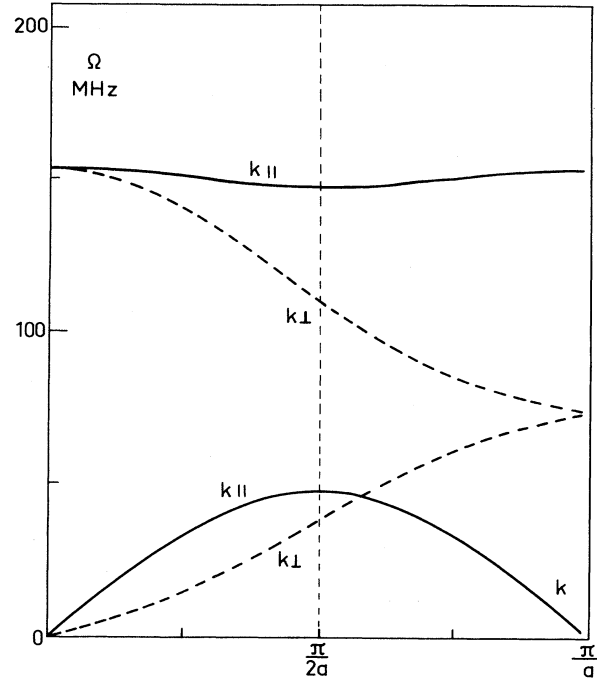


FIG. 23. Spin-wave spectrum of the udd phase within a two-parameter model ($J_i = -0.1$ mK; $K_P = -0.355$ mK). The eigenenergies are plotted vs k for two particular directions: solid lines, k_{\parallel} parallel to the anisotropy direction (001), i.e., perpendicular to the ferromagnetic planes; dashed lines, k_{\perp} perpendicular to (001), in the ferromagnetic planes. The zero- k frequency of the optical mode is $16\sqrt{K_P J_i} \simeq 150$ MHz.

2. Possible experimental investigations on the optical mode

It is interesting to speculate on how this mode might be observed. The optical mode corresponds to small variations of the relative angle between the directions of the two antiferromagnetic sublattices (A, A') and (BB'), with each antiferromagnetic sublattice conserving a zero magnetization. Consequently if we neglect the dipolar Hamiltonian \mathcal{H}_D we cannot excite the optical mode at $k=0$ by a uniform radiofrequency field of frequency ω . (If $[\mathcal{H}, \mathcal{H}_D] = 0$ we can only excite the Larmor frequency $\omega = \gamma H$ at $k=0$.)

The dipolar Hamiltonian, by itself, shows a coupling, reduced by the ratio $\langle \mathcal{H}_D \rangle / \langle \mathcal{H} \rangle$. This coupling is quite weak; therefore we can probably rule out magnetic resonance. However, the exchange Hamiltonian is strongly coupled to the phonons. By measuring the velocity and damping of sound waves, we could expect some effect at the crossing with the optical mode ($\omega \simeq 150$ MHz). The dependence of these measurements upon the orientation of the sound wave with respect to the crystal axis could give interesting information on the anisotropic variations of the exchange parameters in terms of the lattice deformations. Up to now the low-field phase has not been identified with certainty (see Sec. II.A.1). The experimental investigation of this mode would be a good test for the udd phase and the validity of our theory.

3. Experimental evidence of the acoustic mode at low temperature

At zero magnetic field the acoustical mode is accessible through measurement of the entropy as a function of temperature. Osheroff and Yu (1980) have measured the low-temperature pressure dependence of the phase line between the solid and the liquid. They find a T^4 variation in agreement with spin-wave theory. They find a T^3 specific heat,

$$\frac{C_v}{V} = \frac{4\pi^2}{15} \frac{k_B}{\hbar} (k_B T^3) \frac{1}{C^3}, \quad (9.14)$$

with the mean spin-wave velocity $C = 8.4$ cm/s.

This "mean spin-wave velocity C " can be calculated within our model. At low k , we can write

$$\lambda_+(k) = |k| (v_{\perp}^2 \sin^2 \theta + v_{\parallel}^2 \cos^2 \theta)^{1/2} = |k| C(\theta). \quad (9.15)$$

θ is the angle between k and the anisotropy direction OZ ; v_{\parallel} and v_{\perp} are the slopes at $k \simeq 0$ of the curves represented on Fig. 23 for k , parallel to $OZ = (001)$ and (100) , respectively (k is supposed small compared to $1/a$, but sufficiently large to neglect the dipolar anisotropy).

The magnetic energy and specific heat are obtained from the spin-wave acoustic modes $\lambda_+(k)$ in the same way that we usually calculate the lattice energy and specific heat from phonon modes. The only difference in the final formula is a factor $\frac{2}{3}$ due to the ratio of the number of spin-wave acoustic modes (two degenerate modes) to the number of phonon modes (three).

The number C defined in Eq. (9.14) is given by

$$\frac{1}{C^3} = \int \frac{1}{C^3(\theta)} \frac{d\Omega}{4\pi} = \frac{1}{v_{\parallel} v_{\perp}^2}. \quad (9.16)$$

The coefficients v_{\parallel}^2 and v_{\perp}^2 can be obtained in a straightforward way using Eq. (9.6) and expanding $\omega, \gamma, \nu, \eta$ [Eq. (9.2)] to second order in k . After tedious algebra some simplifications appear; the term

$$\chi_{\perp}^{-1} = -C_1^{-1} 2(2J_1 + J_2 + 4J_3 + 3K_P), \quad (9.17)$$

representing the inverse susceptibility χ_{\perp}^{-1} of the uudd phase, can be factored. We obtain finally (see Appendix D),

$$\begin{aligned} v_{\parallel}^2 &= \left[\frac{a}{\hbar} \right]^2 4(2J_1 + J_2 + 4J_3 + 3K_P) \\ &\quad \times [J_2 + 4J_3 - K_F - J_1^2 / (3K_P + K_F)], \\ v_{\perp}^2 &= \left[\frac{a}{\hbar} \right]^2 4(2J_1 + J_2 + 4J_3 + 3K_P)(K_F - J_2). \end{aligned} \quad (9.18)$$

This factorization is easily understood if we write the equations of spin hydrodynamics in solid ^3He , which are identical to those obtained in the anisotropic A phase of superfluid liquid ^3He (Graham and Pleiner, 1975). The order parameter is represented by the spin direction $\mathbf{n} = \mathbf{d}$.

\mathbf{l} is the anisotropy axis perpendicular to the ferromagnetic planes of the uudd phase.

From Eq. (13) of Graham and Pleiner (1975),

$$C = [(M_{\perp} k_{\perp}^2 + M_{\parallel}^2 k_{\parallel}^2) \cdot \chi_{\perp}^{-1} \cdot k^2]^{1/2},$$

we have

$$v_{\parallel}^2 = \frac{M_{\parallel}}{\chi_{\perp}} \quad \text{and} \quad v_{\perp}^2 = \frac{M_{\perp}}{\chi_{\perp}}. \quad (9.19)$$

χ_{\perp} is the perpendicular susceptibility [Eq. (9.17)]. M_{\perp} and M_{\parallel} represent the increase of the energy due to small gradients of the order parameter perpendicular and parallel, respectively, to \mathbf{l} . M_{\perp} and M_{\parallel} are calculated in Appendix C within the MFA. The expressions thus obtained give precisely Eq. (9.18) after using Eq. (9.19).

From Eq. (9.16) we obtain

$$\begin{aligned} C &= \left[\frac{a}{\hbar} \right] 2(2J_1 + J_2 + 4J_3 + 3K_P)^{1/2} (K_F - J_2)^{1/3} \\ &\quad \times \left[J_2 + 4J_3 - K_F - \frac{J_1^2}{3K_P + K_F} \right]^{1/6}. \end{aligned} \quad (9.20)$$

The energies (at $T=0$) of the uudd and ssqaf phases are, respectively,

$$\begin{aligned} E_{\text{uudd}} &= -\frac{N}{2} [J_2 - 2J_3 - (K_F + 3K_P)], \\ E_{\text{ssqaf}} &= \frac{N}{2} [J_2 + 2J_3 + 3K_P - K_F]. \end{aligned} \quad (9.21)$$

The spin-wave velocity cancels at the limit of stability between the two phases:

$$(E_{\text{uudd}} = E_{\text{ssqaf}}) \Leftrightarrow (K_F - J_2 = 0).$$

Our two-parameter fit ($J_i = -0.1$ mK, $K_P = -0.355$ mK) is close to this boundary. We obtain [see Eq. (5.11)] $K_F = 0$ and $J_2 = -4J_i + K_P \simeq 0.045$ mK. Thus the theoretical value of the velocity $C \simeq 5.8$ cm s $^{-1}$ is too small compared to Osheroff's value. Osheroff's experiments measure directly the cube of C . Thus we believe C to be known with good accuracy. In Sec. X we readjust our parameters to move away from the boundary $K_F - J_2 = 0$ to see if fitting C is compatible with other experimental information.

C. Spin fluctuation at $T=0$. Numerical evaluations

The spin fluctuations cause a lowering of the energy of the system. Their magnitude gives some idea of the importance of corrections to the molecular-field theory.

1. Corrections to the molecular-field energy at $T=0$

At zero temperature, the spin-wave energy differs from the molecular-field energy E_0 by the term [Eq. (9.3)]

$$\Delta E = \sum_k [\lambda_+ + \lambda_- - 2\omega(k)].$$

(It can be shown that this energy shift is always negative.)

After transforming the summation over the reciprocal lattice by an integration over the first Brillouin zone, we have calculated ΔE by Gaussian quadrature for the two-parameter model, $J_t = -0.1$ mK, $K_P = -0.355$ mK. We find for the uudd phase $\Delta E = -0.499$ mK. In the naf (spin-flop) phase at 0.9 T we find $\Delta E = -0.26$ mK.

The fact that the naf energy correction is smaller than that for the uudd means simply that the fluctuations are larger for the uudd phase. Consequently the transition field between the uudd and naf phases at $T=0$ is still larger in the spin-wave approximation than in the molecular-field approximation.

This seems in contradiction with the experiment giving a field of about 4 kG (Osherooff, 1982). However, the spin-wave corrections to the molecular-field energy are of the same order of magnitude as the difference of the molecular-field energy between the uudd and naf phase! It is consequently probable that even the spin-wave approximation is not reliable for evaluation of the transition field.

2. Zero-point spin deviation

The ground state $|0\rangle$ being different from the molecular-field state, the mean value of

$$\langle S_z \rangle = \frac{4}{N} \sum_{i \in \varphi_1} \langle 0 | S_z^i | 0 \rangle$$

differs from $\frac{1}{2}$. The spin deviation is

$$\begin{aligned} \langle \Delta S_z \rangle &= \frac{1}{2} - \langle S_z \rangle = \frac{4}{N} \sum_{i \in \varphi_1} \langle 0 | \alpha_{l,i}^+ \alpha_{l,i} | 0 \rangle \\ &= \frac{4}{N} \sum_{k \in \mathcal{R}_1} \langle 0 | \alpha_l^+(k) \alpha_l(k) | 0 \rangle. \end{aligned}$$

The α_l are expressed in terms of the e_i by solving Eq. (9.4), using the definitions given by Eqs. (9.5) and (9.7)–(9.10). With the obvious identities

$$\langle 0 | e_i^+ e_j | 0 \rangle = 0 \text{ and } \langle 0 | e_i e_j^+ | 0 \rangle = \delta_{ij},$$

we obtain

$$\begin{aligned} \langle 0 | \alpha_l^+(k) \alpha_l(k) | 0 \rangle &= r_- r_-^* + s_- s_-^* \\ &= \frac{1}{4} \left[\sum_{\substack{\varepsilon = \pm 1 \\ \varepsilon' = \pm 1}} (\mu_{\varepsilon'}^\varepsilon)^2 \right] \\ &\quad - \frac{1}{4} (\mu_+^+ \mu_-^+ + \mu_+^- \mu_-^-) (e^{2it} + e^{-2it}). \end{aligned}$$

The last term is simply $-\frac{1}{2}$ [see Appendix D, Eq. (D44)]. The first term is deduced from Eq. (9.9). We finally obtain

$$\begin{aligned} \langle \Delta S_z \rangle &= \frac{4}{N} \sum_k \left\{ \frac{1}{4} \left[\omega \left(\frac{1}{\lambda_+} + \frac{1}{\lambda_-} \right) \right. \right. \\ &\quad \left. \left. + \frac{\text{Re}(v\eta)}{(|v|^2 - c^2)^{1/2}} \left(\frac{1}{\lambda_+} - \frac{1}{\lambda_-} \right) \right] \right. \\ &\quad \left. - \frac{1}{2} \right\}, \end{aligned} \quad (9.22)$$

with [see Eq. (9.6)]

$$\text{Re}(v\eta) = 2[\omega |\eta|^2 - \gamma |v| |\eta| \cos akz].$$

Within the two-parameter model, $J_t = -0.1$ mK, $K_P = -0.355$ mK, we obtain $\langle \Delta S_z \rangle \simeq 0.175$, much larger than the value obtained for an ordinary antiferromagnet within a HNNA model ($\langle \Delta S_z \rangle \simeq 0.07$). The polarization at zero temperature is

$$p \simeq 1 - 2 \langle \Delta S_z \rangle \simeq 0.65.$$

Such large fluctuations call into question the validity of the molecular-field approximation and even the validity of this noninteracting spin-wave theory. This phase being “frustrated” (see Sec. VIII), such effects are not surprising. Further approaches using the random-phase approximation have been recently investigated by Iwahashi and Masuda (1981). The decoupling schemes used in such approximation are never fully consistent (even applied to the simple HNNA model). These decoupling schemes seem to us even more arbitrary if one attempts to generalize them to the four-spin Hamiltonian.

X. REFITTED TWO-PARAMETER MODEL, TAKING INTO ACCOUNT THE SPIN-WAVE VELOCITY

A. Determination of the parameters

The most accurate experimental data known about the nuclear magnetic order of bcc solid ^3He are certainly

- (i) the temperature of first-order transition $T_{C1} = 1$ mK,
- (ii) the high-temperature coefficient $\bar{\varepsilon}_2 \simeq 7 \pm 0.3$ mK,
- (iii) the mean spin-wave velocity $C \simeq 8.4 \pm 0.4$ cm s $^{-1}$.

The molecular-field theory can give only a rough evaluation of T_{C1} , and approximations beyond mean field seem very difficult to work with, especially with four-spin exchange. In contrast, the high-temperature coefficient $\bar{\varepsilon}_2$ has been exactly calculated with four-spin exchange, and we think the spin-wave theory developed in Sec. IX may give a reliable estimate of C at low temperature. Hence it now seems natural to use these two accurate data, $\bar{\varepsilon}_2$ and C , to determine the parameters J_t and K_P of a two-parameter model. Even if C is not calculated correctly, it is interesting to see what effect it has on the fits if we use it rather than T_{C1} as the crucial low-temperature parameter.

Figure 24 represents the variations of $\bar{\varepsilon}_2$ (solid lines) and C (dashed lines) in terms of (J_t, K_P) . The experimental results (ii) and (iii) above restrict the parameters to the shaded area. We note that this area is somewhat outside the domain limited by the errors on the measurements of Θ :

$$-3.3 \lesssim \Theta \lesssim -2.5 \text{ mK}.$$

Within the shaded area we choose a point M_2 giving the largest value of $|\Theta|$:

$$\begin{aligned} J_t &= -0.13 \text{ mK}, \\ K_P &= -0.385 \text{ mK}. \end{aligned}$$

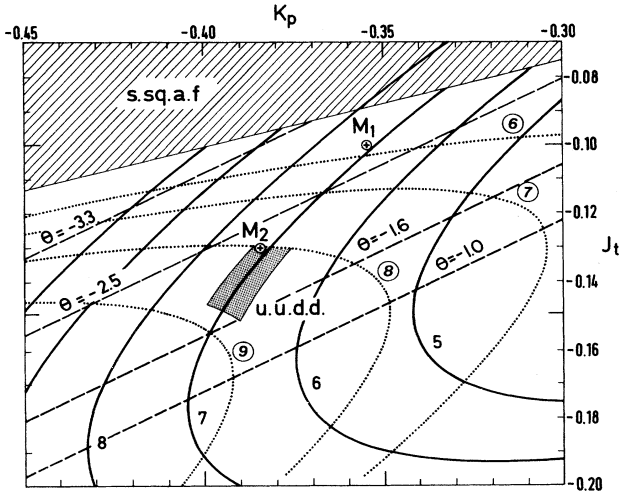


FIG. 24. Two-parameter model, planar four-spin exchange K_P and triple exchange J_t ; solid lines variation of $\bar{\epsilon}_2$ (in mK^2); dotted lines spin-wave velocity C (cm sec^{-1}). The experimental results on ϵ_2 and C restrict the parameters to the dotted area. The straight dashed lines are lines of constant Θ . Our first fit, represented by M_1 , is outside the domain given by Osheroff's results on C . The fit M_2 gives a value of Θ slightly below our estimation of the lower limit of Θ from the experiments. Considering the large experimental uncertainties, it can be considered as acceptable.

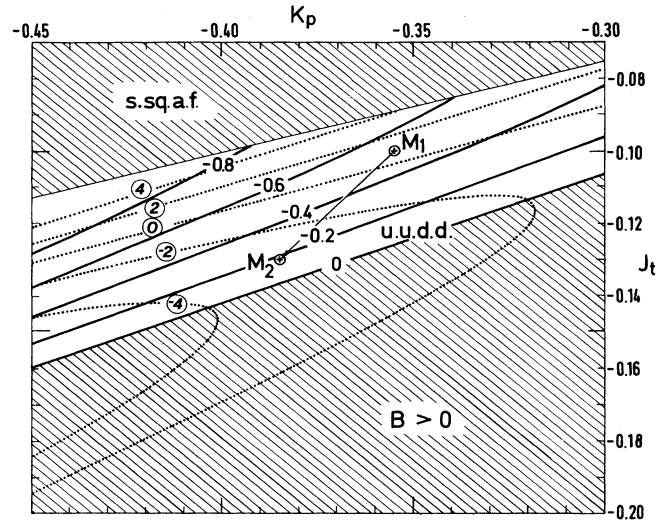


FIG. 25. Variations of B (mK^2) (solid lines) and $\bar{\epsilon}_3$ (mK^3) (dotted lines) within the same model (see Fig. 24). We exclude the lower dashed area corresponding to $B > 0$, which contradicts the experiments. In the rest of the domain, B is negative but small in magnitude. $\bar{\epsilon}_3$ is small but positive or negative. Our fit M_2 gives $\bar{\epsilon}_3 \approx -3 \text{ mK}^3$, which seems in contradiction with the experimental results available to date; however, more accurate measurements, taking into account higher terms, are needed.

We obtain $\Theta \approx -2.25 \text{ mK}$, which, given the low precision of the measurements, can still be considered reasonable.

Thus we have moved to M_2 at constant $\bar{\epsilon}_2$ from our first fit represented by M_1 , away from the boundary between the uudd and ssqaf phase, in order to increase the mean spin-wave velocity. The high-temperature coefficients B and $\bar{\epsilon}_3$ are represented in Fig. 25. At M_2 , $B = -0.2 \text{ mK}^2$ is smaller in magnitude than our first fit ($B \approx -0.6 \text{ mK}^2$) and $\bar{\epsilon}_3 = -3 \text{ mK}^3$ is negative but small.

Prewitt and Goodkind (1980) give a larger negative value of B ($B \approx -2.7 \text{ mK}^2$), while Hebral *et al.* (1979), Halperin (1979), Dundon and Goodkind (1975), and Mamiya *et al.* (1981) show that $\bar{\epsilon}_3 > 0$. However, it is probable that at low temperature the behavior of the susceptibility and specific heat involves a lot of higher-order terms. The discrepancy, therefore, with "apparent" values of B and $\bar{\epsilon}_3$, which are not very well measured (Hetherington, 1978), is perhaps not significant.

B. Phase diagram

The phase diagram, Fig. 26, differs only slightly from Fig. 21. The critical temperature T_{C1} of the first-order transition to the uudd phase is slightly higher, $T_{C1} \approx 1.2 \text{ mK}$. Since we know that the molecular-field approximation generally overestimates the critical temperature, this result is not unsatisfying. The helical phase $H100$ disappears. The critical field of transition between the udd and naf phase remains high: $H_c \approx 16 \text{ kG}$ at $T=0$, but

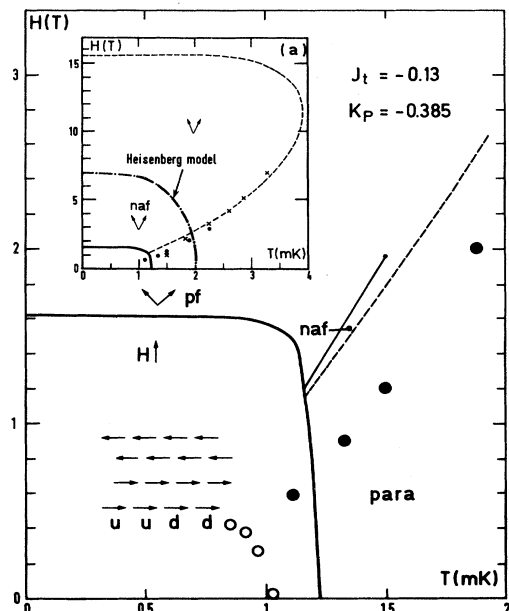


FIG. 26. Molecular-field phase diagram obtained with the two-parameter model $J_t = -0.13 \text{ mK}$; $K_P = -0.385 \text{ mK}$: solid line, first-order transition; dashed line, second-order transition. We compare to the experimental results: \times , second-order transition from Godfrin *et al.* (1980); \bullet , second-order transition obtained by Kummer *et al.* (1975, 1977); \circ , first-order transition from Kummer *et al.* (1975, 1977).

again both phases are almost degenerate, and we cannot trust the theoretical evaluation of this field within the molecular-field approximation.

The diagram of the high-field phase is comparable to that obtained with the first model and fits the experimental data of Godfrin *et al.* (1980) and Adams, Delrieu, and Landesman (1978) just as well.

C. Magnetization of the high-field phase

The theoretical curves of limiting pressure and magnetization in terms of the external field H are compared to the experimental results of Godfrin *et al.* (1980) in Fig. 27. The agreement is comparable to that obtained with the fit discussed in Sec. VIII (Fig. 22).

D. Susceptibility of the uudd phase

The molecular-field approximation gives [Eq. (8.11)]

$$\chi_{\perp} = -C_1[8(-4J_t + 3K_p)]^{-1} = C_1/5.08 \text{ mK} .$$

Prewitt and Goodkind (1977) give $\chi_{\perp} = C_1/5.2 \text{ mK}$; and Morii *et al.* (1978) give $C_1/5.9 \text{ mK} \lesssim \chi_{\perp} \lesssim C_1/5.2 \text{ mK}$.

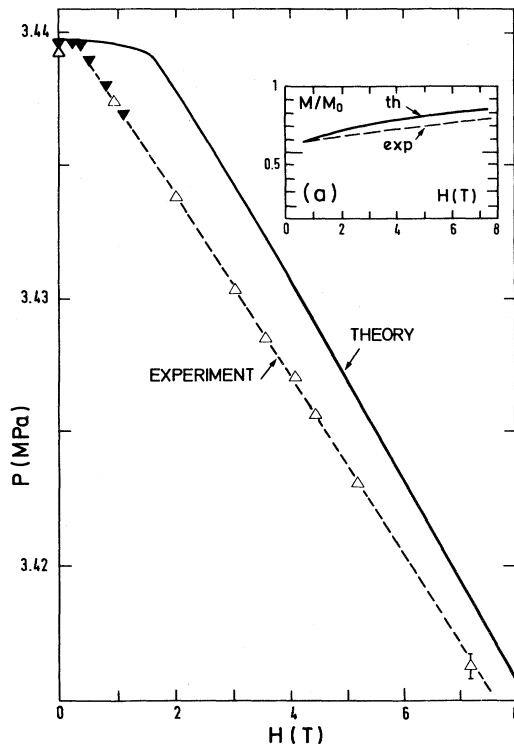


FIG. 27. Comparison of theory with experimental measurements of the limiting pressure $P(H)$ in a Pomeranchuk cell: dashed line, Δ experiments of Godfrin *et al.* (1980); \blacktriangledown , Kummer *et al.* (1977) as analyzed by Adams, Delrieu, and Landesman (1978); solid line, theoretical prediction of our two-parameter models. Inset (a) compares the experimental and theoretical magnetizations deduced from the slope $dP(H)/dH$.

As the fluctuations can lower the molecular-field value by 10–15% (as in an “ordinary” antiferromagnet), the agreement with experiment is satisfying.

E. Spin-wave calculations

1. Optical mode

The $k=0$ frequency of the optical mode is [see Eq. (D57)]

$$16\sqrt{6K_p J_t} \simeq 180 \text{ MHz} .$$

2. Mean spin-wave deviation at zero temperature

Using Eq. (9.22), we obtain

$$\langle \Delta S_z \rangle \simeq 0.13 .$$

The polarization is $\simeq 0.74$.

3. Nuclear-magnetic-resonance frequency in zero field

Taking the experimental results on the susceptibility [Eq. (8.12)], we evaluated in Sec. VIII, Eq. (8.13), the zero-field resonance frequency in MFA,

$$1150 \lesssim \Omega_0 \lesssim 1225 \text{ Hz} .$$

When we neglect the terms in $\sigma_i^+ \sigma_j^-$, the renormalization of the dipolar energy by the spin waves gives

$$851 \lesssim \Omega'_0 \simeq p \Omega_0 \lesssim 907 \text{ kHz} .$$

Finally the renormalization factor due to the motion of atoms (Sec. VIII) $\sqrt{0.95}$, gives

$$829 \lesssim \Omega''_0 \lesssim 884 \text{ kHz} ,$$

in good agreement with Osheroff's value.

4. Variation of the zero-field resonance frequency with the temperature

At low temperature, the polarization $p(T)$ can be estimated by applying boson statistics:

$$\langle 0 | e_i^+(k) e_i(k) | 0 \rangle = n_k = [\exp(\lambda_i/k_B T) - 1]^{-1} .$$

We have $p(T) = (1 - 2\langle \Delta S_z \rangle)$ and, from Sec. IX,

$$\langle \Delta S_z \rangle = \frac{4}{N} \sum_{k \in \mathcal{R}_1} \langle | \alpha_l^+(k) \alpha_l(k) | \rangle .$$

The $\alpha_l(k)$ are transformed into the $e_i(k)$ by the relations in Sec. IX.

We finally obtain for $\langle \Delta S_z \rangle$, Eq. (9.22) except that the λ 's are replaced by their thermal averages,

$$\frac{1}{\langle \lambda_{\pm} \rangle} = \frac{1}{\lambda_{\pm}} \left\{ \frac{2}{\exp(\lambda_{\pm}/h_B T) - 1} + 1 \right\}$$

and $p(T) = 1 - 2\langle \Delta S_z \rangle$.

The variations of $p^2(T)/p^2(0)$ so determined are compared to the curve $\Omega^2(T)/\Omega^2(0)$ obtained by Osheroff in Fig. 28.

The difference between the two curves does not exceed 10%. This comparison presupposes that the dipolar energy is essentially renormalized by a factor p , neglecting the terms in $\langle \sigma_i^+ \sigma_j^- \rangle$. Calculation of the dipolar energy in the complete spin-wave approximation should give a more reliable comparison.

XI. THREE-PARAMETER MODELS

Up to now we have completely neglected pair exchange J_{NN} and folded four-spin exchange K_F . It is interesting to see whether we can improve the quantitative agreement with all available data by including one of these types of exchange.

A. Three-parameter model including J_t, K_P, K_F

1. High-temperature results

As emphasized before, the high-temperature coefficient determined experimentally with best accuracy is certainly

$$\tilde{\epsilon}_2 \simeq 7.0 \pm 0.3 \text{ mK}^2.$$

From Sec. VI we have [Eq. (6.13)]

$$\begin{aligned} \tilde{\epsilon}_2 = & 576J_t^2 - (144J_{\text{NN}} + 576K_F + 504K_P)J_t \\ & + 12J_{\text{NN}}^2 + 72J_{\text{NN}}(K_F + K_P) + 175.5K_F^2 \\ & + 153K_P^2 + 252K_F K_P. \end{aligned} \quad (11.1)$$

For the first model, we assume $J_{\text{NN}} = 0$. We choose K_F and K_P as independent variables, and take $\tilde{\epsilon}_2 = 7$, so that Eq. (11.1) is a second-order equation for J_t . Of the two solutions, we retain only that with the plus sign before the

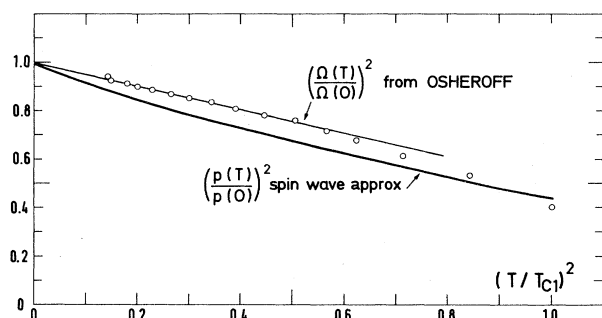


FIG. 28. The variation of the zero-field resonance frequency Ω vs T , obtained by Osheroff, Cross, and Fisher (1980), compared to the theoretical calculation of the polarization $\langle T \rangle$ in the spin-wave theory. Both $\Omega(T)$ and $p(T)$ are normalized to the values at $T=0$. The two curves agree within 10%. This rough comparison neglects the terms in $\langle \sigma^+ \sigma^- \rangle$ in the spin-wave calculation of the dipolar energy.

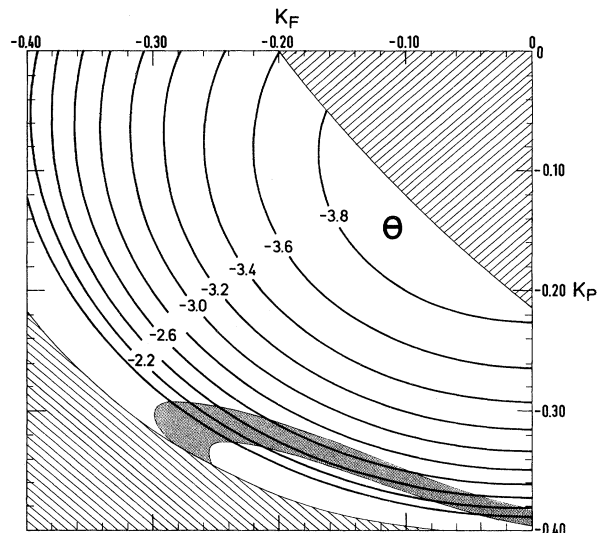


FIG. 29. Three-parameter models including triple exchange J_t and the two kinds of four-spin exchanges K_P and K_F . From accurate experimental results we take $\tilde{\epsilon}_2 = 7$. This gives a quadratic relation between the parameters. We choose K_F and K_P as independent variables. The quadratic equation has no real root in the lower dashed area. The upper dashed area corresponds to $J_t < 0$ and is also excluded. The contours are lines of constant Θ in mK. The shaded area corresponds (cf. Fig. 31) to a spin-wave velocity $8 < C < 8.8 \text{ cm s}^{-1}$ according to Osheroff's results.

radical, the other giving unphysical low negative or positive values of Θ . The high-temperature coefficient Θ is shown in Fig. 29 in terms of K_F, K_P .

2. Stable phase at $T=0$ and $H=0$

We have minimized the free energy by computer, according to the method described in Sec. VII for a limited number of points distributed in the plane (K_F, K_P) . (J_t is determined as described.) Four possible phases have thus been found, depending on the parameters: scaf, ssqaf, pf, uudd. The stability domains of each phase are shown in Fig. 30.

3. Mean spin-wave velocity

For the uudd phase, the mean spin-wave velocity is represented in Fig. 31. Osheroff's result, $C = 8.4 \pm 0.4 \text{ cm s}^{-1}$, restricts the parameters to the shaded area in Figs. 29 and 31. Figure 31 shows that with C constant, B increases with K_F . Introducing K_F can also slightly increase the value of $|\Theta|$. Inside the shaded area $\tilde{\epsilon}_3$ remains quite low: $\tilde{\epsilon}_3 \lesssim 2 \text{ mK}^3$.

4. Choice of a set of parameters

We determine the parameters in order to fit the spin-wave velocity of Osheroff (shaded area) and the value of $B \simeq -2.7 \text{ mK}^2$ given by Prewitt and Goodkind. The

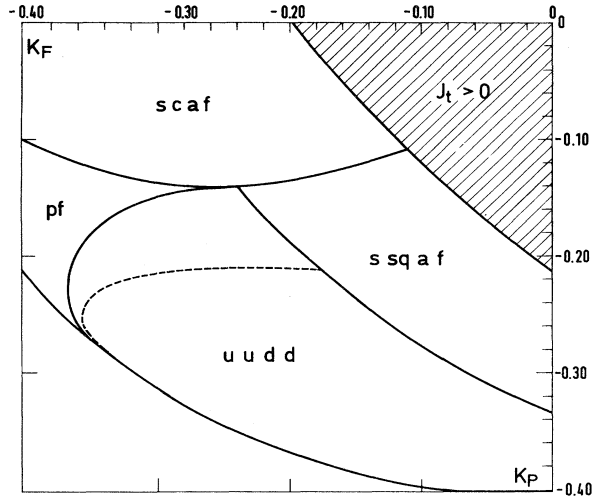


FIG. 30. Phases found in mean-field theory at zero field and low temperature as a function of K_F and K_P , where J_t is determined by the constraint $\bar{\epsilon}_2 = 7 \text{ mK}^2$ as in the previous figure.

point in the (K_F, K_P) plane is chosen at the upper limit of the shaded area in order to obtain the largest possible values of $\Theta \simeq 2.7 \text{ mK}$ and $\bar{\epsilon}_3 \simeq 2 \text{ mK}^3$.

We therefore propose

$$K_P = -0.33 \text{ mK},$$

$$K_F = -0.15 \text{ mK},$$

$$J_t = -0.165 \text{ mK},$$

and thus have $C \simeq 8 \text{ cm s}^{-1}$ and $\bar{\epsilon}_2 = 7 \text{ mK}^2$. Furthermore, $\bar{\epsilon}_3 \simeq +2 \text{ mK}^3$, and thus is positive in agreement with the experimental results, while $\Theta \simeq -2.7 \text{ mK}$, and $B \simeq -2.7 \text{ mK}^2$, in agreement with Prewitt and Goodkind (1980). All high-temperature results plus the spin-wave velocity are thus quantitatively satisfied.

5. Phase diagram

The phase diagram obtained with this parameter set is represented in Fig. 32.

The critical temperature of the first-order transition in zero field is approximately (see Sec. VIII)

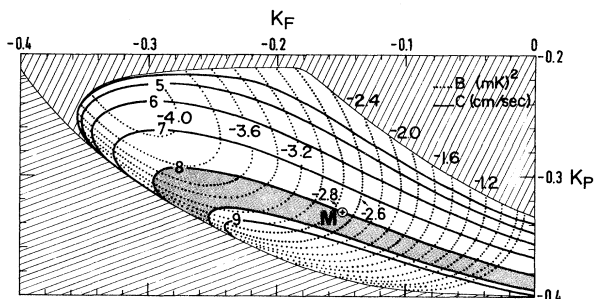


FIG. 31. The variation of the quantities B and C in the uudd part of the phase diagram of the previous figure.

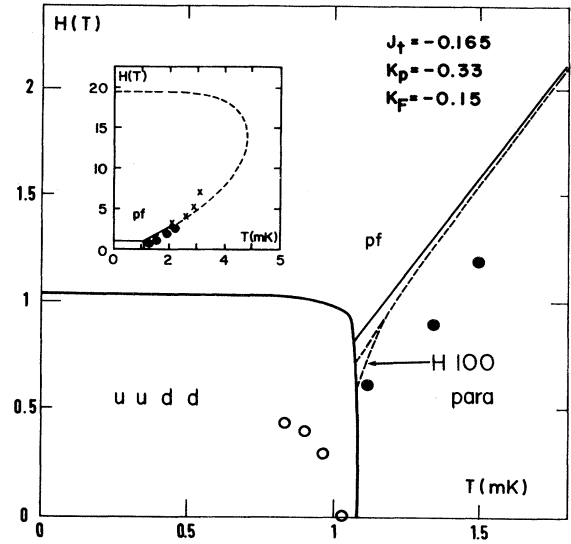


FIG. 32. The phase diagram in the H - T plane as determined by mean-field theory with parameter values corresponding to point M of Fig. 31.

$$T_{C1} \simeq -E_{\text{uudd}}(T=0)/\ln 2,$$

$$T_{C1} \simeq -(2J_t + \frac{3}{2}K_P - \frac{1}{2}K_F)/\ln 2 \simeq 1.08 \text{ mK}.$$

The high-field phase diagram is roughly the same as that obtained in the two-parameter model. The molecular-field value of the critical field at $T=0$ between the uudd and naf phase,

$$H_C \simeq 8 \text{ kG},$$

is lower than that obtained with the preceding models, and in better agreement with the experimental results. Thus this model seems to fit all the experimental data better. We note that the first-order transition line between the pf and naf phase (see Sec. VII) goes up to a very high field, of the order of 20 kOe.

6. Susceptibility and zero-field resonance frequency

The molecular field susceptibility is

$$\chi = -C_1 [8(-4J_t + 2K_F + 3K_P)]^{-1} \simeq \frac{C_1}{5.04} \text{ mK},$$

in agreement with the experimental value.

The spin-wave calculation gives

$$p \simeq 0.65.$$

Taking the experimental value of the susceptibility, we obtain after renormalization (see Sec. VIII)

$$730 < \Omega_0'' < 780 \text{ kHz}.$$

The performance of this three-parameter model is among those compared in Table I below.

B. Three-parameter model including J_{NN}, J_t, K_P

For this model we follow the same scheme as in the preceding paragraph. We take $\bar{\epsilon}_2 = 7 \text{ mK}^2$ and choose (J_{NN}, K_P) as independent variables; J_t is given by Eq. (11.1), with $K_F \equiv 0$. As in the preceding case, only one of the two roots gives physical values of Θ . Osheroff's result on the spin-wave velocity is used to restrict the parameters. With this restriction,

- (i) B remains negative but small, $|B| < -0.5 \text{ mK}^2$;
- (ii) e_3 is negative ($\bar{\epsilon}_3 \leq -2$);
- (iii) $|\Theta|$ is small, $|\bar{\Theta}| \lesssim 2.4 \text{ mK}$.

Thus introducing J_{NN} does not improve the agreement with the high-temperature results.

On the phase diagram, the main tendency of pair exchange J_{NN} is to favor the naf phase. (We recall that the naf phase is the phase which appears with only J_{NN} , i.e., the HNNA model.) Hence, with J_{NN} sufficiently large,

- (i) the transition field at $T=0$ between the udd and naf phase decreases;
- (ii) the ferromagnetic tendencies decrease; in particular, the first-order transition line between the naf and pf phases ends at lower field;
- (iii) the second-order critical temperature of the naf phase increases and is larger than the critical temperature of first-order transition to the udd phase, within the MFA; we thus obtain a molecular-field phase diagram similar to that presented by Hetherington and Willard (1975).

Thus, although an admixture of J_{NN} exchange is not eliminated, it does not seem to significantly improve the overall fit to the data.

XII. SUMMARY

The theoretical predictions of the multiple exchange models are summarized in Table I (columns 1 and 3). They all agree qualitatively (also quantitatively, for most of them) with the experimental results shown in column 1. The contrast with the predictions of the HNNA model is underlined again in column 4.

Columns 2 and 3 represent, respectively,

Model 1. The two-parameter fit $J_t = -0.13 \text{ mK}$; $K_P = -0.385 \text{ mK}$, $K_F = 0$ proposed in Sec. X.

Model 2. The three-parameter fit $J_t = -0.165 \text{ mK}$; $K_F = -0.15 \text{ mK}$, $K_P = -0.33 \text{ mK}$ discussed in Sec. XI.

Both models agree qualitatively with the data. Model 2 gives a better quantitative agreement with high temperature results.

A. Phase diagram

The essential feature of the phase diagram is the evidence of two almost degenerate phases with absolutely

different characters which compete at low field.

At low field, the stable phase is antiferromagnetic. Its noncubic udd structure gives a resonance spectrum with a large zero-field resonance frequency in quantitative agreement with the results of Osheroff *et al.* (1980). Its low-field susceptibility agrees with the experimental results (Prewitt and Goodkind, 1977; Morii *et al.*, 1978). The spin-wave spectrum gives, at low k , a mean spin-wave velocity in quantitative agreement with the results of Osheroff and Yu (1980). At $T \simeq 1 \text{ mK}$ this phase undergoes a strong first-order transition to the paramagnetic phase.

When the magnetic field is increased, our model predicts a first-order transition to a two-sublattice phase with strong ferromagnetic tendencies. Its symmetry is that of a "normal antiferromagnetic" spin-flopped phase. However, its uniqueness lies in its large spin-flopped angle, giving an unusually large magnetization (0.6 times the saturation magnetization M_0 at the transition field), varying slowly with the field and extrapolating to a finite value $\simeq 0.5M_0$ at zero field. This is in perfect quantitative agreement with the experimental results of Godfrin *et al.* (1980).

As the temperature is increased, this phase undergoes a second-order transition to the paramagnetic phase at a critical temperature $T_{c_2}(H)$, increasing with H up to $H \simeq 12 \text{ T}$. Then $T_{c_2}(H)$ decreases with H to reach zero at a critical field H_{c_2} of order 15 T. The phase diagram has been investigated up to 7 T by Godfrin *et al.* (1980) and agrees with our theory. We urge experimentalists to explore the upper part of the phase diagram, which remains unknown. As shown recently by Hetherington (1981), the value of H_{c_2} calculated in MFA is exact. Thus we expect the MFA to be very accurate at high field and to lead to a reliable comparison with experimental results.

In contrast, at low field, we do not expect from the MFA more than qualitative information. In particular, our prediction of the field of transition between the udd and high-field phase, which results from the comparison between two almost degenerate energies, cannot be stated with accuracy. It is estimated to be 1.5 T in Model 1 and $\simeq 1 \text{ T}$ in Model 2. The experimental value of this first-order transition field, recently measured at 0.5 mK by Osheroff (1982), is 0.4 T.

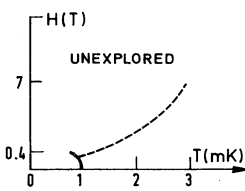
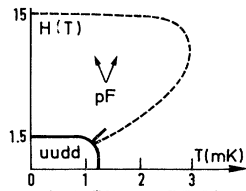
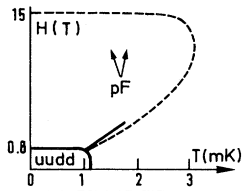
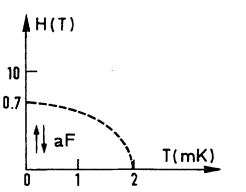
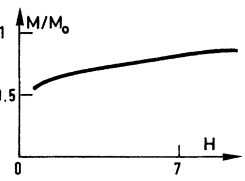
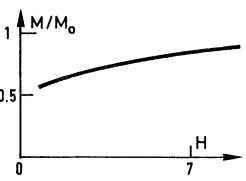
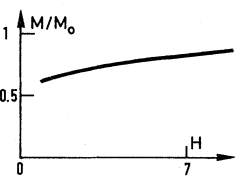
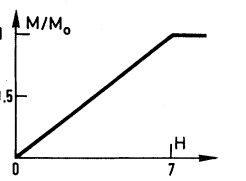
Our model also gives in the high-field phase a first-order transition line, ending at some critical point corresponding to a change of the spin-flopped angle and a change in the sublattice polarization. We point out that Osheroff (1982) recently observed in this region a first-order transition which could correspond to this line. Further experimental investigations in this area—where several transition lines meet—are needed. In addition, approximations beyond the MFA are needed in the critical region.

B. High-temperature series expansions

1. Zero-field expansion of the partition function

Our parameters have always been adjusted to fit the coefficient $\bar{\epsilon}_2$ of the T^{-2} term, which is experimentally

TABLE I. Comparison of various models of solid ^3He with experimental results.

	Experimental results	Triple exchange and planar four-spin exchange $J_t = -0.13$ mK $K_P = -0.385$ mK	Triple exchange + both kinds of four-spin exchange $J_t = -0.165$ mK $K_F = -0.15$ mK $K_P = -0.33$ mK	Heisenberg first neighbor $J_1 = -0.75$ mK
High-temp data				
Susceptibility	$\Theta \approx \begin{cases} -3 \text{ mK}^a \\ -2.6 \text{ mK}^b \end{cases}$	$\Theta \approx -2.25$ mK	$\Theta \approx -2.7$ mK	$\Theta = -3$ mK
$\chi^{-1} = c(T - \Theta + \frac{B}{T} \dots)$	$B = -2.7 \text{ mK}^{2b}$	$B \approx -0.2 \text{ mK}^2$	$B \approx -2.7 \text{ mK}^2$	$B = +2.25 \text{ mK}^2$
Specific heat	$\tilde{e}_2 = 7 \text{ mK}^{2c}$	$\tilde{e}_2 \approx 7 \text{ mK}^2$	$\tilde{e}_2 \approx 7 \text{ mK}^2$	$e_2 = 6.8 \text{ mK}^2$
$C_v = \frac{R}{4} \left(\frac{\tilde{e}_2}{T^2} - \frac{\tilde{e}_3}{T^3} \right)$	$\tilde{e}_3 = \begin{cases} 24 \text{ mK}^d \\ 2 \text{ mK}^{3e} \end{cases}$	$\tilde{e}_3 \approx -3 \text{ mK}^3$	$\tilde{e}_3 \approx +2 \text{ mK}^3$	$\tilde{e}_3 = -5 \text{ mK}^3$
PHASE DIAGRAM				
Low-field phase				
Structure	Resonance spectrum ^f in agreement with uudd	uudd	uudd	antiferromagnetic
Susceptibility	$\frac{c}{5.9} < \chi < \frac{c}{5.2}^g$	$\chi = \frac{c}{5.08}$	$\chi = \frac{c}{5.04}$	$\chi = \frac{c}{6}$
Zero-field resonance frequency	$\Omega_0 = 825 \text{ kHz}^f$	$800 \lesssim \Omega_0 \lesssim 860 \text{ kHz}$	$700 \lesssim \Omega_0 \lesssim 760 \text{ kHz}$	cubic anisotropy $\Omega_0 \lesssim 1 \text{ kHz}$
Mean spin-wave velocity	$c = 8.4 \pm 0.4 \text{ cm s}^{-1h}$	$c = 8 \text{ cm s}^{-1}$	$c = 8 \text{ cm s}^{-1}$	
High-field phase				
	High magnetization varying from $0.6M_0$ to $0.75M_0$ between 4 and 72 kG ⁱ	High magnetization varying from $0.6M_0$ at 15 kG to $0.8M_0$ at 72 kG	High magnetization varying from $0.6M_0$ at 8 kG to $0.8M_0$ at 72 kG	Only one phase antiferromagnetic
Magnetization curves				

^aKirk, Osgood, and Garber 1969.^bPrewitt and Goodkind, 1977.^cPanczyk and Adams, 1970.^dDundon and Goodkind, 1974, 1975.^eHebral *et al.* 1979.^fOsheroff, *et al.*, 1980.^gMorii *et al.*, 1978.^hOsheroff and Yu, 1980.ⁱGodfrin *et al.*, 1980.

measured with accuracy. The next coefficient $\tilde{\epsilon}_3$ is not determined with good precision but is proved to be positive. Recent measurements (Mamiya *et al.*, 1981) indicate that it is quite large. Our first fit (Model 1) gives $\tilde{\epsilon}_3$ small and negative, while the second fit (Model 2) leads to a positive but too small value of $\tilde{\epsilon}_3$.

2. Susceptibility

Both fits give a theoretical value of Θ in agreement with the experimental results (taking into account the low precision on the experimental value).

One of the first observed unexpected features of bcc ^3He was the increase in susceptibility with respect to the Curie-Weiss law corresponding to $B < 0$. Both fits 1 and 2 give negative values of B . Only fit 2 gives a large $|B|$ in agreement with the results of Prewitt and Goodkind.

Such a long list of data fitted with only two or three adjustable parameters gives good confidence in the validity of the multiple exchange model. Of course some features of the model are not exclusive properties of a multiple exchange Hamiltonian. In particular, it has been proven by renormalization-group methods that the udd structure always gives a first-order transition to the paramagnetic phase, independently of any model (Bak and Rasmussen, 1981). However, this general technique does not tell us if the first-order transition is sufficiently strong. One also needs a model that explains why the udd phase appears, which the multiple exchange model does.

Perhaps the strongest evidence for the multiple exchange model is the observation of the high-field phase, whose unusual features are qualitatively predicted if strong four-spin exchange (of any kind!) is introduced.

XIII. GENERAL PERSPECTIVE

The great theoretical fascination with solid ^3He is that it represents a system wherein one might hope to comprehend all the physical phenomena directly in terms of electromagnetic interactions and quantum mechanics. Few if any other solids offer this hope. In addition, the quantum effects are large in helium and intrinsically interesting. The path is rather long nevertheless: First, one calculates the wave function for helium atoms, then the Lennard-Jones potential, and then the wave function for the solid. Furthermore, we have that in order to understand the magnetic properties, we must deduce the solid wave function in a difficult region of configuration space and from that calculate the quantum tunneling exchange rate. Finally, one obtains from this a pseudo-Hamiltonian, which must be solved for the magnetic properties and phase diagram. It is now possible to think that we know the basic physics behind each of these steps and that improvements will be made by better approximations at each step of the way rather than by new concepts of what must be approximated. At this time we cannot be sure of this. The physics behind the exchange may be more complicated than that proposed here or different.

However, any completely new theory must fit the rather large number of parameters and qualitative features that we have been able to fit with two or three parameters.

Perhaps the most puzzling conceptual question is why more than one exchange (J_t , K_P , and perhaps K_F) is necessary (see Sec. VIII.A) to obtain successful fits. A simple argument based on the tunneling theory we have presented leads one to think that in all probability only one type of exchange would dominate: The tunneling is an exponential of a quantity which should be very different from one type of exchange to another. Therefore, it seems improbable that if the tunnelings are distinct processes they should happen to be nearly of the same order of magnitude.

Furthermore, all data which have been so far obtained above the melting pressure can be correlated by assuming that the Hamiltonian depends essentially on one unique parameter, which scales with the specific volume approximately as v^{18} . If these results are confirmed, one might conjecture that the various types of exchange go by some single mechanism we have not investigated. For instance, if ground-state vacancies exist and are in sufficient number, they may play an essential role in the exchange mechanism.

Another mechanism which would explain the near equality of the magnitudes of the exchanges is the possibility of a liquidlike intermediate state ("doorway state" in nuclear physics parlance). A few atoms could transform to this liquid ordering in a sort of bubble, then return to the solid form again with several more or less equally probable permutations. As pressure is increased, this bubble would have higher energy and might therefore lead to a single functional variation with volume, at least over a limited volume range. The basic ideas of Sec. IV would still be valid, but would require careful calculation.

It is possible of course that two exchange mechanisms just happen to be of the same size and because the exchange path lengths and potential barriers are approximately equal, they might also vary the same way with volume.

As we move to a higher pressure regime, our conjecture that one exchange should dominate may become more correct. One might expect either K_P or J_t exchange to become most prominent at, say, 21 cc/mole. In this case we would expect either a ferromagnetic second-order transition, if J_t dominates, or the ssqaf phase at low field if K_P dominates (K_F would lead to the scaf phase). As pointed out, because of the triangular coordination in the hcp solid, one would expect mainly triple exchange J_t and thus ferromagnetism at about 50 μK and 100 atmospheres.

But these speculations have a certain mundane quality, while solid ^3He can surely be depended upon for still more surprises.

APPENDIX A: VARIATIONAL METHOD FOR THE TUNNELING PSEUDOPOTENTIAL

In Sec. IV.C we propose to correct the usual trial wave function $\phi(\mathbf{r})$ (i.e., the product of a Jastrow wave function

and a phonon eigenfunction), along the line $\mathcal{L}(t)$, following the middle of the "duct," by multiplying it by an appropriate one-dimensional function $f(t)$:

$$\psi(\mathbf{r}) = \phi(\mathbf{r})f(t(\mathbf{r})) .$$

\mathbf{r} is a $3N$ -dimensional variable represented by a point $M(\mathbf{r})$ in the configuration space; t is the curvilinear coordinate of the orthogonal projection (i.e., closest point) of $M(\mathbf{r})$ on the path $\mathcal{L}(t)$. From the variational principle the one variable function $f(t)$ is determined to minimize the quantity

$$I = \langle |(\nabla\psi)^2| - (E - U)|\psi|^2 \rangle . \quad (\text{A1})$$

$\langle \rangle$ means the integration over the $3N$ -dimensional configuration space. We now prove that the condition

$$\delta I = 0 \quad (\text{A2})$$

leads to a simple one-dimensional Schrödinger equation for $f(t)$.

With

$$\delta\psi = \phi\delta f \quad (\phi \text{ is given})$$

Eq. (A2) gives

$$\delta I = \delta f \{ \langle \phi \nabla^2(\phi f) \rangle_{\perp} + \langle (E - U)\phi^2 f \rangle_{\perp} \} = 0 , \quad (\text{A3})$$

$\langle \rangle_{\perp}$ meaning the integration over the $(3n - 1)$ -dimensional space orthogonal to the tangent to the trajectory $\mathcal{L}(t)$ at the point of coordinate t .

If $\mathcal{L}(t)$ is a straight line, we can easily separate, in Eq. (A2), t and the $3N - 1$ orthogonal variables. Using the relation

$$\nabla^2(\phi f) = \phi \nabla^2 f + 2\nabla\phi \cdot \nabla f + f \nabla^2 \phi ,$$

we can write Eq. (A3)

$$\begin{aligned} \frac{\partial^2 f}{\partial t^2} \cdot \langle \phi^2 \rangle_{\perp} + 2 \frac{\partial f}{\partial t} \left\langle \phi \frac{\partial}{\partial t} \phi \right\rangle_{\perp} \\ + f \langle \phi \nabla^2 \phi \rangle_{\perp} + f \langle (E - U)\phi^2 \rangle_{\perp} = 0 . \end{aligned} \quad (\text{A4})$$

This equation can be simplified if we define a new function $\tilde{\phi}$ such that, for each value of t ,

$$\langle \tilde{\phi}^2 \rangle_{\perp} = 1 .$$

Hence we take

$$\begin{aligned} \tilde{\phi} &= \phi\theta(t), \quad \tilde{f}(t) = \theta^{-1}(t)f(t), \\ \psi &= \tilde{\phi}\tilde{f}(t) \end{aligned} \quad (\text{A5})$$

with

$$\theta(t) = \langle \phi^2 \rangle_{\perp}^{-1/2} .$$

With this choice, the second term of Eq. (A4),

$$2 \frac{\partial f}{\partial t} \left\langle \phi \frac{\partial}{\partial t} \phi \right\rangle_{\perp} = \frac{\partial f}{\partial t} \left\langle \frac{\partial}{\partial t} \phi^2 \right\rangle_{\perp} = \left[\frac{\partial f}{\partial t} \right] \left[\frac{\partial}{\partial t} \langle \phi^2 \rangle_{\perp} \right] ,$$

is null ($\langle \tilde{\phi}^2 \rangle_{\perp}$ being constant). Equation (A4) can be written

$$-\frac{\partial^2}{\partial t^2} \tilde{f}(t) + (\langle U\tilde{\phi}^2 \rangle_{\perp} - \langle \tilde{\phi} \nabla^2 \tilde{\phi} \rangle_{\perp}) \tilde{f}(t) = E \tilde{f}(t) . \quad (\text{A6})$$

Hence $\tilde{f}(t)$ is a solution of a one-dimensional Schrödinger equation with effective potential

$$\tilde{V}(t) = \langle U\tilde{\phi}^2 \rangle_{\perp} - \langle \tilde{\phi} \nabla^2 \tilde{\phi} \rangle_{\perp} .$$

We usually take $\tilde{\phi}$ as a product of one-particle wave functions. In this case it is useful to express $\tilde{\phi} \nabla^2 \tilde{\phi}$ in a more convenient form. For any function ϕ , we can write

$$\nabla^2 \tilde{\phi} = e^{\ln \nabla^2 \tilde{\phi}} = \nabla(\tilde{\phi} \nabla \ln \tilde{\phi}) = \tilde{\phi} \nabla^2 \ln \tilde{\phi} + (\nabla \phi) \nabla \ln \tilde{\phi} .$$

Thus

$$\langle \tilde{\phi} \nabla^2 \tilde{\phi} \rangle_{\perp} = \langle \tilde{\phi}^2 \nabla^2 \ln \tilde{\phi} \rangle_{\perp} + \langle (\nabla \tilde{\phi})^2 \rangle_{\perp} .$$

On the other hand, the integration by parts of $\langle \tilde{\phi} \nabla^2 \tilde{\phi} \rangle_{\perp}$ gives

$$\langle \tilde{\phi} \nabla^2 \tilde{\phi} \rangle_{\perp} = - \langle (\nabla \tilde{\phi})^2 \rangle_{\perp} .$$

Adding these two last equations, we obtain

$$2 \langle \tilde{\phi} \nabla^2 \tilde{\phi} \rangle_{\perp} = \langle \tilde{\phi}^2 \nabla^2 \ln \tilde{\phi} \rangle_{\perp} .$$

If ϕ is a product, it is easier to deal with the right-hand side of this equation. With $\tilde{\phi} = \phi\theta(t)$ we obtain

$$\begin{aligned} \langle \tilde{\phi} \nabla^2 \tilde{\phi} \rangle_{\perp} &= \frac{1}{2} \langle \tilde{\phi}^2 \nabla^2 \ln \tilde{\phi} \rangle_{\perp} \\ &= \frac{1}{2} \theta^2 \langle \phi^2 \nabla^2 \ln \phi \rangle_{\perp} + \frac{1}{2} \theta^2 \langle \phi^2 \rangle_{\perp} \frac{\partial^2}{\partial t^2} \ln \theta . \end{aligned}$$

Since $\theta = \langle \phi^2 \rangle_{\perp}^{-1/2}$, the second term can be written $-\frac{1}{4} (\partial^2 / \partial t^2) \ln \langle \phi^2 \rangle_{\perp}$. Substituting in Eq. (A6), we finally obtain

$$-\frac{\partial^2}{\partial t^2} \tilde{f}(t) + V(t) \tilde{f}(t) = E \tilde{f}(t) , \quad (\text{A7})$$

with

$$V(t) = \frac{\langle U\phi^2 \rangle_{\perp}}{\langle \phi^2 \rangle_{\perp}} - \frac{1}{2} \frac{\langle \phi^2 \nabla^2 \ln \phi \rangle_{\perp}}{\langle \phi^2 \rangle_{\perp}} - \frac{1}{4} \frac{\partial^2}{\partial t^2} \ln \langle \phi^2 \rangle_{\perp} . \quad (\text{A8})$$

APPENDIX B: SERIES EXPANSION DETAILS

We give here some details of the high-temperature series expansion described in Sec. VI.

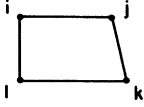
We are led to calculate $\langle \mathcal{H}_{\text{ex}}^n \rangle = \text{tr} \mathcal{H}_{\text{ex}}^n e^{-\beta \mathcal{H}_z}$. The exchange Hamiltonian \mathcal{H}_{ex} contains two-spin terms $\sigma_i \cdot \sigma_j$, represented by

$$\overline{ij}$$

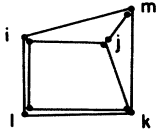
and four-spin terms,

$$\begin{aligned} \mathcal{L}_{ijkl}^{\lambda_{\alpha}} &= (\sigma_i \cdot \sigma_j)(\sigma_k \cdot \sigma_l) + (\sigma_i \cdot \sigma_l)(\sigma_j \cdot \sigma_k) \\ &\quad + \lambda_{\alpha} (\sigma_i \cdot \sigma_k)(\sigma_j \cdot \sigma_l) , \end{aligned}$$

schematized by



$\mathcal{H}_{\text{ex}}^n$ is expanded as a sum of products of these elementary terms; each product is represented by a diagram. For instance,



represents $\mathcal{S}_{ijkl}^{\lambda_\alpha} \mathcal{S}_{imkl}^{\lambda_\beta} \sigma_j \cdot \sigma_m$ in $\mathcal{H}_{\text{ex}}^3$.

We list here all the diagrams occurring in the calculation of $\langle \mathcal{H}^n \rangle$, $n \leq 3$, their respective number, trace (weighted by $e^{-\beta \mathcal{H}^z}$), and contribution to the cumulants K_n (see Sec. VI). Table II represents the results concerning the second-order term in β^2 : $K_2 = \langle \mathcal{H}^2 \rangle - \langle \mathcal{H} \rangle^2$. The topological structure of each diagram is sketched in the second column. In the first column we indicate the product of the coefficients $(-K_\alpha/4)^p \cdot (-J_n/2)^q$, $p+q=n$ [see Eq. (6.1)] corresponding to each diagram.

The same labeled diagram, representing a product of n terms in \mathcal{H}^n , occurs ν times in \mathcal{H}^n , ν being the number of ways of ordering the different terms of the product ($\nu/n!$ is usually called the symmetry factor of the diagram). ν is indicated in column 3. The number of unlabeled diagrams of each type is shown in column 4. The trace of each term is shown in column 5. Column 7 represents the contribution of the corresponding disconnected diagram for $-\langle \mathcal{H} \rangle^2$. The contribution of each diagram to the cumulant (difference between columns 5 and 7) is reported in column 8). Thus the net contribution of each diagram to K_n is obtained by multiplying columns 1, 3, 4, and 8.

Remarks: (i) The free energy being an extensive function, disconnected diagrams do not contribute. (ii) The free energy is an even function of H or \tilde{p} ; hence only diagrams with an even number of single nodes have nonzero trace. (iii) In the limit $H \rightarrow \infty$ or $\tilde{p} \rightarrow 1$, the partition function reduces to the zeroth-order term $Z = \text{tr} e^{-\beta \mathcal{H}^z}$, thus all the other terms of the series cancel for $\tilde{p} = 1$, and $(1 - \tilde{p}^2)$ can be factored out.

The calculation of the third-order term at $H=0$ is summarized in Table III with the same conventions. With $H=0$, we have $\langle \mathcal{H}_{\text{ex}} \rangle = 0$, and the cumulant K_3 reduces to $\langle \mathcal{H}_{\text{ex}}^3 \rangle$. The contribution of each diagram to $\langle \mathcal{H}_{\text{ex}}^3 \rangle = K_3$ is obtained by multiplying columns 1, 3, 4, and 5. Only the diagrams with no single nodes contribute to the zeroth-order term in H . More details about this high-temperature expansion are given in Roger (1980). In particular, there are a lot of ways (more or less sophisticated) to calculate the traces explicitly (Rushbrooke, Baker, and Wood, 1974). A simple straightforward way is suitable for up to third order, as presented in Roger (1980).

APPENDIX C: CALCULATION OF THE SPIN-WAVE VELOCITY IN THE UDD PHASE

1. General hydrodynamic equations

We refer the reader to the paper of R. Graham and G. Pleiner (1975; hereafter referred to as GP) on the spin hydrodynamics of ^3He in the anisotropic A phase. The same equations apply for spin dynamics in a solid antiferromagnet.

To the orbital anisotropy axis l corresponds the anisotropy axis l of the magnetic phase (l perpendicular to the 100 ferromagnetic planes for the udd phase). In the solid, the order parameter \mathbf{n} is the direction of the spins.

A small spatial gradient $\nabla \mathbf{n}$ of the order parameter creates a change of energy (using the summation convention)

$$\varepsilon = M_{jl} (\delta_{ik} - \hat{n}_i^0 \hat{n}_k^0) \cdot \frac{1}{2} (\nabla_l n_k) (\nabla_j n_i). \quad (\text{C1})$$

Here we use Eq. (8) of GP, and the definition of ψ_{ij} as conjugate parameter of $\nabla_j n_i$,

$$d\varepsilon = \psi_{ij} d(\nabla_j n_i).$$

In a reference frame with OZ parallel to the anisotropy axis l , M_{ij} is diagonal and has only two different components $M_{||}, M_{\perp}$:

$$M_{ij} = M_{\perp} (\delta_{ij} - l_i l_j) + M_{||} l_i l_j. \quad (\text{C2})$$

The spin-wave velocity is given in terms of the ‘‘mass densities’’ $M_{||}$ and M_{\perp} defined in Eq. (C2), and the perpendicular susceptibility is given χ_{\perp} by Eq. (13) of GP:

$$C = \gamma [(M_{\perp} k_{\perp}^2 + M_{||} k_{||}^2) / \chi_{\perp} |k|^2]^{1/2}. \quad (\text{C3})$$

The ‘‘perpendicular’’ and parallel spin-wave velocities are then

$$C_{\alpha} = \gamma (M_{\alpha} / \chi_{\perp})^{1/2} \quad \alpha = || \text{ or } \perp. \quad (\text{C4})$$

This proves that the factorization of the inverse perpendicular susceptibility is a very general property, independent of any model Hamiltonian.

We now need to calculate χ_{\perp} and the M_{α} within the multiple exchange model. An exact calculation is not possible, so we simply use the molecular-field approximation, which, as we shall prove, leads to the same results as the spin-wave approximation developed in Sec. IX and Appendix D. (This illustrates the fact that the spin-wave approximation is no more than a quantization of the fluctuations around the molecular-field state.)

2. Mean spin-wave velocity in the molecular-field approximation

a. Susceptibility

For obvious symmetry reasons, in a magnetic field \mathbf{H} the magnetizations of each of the four sublattices, initially perpendicular to \mathbf{H} , are tilted at the same angle α toward \mathbf{H} .

TABLE II. Diagrams and factors used in calculating $\bar{\epsilon}_2(p)$.

1	2	3	4	5	6	7	8
Coef.	diagram of $\langle H^2 \rangle$	choice HxH	no. Nx	$\langle H^2 \rangle$	diagram of $-\langle H \rangle^2$	$-\langle H \rangle^2$	$K_2 = \langle H^2 \rangle - \langle H \rangle^2$ Common factor $(1 - \bar{p}^2) \times$
$J_1^2/4$			4	$3-2\bar{p}^2$			
$J_2^2/4$		1	3			$-\bar{p}^4$	$3+\bar{p}^2$
$J_3^2/4$			6				
$J_1^2/4$			$8 \times 7/2$				
$J_2^2/4$			$6 \times 5/2$				
$J_3^2/4$		2	12x11	\bar{p}^2		$-\bar{p}^4$	\bar{p}^2
$J_1 J_2/4$			8x6				
$J_1 J_3/4$			8x12				
$J_2 J_3/4$			6x12				

1	2	3	4	5	6	7	8
Coef.	diagram of $\langle H^2 \rangle$	Choice HxH	no. Nx	$\langle H^2 \rangle$	diagram of $-\langle H \rangle^2$	$-\langle H \rangle^2$	$K_2 = \langle H^2 \rangle - \langle H \rangle^2$ Common factor $(1 - \bar{p}^2) \times$
$J_1 K_F/8$		2	24	$(4 + \lambda_F) \bar{p}^2 - 2 \bar{p}^4$		$-(2 + \lambda_F) \bar{p}^6$	$\bar{p}^2 [4 + \lambda_F + (2 + \lambda_F) \bar{p}^2]$
$J_1 K_P/8$			24	$(4 + \lambda_P) \bar{p}^2 - 2 \bar{p}^4$		$-(2 + \lambda_P) \bar{p}^6$	$\bar{p}^2 [4 + \lambda_P + (2 + \lambda_P) \bar{p}^2]$
$J_2 K_F/8$		2	12	$(2 + 3 \lambda_F) \bar{p}^2 - 2 \lambda_F \bar{p}^4$		$-(2 + \lambda_F) \bar{p}^6$	$\bar{p}^2 [2 + 3 \lambda_F + (2 + \lambda_F) \bar{p}^2]$
$J_2 K_P/8$			6	$(2 + 3 \lambda_P) \bar{p}^2 - 2 \lambda_P \bar{p}^4$		$-(2 + \lambda_P) \bar{p}^6$	$\bar{p}^2 [2 + 3 \lambda_P + (2 + \lambda_P) \bar{p}^2]$
$J_3 K_P/8$			6	"		"	"
$J_1 K_F/8$		2	$4 \times 6 \times 6$	$(2 + \lambda_F) \bar{p}^4$		$-(2 + \lambda_F) \bar{p}^6$	$(2 + \lambda_F) \bar{p}^4$
$J_2 K_F/8$		$4 \times 5 \times 6$					
$J_3 K_F/8$		$4 \times 12 \times 6$					
$J_1 K_P/8$			$4 \times 6 \times 6$	$(2 + \lambda_P) \bar{p}^4$		$-(2 + \lambda_P) \bar{p}^6$	$(2 + \lambda_P) \bar{p}^4$
$J_2 K_P/8$		$2 \times 5 \times 6$ $+ 2 \times 6 \times 6$					
$J_3 K_P/8$		$2 \times 11 \times 6$ $+ 2 \times 12 \times 6$					

TABLE II. (Continued.)

1	2	3	4	5	6	7	8
Coef.	diagram of $\langle H^2 \rangle$	Choice HxH	no. N _x	$\langle H^2 \rangle$	diagram of $-\langle H \rangle^2$	$-\langle H \rangle^2$	$K_2 = \langle H^2 \rangle - \langle H \rangle^2$ Common factor $(1 - \tilde{\rho}^2) \times$
$\frac{K_F^2}{16}$ $\frac{K_P^2}{16}$		1	6 6	$24 + 12 \lambda_\alpha + 9 \lambda_\alpha^2$ $-(32 + 16 \lambda_\alpha + 12 \lambda_\alpha^2) \tilde{\rho}^2$ $+(12 + 8 \lambda_\alpha + 4 \lambda_\alpha^2) \tilde{\rho}^4$ $\alpha = F \text{ or } \alpha = P$		$-(2 + \lambda_\alpha)^2 \tilde{\rho}^8$	$24 + 12 \lambda_\alpha + 9 \lambda_\alpha^2$ $-(8 + 4 \lambda_\alpha + 3 \lambda_\alpha^2) \tilde{\rho}^2$ $+(2 + \lambda_\alpha) \tilde{\rho}^4$ $+(2 + \lambda_\alpha)^2 \tilde{\rho}^6$
$\frac{K_F K_P}{16}$ $\frac{K_F^2}{16}$		2	4x6 $\frac{4 \times 6}{2}$	$(8 + 2 \lambda_F + 2 \lambda_P + 3 \lambda_F \lambda_P) \tilde{\rho}^2$ $-2(2 + \lambda_F \lambda_P) \tilde{\rho}^4$ $(8 + 4 \lambda_F + 3 \lambda_F^2) \tilde{\rho}^2$ $-2(2 + \lambda_F^2) \tilde{\rho}^4$		$-(2 + \lambda_F)(2 + \lambda_P) \tilde{\rho}^8$ $-(2 + \lambda_F)^2 \tilde{\rho}^8$	$\tilde{\rho}^2 [8 + 2(\lambda_F + \lambda_P) + 3 \lambda_F \lambda_P$ $+ (2 + \lambda_F)(2 + \lambda_P)(\tilde{\rho}^2 + \tilde{\rho}^4)]$ $\tilde{\rho}^2 [8 + 4 \lambda_F + 3 \lambda_F \lambda_P$ $+ (2 + \lambda_F)^2 (\tilde{\rho}^2 + \tilde{\rho}^4)]$
$\frac{K_F K_P}{16}$ $\frac{K_F^2}{16}$ $\frac{K_P^2}{16}$		2	4x4x6 $\frac{4 \times 3 \times 6}{2}$ $\frac{4 \times 5 \times 6}{2}$	$(6 + 2 \lambda_F + 2 \lambda_P + \lambda_F \lambda_P) \tilde{\rho}^4$ $-2 \tilde{\rho}^6$ $(6 + 4 \lambda_F + \lambda_F^2) \tilde{\rho}^4$ $-2 \tilde{\rho}^6$ $(6 + 4 \lambda_P + \lambda_P^2) \tilde{\rho}^4$ $-2 \tilde{\rho}^6$		$-(2 + \lambda_F)(2 + \lambda_P) \tilde{\rho}^8$ $-(2 + \lambda_F)^2 \tilde{\rho}^8$ $-(2 + \lambda_P)^2 \tilde{\rho}^8$	$\tilde{\rho}^4 [6 + 2(\lambda_F + \lambda_P) + \lambda_F \lambda_P$ $+ (2 + \lambda_F)(2 + \lambda_P) \tilde{\rho}^2]$ $\tilde{\rho}^4 [6 + 4 \lambda_F + \lambda_F^2$ $+ (2 + \lambda_F)^2 \tilde{\rho}^2]$ $\tilde{\rho}^4 [6 + 4 \lambda_P + \lambda_P^2$ $+ (2 + \lambda_P)^2 \tilde{\rho}^2]$

1	2	3	4	5	6	7	8
Coef.	diagram of $\langle H^2 \rangle$	Choice HxH	no. N _x	$\langle H^2 \rangle$	diagram of $-\langle H \rangle^2$	$-\langle H \rangle^2$	$K_2 = \langle H^2 \rangle - \langle H \rangle^2$ Common factor $(1 - \tilde{\rho}^2) \times$
$\frac{K_F K_P}{16}$ $\frac{K_F^2}{16}$ $\frac{K_P^2}{16}$		2	=0 $\frac{2 \times 6}{2}$ $\frac{1 \times 6}{2}$	$(4 + 4 \lambda_F + 3 \lambda_F^2) \tilde{\rho}^4 - 2 \lambda_F^2 \tilde{\rho}^6$ $(4 + 4 \lambda_P + 3 \lambda_P^2) \tilde{\rho}^4 - 2 \lambda_P^2 \tilde{\rho}^6$		$-(2 + \lambda_F)^2 \tilde{\rho}^8$ $-(2 + \lambda_P)^2 \tilde{\rho}^8$	$\tilde{\rho}^4 [4 + 4 \lambda_F + 3 \lambda_F^2 + (2 + \lambda_F)^2 \tilde{\rho}^2]$ $\tilde{\rho}^4 [4 + 4 \lambda_P + 3 \lambda_P^2 + (2 + \lambda_P)^2 \tilde{\rho}^2]$
$\frac{K_F K_P}{16}$ $\frac{K_F^2}{16}$ $\frac{K_P^2}{16}$		2	$\frac{4 \times (7 \times 6)}{6}$ $4 \times 13 \times 6$ $2(12 + 13 \times 6)$	$(2 + \lambda_F)(2 + \lambda_P) \tilde{\rho}^5$ $(2 + \lambda_F)^2 \tilde{\rho}^5$ $(2 + \lambda_P)^2 \tilde{\rho}^5$		$-(2 + \lambda_F)(2 + \lambda_P) \tilde{\rho}^8$ $-(2 + \lambda_F)^2 \tilde{\rho}^8$ $-(2 + \lambda_P)^2 \tilde{\rho}^8$	$(2 + \lambda_F)(2 + \lambda_P) \tilde{\rho}^5$ $(2 + \lambda_F)^2 \tilde{\rho}^5$ $(2 + \lambda_P)^2 \tilde{\rho}^5$

The corresponding change in energy is [see Eq. (5.10)]

$$\Delta E = E(H) - E(0)$$

$$= N(2J_1 + J_2 + 4J_3 + 3K_P)u^2 - N(\gamma \hbar / 2)Hu$$

with $u = \sin \alpha$.

Its minimization with respect to u

$$\left. \frac{\partial E}{\partial u} \right|_{u=u_0} = 0$$

TABLE III. Diagrams and factors used in calculating $\tilde{\epsilon}_3(0)$.

Coefficient	diagram	choice $H \times H \times H$	number N_x	$K_3 = \langle H^3 \rangle$ ($\tilde{p}=0$)
$-\frac{J_1^3}{8}$		1	4	-6
$-\frac{J_2^3}{8}$			3	
$-\frac{J_3^3}{8}$			6	
$-\frac{J_1^2 J_2}{8}$		6	12	+3
$-\frac{J_1^2 J_3}{8}$			12	
$-\frac{J_2^2 J_3}{8}$			12	
$-\frac{J_3^3}{8}$			8	

Coefficient	diagram	choice $H \times H \times H$	number N_x	$K_3 = \langle H^3 \rangle$ ($\tilde{p}=0$)	
$-\frac{K_F J_1^2}{16}$		6	12	$12 + 3\lambda_F$	
$-\frac{K_P J_1^2}{16}$			12	$12 + 3\lambda_P$	
$-\frac{K_F J_2^2}{16}$		6	6	$6 + 9\lambda_F$	
$-\frac{K_P J_2 J_3}{16}$			6	$6 + 9\lambda_P$	
$-\frac{K_F^2 J_1}{32}$		3	4×6	-30	
$\frac{K_P^2 J_1}{32}$					
$-\frac{K_F^2 J_2}{32}$		3	2×6	$12 - 24\lambda_F - 18\lambda_F^2$	
$-\frac{K_P^2 J_2}{32}$			1×6		$12 - 24\lambda_P - 18\lambda_P^2$
$-\frac{K_P^2 J_3}{32}$			1×6		

TABLE III. (Continued.)

Coefficient	diagram	choice $H \times H \times H$	number $N \times$	$K_3 = \langle H^3 \rangle$ ($\tilde{\rho}=0$)
$-\frac{K_F K_P J_2}{32}$		6	4x6	$24+6\lambda_F+6\lambda_P+9\lambda_F\lambda_P$
$-\frac{K_F^2 J_3}{32}$		6	2x6	$24+12\lambda_F+9\lambda_F^2$
$-\frac{K_F^3}{64}$		1	6	$36(4+3\lambda_F+2\lambda_F^2+\lambda_F^3)$
$-\frac{K_P^3}{64}$		1	6	$36(4+3\lambda_P+2\lambda_P^2+\lambda_P^3)$
$-\frac{K_F^2 K_P}{64}$		6	2x6	$6(-2+4\lambda_F+2\lambda_P-2\lambda_F^2-4\lambda_F\lambda_P-3\lambda_F^2\lambda_P)$

leads to

$$\chi_{\perp} = N \frac{\gamma \hbar}{2} \frac{u_0}{H} = -N \left[\frac{\gamma \hbar}{2} \right]^2 [4J_1 + 2J_2 + 8J_3 + 6K_P]^{-1}. \quad (\text{C5})$$

b. Calculation of M_{\parallel}

The initial direction of the spin is perpendicular to \mathbf{l} : $\mathbf{l} \parallel \text{OZ}$; $\mathbf{n}_0 \parallel \text{OX}$. The udd phase belongs to the structures $(A, B, -A, -B)$ (see Sec. VII) with two interleaved antiferromagnetic sublattices A and B . We consider separately each antiferromagnetic sublattice, as shown in Fig. 33(a). For each sublattice we take the same gradient of the order parameter in the direction parallel to the anisotropy axis \mathbf{l} : i.e., within one sublattice going from one plane perpendicular to the anisotropy axis to the next, the order parameter turns by an angle θ . From Eqs. (C1) and (C2), we obtain

$$\varepsilon = M_{\parallel} \cdot \frac{1}{2} [(\nabla_{\parallel} n_x)^2 + (\nabla_{\parallel} n_y)^2] = \frac{1}{2} M_{\parallel} \left[\frac{\theta}{a} \right]^2. \quad (\text{C6})$$

The angle θ' between the order parameters of the two sublattices (see Fig. 33) must be chosen in order to minimize the variation of energy $\varepsilon(\theta, \theta')$.

In the molecular-field approximation, the energy variation is

$$\varepsilon(\theta, \theta') = -N \left[\left[\frac{J_1}{2} + \frac{J_2}{4} + J_3 + \frac{3K_P}{4} \right] \theta^2 + [J_1 - (3K_P + K_F)] \theta \theta' - (3K_P + K_F) \theta'^2 \right].$$

Minimizing with respect to θ' , we obtain

$$\theta' = \frac{1}{2} \left[1 - \frac{J_1}{3K_P + K_F} \right] \theta$$

and

$$\varepsilon = \frac{N}{4} \theta^2 \left[-J_2 - 4J_3 + K_F + \frac{J_1^2}{3K_P + K_F} \right]$$

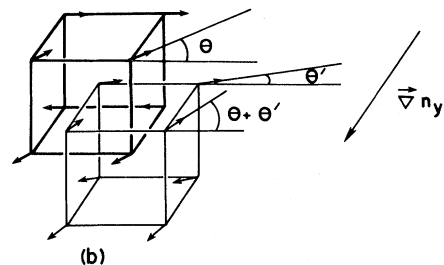
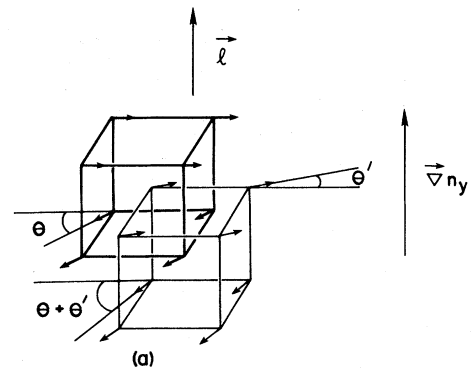


FIG. 33. Sublattice spin orientations for calculation of (a) M_{\parallel} and (b) M_{\perp} .

which gives with Eq. (C6)

$$M_{\parallel} = \frac{Na^2}{2} \left[-J_2 - 4J_3 + K_F + \frac{J_1^2}{3K_P + K_F} \right]. \quad (\text{C7})$$

c. Calculation of M_{\perp}

We take a gradient $\nabla_{\perp} n_i$ in the direction OX perpendicular to the anisotropy direction (l axis), as shown in Fig. 33(b). As explained before, the lattice is split into two simple cubic antiferromagnetic sublattices A and B . In each sublattice, the order parameter turns by an angle θ as one goes from one plane perpendicular to OX to the next.

The variation of energy is

$$\varepsilon = M_{\perp} \frac{1}{2} [(\nabla_{\perp} n_y)^2 + (\nabla_{\perp} n_z)^2] = \frac{1}{2} M_{\perp} \left[\frac{\theta}{a} \right]^2.$$

The angle θ' between the order parameters of the two sublattices is determined so as to minimize the variation of energy. We obtain in molecular-field approximation

$$\varepsilon(\theta, \theta') = N \left[\left[\frac{J_2}{4} - \frac{3K_P}{4} - \frac{K_F}{2} \right] \theta^2 - (3K_P + K_F)(\theta'^2 - \theta\theta') \right].$$

The minimum in terms of θ' is obtained for $\theta' = \theta/2$. Thus

$$\varepsilon = \frac{N\theta^2}{4} (J_2 - K_F).$$

We deduce

$$M_{\perp} = \frac{Na^2}{2} (J_2 - K_F). \quad (\text{C8})$$

Substituting Eqs. (C7) and (C8) in (C3), we obtain the spin-wave velocities C_{\parallel} and C_{\perp} . The results are the same as those given by a straightforward but tedious expansion at low T of the dispersion relation of the spin waves (see Sec. IX).

APPENDIX D: SPIN-WAVE APPROXIMATION

In this section we present the spin-wave calculation for the main phases, uudd, naf, ssqaf, and scaf, which can occur with four-spin interactions. Although the ssqaf and scaf phases do not appear experimentally at the melting curve molar volume, they are not excluded at higher densities. In particular, if J_i decreases faster than K_P when the molar volume is decreased, the ssqaf phase can become stable.

1. Generalities on the spin-wave approximation

a. Quantization of the spin fluctuation in the Holstein-Primakoff (1940) formalism (for spin $1/2$)

For each site i , the spin is quantized along the direction OZ of the molecular field. We assign to the two states

$S_i^z = +\frac{1}{2}$, $S_i^z = -\frac{1}{2}$ the respective boson states $|0\rangle$, $|1\rangle$. We introduce the corresponding boson creation and annihilation operators α_i^{\dagger} and α_i . From the boson commutation rules, it is easily proved that the operators

$$\begin{aligned} S_i^z &= \frac{1}{2} - \alpha_i^{\dagger} \alpha_i, \\ S_i^+ &= (1 - \alpha_i^{\dagger} \alpha_i) \alpha_i, \\ S_i^- &= \alpha_i^{\dagger} (1 - \alpha_i^{\dagger} \alpha_i), \end{aligned} \quad (\text{D1})$$

satisfy the commutation rules for spin operators. The fluctuations with respect to the molecular field are generally weak. Thus at lowest order we retain in the Hamiltonian only the linear and quadratic terms which makes its diagonalization possible. Hence we can write

$$\mathbf{S}_i = \mathbf{S}_i^0 + \delta\mathbf{S}_i.$$

Here

$$\mathbf{S}_i^0 = \begin{pmatrix} 0 \\ 0 \\ \frac{1}{2} \end{pmatrix}$$

is the molecular field, and

$$\delta\mathbf{S}_i \simeq \begin{pmatrix} \frac{1}{2}(\alpha_i^{\dagger} + \alpha_i) \\ \frac{i}{2}(\alpha_i^{\dagger} - \alpha_i) \\ -\alpha_i^{\dagger} \alpha_i \end{pmatrix}. \quad (\text{D2})$$

b. Expansion of the Hamiltonian at second order in $\delta\mathbf{S}_i$

Retaining only the first- and second-order terms in $\delta\mathbf{S}_i$, we can write the Hamiltonian

$$\mathcal{H} = E + \sum_i \left[\frac{\partial E}{\partial \mathbf{S}_i} \right] \cdot \delta\mathbf{S}_i + \frac{1}{2} \sum_{i,j} \delta\mathbf{S}_i \cdot \left[\frac{\partial^2 E}{\partial \mathbf{S}_i \partial \mathbf{S}_j} \right] \cdot \delta\mathbf{S}_j, \quad (\text{D3})$$

where E designates the molecular-field energy (all derivatives are taken at the molecular-field value $\mathbf{S}_i = \mathbf{S}_i^0$).

The derivatives that we need with a four-spin Hamiltonian are simply

(i) two-spin terms,

$$\begin{aligned} \frac{\partial}{\partial \mathbf{S}_i} (\mathbf{S}_i \cdot \mathbf{S}_j) &= \mathbf{S}_j, \\ \delta\mathbf{S}_i \cdot \frac{\partial^2 (\mathbf{S}_i \cdot \mathbf{S}_j)}{\partial \mathbf{S}_i \partial \mathbf{S}_j} \cdot \delta\mathbf{S}_j &= \delta\mathbf{S}_i \cdot \delta\mathbf{S}_j, \end{aligned} \quad (\text{D4})$$

(ii) four-spin terms

$$\begin{aligned} \frac{\partial}{\partial \mathbf{S}_i} (\mathbf{S}_i \cdot \mathbf{S}_j)(\mathbf{S}_k \cdot \mathbf{S}_l) &= (\mathbf{S}_k \cdot \mathbf{S}_l) \mathbf{S}_j, \\ \delta\mathbf{S}_i \cdot \frac{\partial^2 (\mathbf{S}_i \cdot \mathbf{S}_j)(\mathbf{S}_k \cdot \mathbf{S}_l)}{\partial \mathbf{S}_i \partial \mathbf{S}_j} \cdot \delta\mathbf{S}_j &= (\mathbf{S}_k \cdot \mathbf{S}_l)(\delta\mathbf{S}_i \cdot \delta\mathbf{S}_j), \\ \delta\mathbf{S}_i \cdot \frac{\partial^2 (\mathbf{S}_i \cdot \mathbf{S}_k)(\mathbf{S}_j \cdot \mathbf{S}_l)}{\partial \mathbf{S}_i \partial \mathbf{S}_j} \cdot \delta\mathbf{S}_j &= (\mathbf{S}_k \cdot \delta\mathbf{S}_i)(\mathbf{S}_l \cdot \delta\mathbf{S}_j). \end{aligned} \quad (\text{D5})$$

c. Diagonalization of the Hamiltonian

We restrict our attention to an n sublattice magnetic structure. For each sublattice φ_l , we define the spin-wave boson operators $\alpha_{l,i}^+$ and $\alpha_{l,i}$ ($0 \leq l \leq n$). We define the Fourier transforms

$$\begin{aligned}\alpha_l(k) &= \left[\frac{n}{N} \right]^{1/2} \sum_{i \in \varphi_l} \alpha_{l,i} e^{-ikR_i}, \\ \alpha_l^+(k) &= \left[\frac{n}{N} \right]^{1/2} \sum_{i \in \varphi_l} \alpha_{l,i}^+ e^{+ikR_i},\end{aligned}\quad (\text{D6})$$

the summation being taken over one sublattice φ_l , where N is the total number of atoms. Reciprocally, we have

$$\begin{aligned}\alpha_{l,i} &= \left[\frac{n}{N} \right]^{1/2} \sum_{k \in \mathcal{P}_l} \alpha_l(k) e^{ikR_i}, \\ \alpha_{l,i}^+ &= \left[\frac{n}{N} \right]^{1/2} \sum_{k \in \mathcal{P}_l} \alpha_l^+(k) e^{-ikR_i},\end{aligned}\quad (\text{D7})$$

the summation being taken over the reciprocal lattice \mathcal{P}_l of φ_l .

The linear terms in the spin-wave Hamiltonian cancel because the stable structure corresponds to a minimum of the molecular-field energy. Using Eq. (D7), we obtain a quadratic form of the Hamiltonian in terms of the $\alpha_l(k)$, $\alpha_n^+(k)$. Taking into account the Hermitian properties, we can write the Hamiltonian

$$\mathcal{H} = E_0 + \sum_k \left[\sum_{i,j} C_{ij}(k) \alpha_i(k) \alpha_j(-k) + C_{ij}^*(k) \alpha_i^+(k) \alpha_j^+(-k) + C'_{ij}(k) \alpha_i(k) \alpha_j^+(k) + C'_{ij}{}^*(k) \alpha_i^+(k) \alpha_j(k) \right].$$

Because of time-reversal invariance ($t \rightarrow -t$ or $k \rightarrow -k$) and the centrosymmetry of the lattice [$C^*(-k) = C(k)$] we can write

$$\mathcal{H} = E_0 + \text{const} + \sum_k \left[\sum_{i,j} C_{ij}(k) [\alpha_i(k) \alpha_j(-k) + \alpha_i^+(-k) \alpha_j^+(k)] + C'_{ij}(k) [\alpha_i(k) \alpha_j^+(k) + \alpha_i^+(-k) \alpha_j(-k)] \right]$$

or in a matrix form,

$$\mathcal{H} = E_0 + \frac{1}{2} \sum_k \begin{bmatrix} {}^t\alpha^+(k) & {}^t\alpha(-k) \end{bmatrix} M(k) \begin{bmatrix} \alpha(k) \\ \alpha^+(-k) \end{bmatrix} + \text{const} \quad (\text{D8})$$

with

$$\alpha(k) = \begin{bmatrix} \alpha_1(k) \\ \alpha_2(k) \\ \vdots \\ \alpha_n(k) \end{bmatrix}; \quad \alpha^+(k) = \begin{bmatrix} \alpha_1^+(k) \\ \alpha_2^+(k) \\ \vdots \\ \alpha_n^+(k) \end{bmatrix},$$

$${}^t\alpha(k) = [\alpha_1(k), \dots, \alpha_n(k)] \quad \text{and} \quad {}^t\alpha^+(k) = [\alpha_1^+(k), \dots, \alpha_n^+(k)]$$

$$M(k) = \begin{bmatrix} A & B \\ B & A \end{bmatrix}.$$

A and B are two $n \times n$ matrices. The diagonalization of the Hamiltonian can be performed with a linear transformation as

$$\begin{bmatrix} e(k) \\ e^+(-k) \end{bmatrix} = U(k) \begin{bmatrix} \alpha(k) \\ \alpha^+(-k) \end{bmatrix} \quad (\text{D9})$$

with

$$e(k) = \begin{bmatrix} e_1(k) \\ \vdots \\ e_n(k) \end{bmatrix}, \quad e^+(k) = \begin{bmatrix} e_1^+(k) \\ \vdots \\ e_n^+(k) \end{bmatrix}.$$

The transformation $U(k)$ must conserve the commutation relations for the new boson creation and annihilation operators

$$[e_i(k), e_j^+(k)] = \delta_{ij}.$$

Using our vectorial notation, this condition can be written as follows:

$$\begin{aligned}\begin{bmatrix} e(k) \\ e^+(-k) \end{bmatrix} [{}^t e^+(k), {}^t e(-k)] \\ - \begin{bmatrix} e^+(k) \\ e(-k) \end{bmatrix} [{}^t e(k), {}^t e^+(-k)] = \tilde{I} \quad (\text{D10})\end{aligned}$$

with

$$\tilde{I} = \begin{bmatrix} I & 0 \\ 0 & -I \end{bmatrix},$$

where I is the $n \times n$ unity matrix and 0 the $n \times n$ zero matrix. Substituting Eq. (D9) into (D10), we obtain

$$\begin{aligned}U(k) \begin{bmatrix} \alpha(k) \\ \alpha^+(-k) \end{bmatrix} [{}^t\alpha^+(k), {}^t\alpha(-k)] {}^t U^*(k) \\ - U^*(k) \begin{bmatrix} \alpha^+(k) \\ \alpha(-k) \end{bmatrix} [{}^t\alpha(k), {}^t\alpha^+(-k)] {}^t U(k) = \tilde{I}.\end{aligned}\quad (\text{D11})$$

Factoring out $U(k)$ and ${}^t U^*(k)$ in Eq. (D11) and remarking that the $\alpha(k), \alpha^+(-k)$ satisfy the boson commutation relation analogous to (D10), we obtain

$$U(k) \tilde{I} U^+(k) = \tilde{I}. \quad (\text{D12})$$

From this relation we deduce the inverse matrix

$$U^{-1}(k) = \tilde{I}U^+(k)\tilde{I}, \quad (\text{D13})$$

which transforms the $e_i(k)$ into the $\alpha_i(k)$:

$$\begin{bmatrix} \alpha(k) \\ \alpha^+(-k) \end{bmatrix} = \tilde{I}^t U^*(k) \tilde{I} \begin{bmatrix} e(k) \\ e^+(-k) \end{bmatrix}. \quad (\text{D14})$$

U is chosen such that the linear transformation diagonalizes the Hamiltonian:

$$[\tilde{I}U(k)\tilde{I}]M(k)[\tilde{I}U^+(k)\tilde{I}] = \Lambda, \quad (\text{D15})$$

where Λ is a diagonal matrix, $\lambda_{ii} = 0$ for $i \neq j$. Multiplying by \tilde{I} to the left, we obtain

$$[U(k)\tilde{I}][M(k)\tilde{I}][U^+(k)\tilde{I}] = \tilde{I}\Lambda. \quad (\text{D16})$$

$\tilde{I}\Lambda$ is also a diagonal matrix. $U(k)\tilde{I}$ and $U^+(k)\tilde{I}$ are inverse matrices [see Eq. (D13)]. Thus we are simply led to diagonalize the $2n \times 2n$ matrix:

$$M(k)\tilde{I} = \begin{bmatrix} A & -B \\ B & -A \end{bmatrix}. \quad (\text{D17})$$

Because of the symmetry of this $2n \times 2n$ matrix, the problem can be reduced to the diagonalization of an $n \times n$ matrix, in the following way:

Let $\mathcal{Y} = \begin{pmatrix} U \\ V \end{pmatrix}$ be an eigenvector of $M\tilde{I}$ with eigenvalue λ (U and V are two n -dimensional vectors). The vectors \mathcal{Y} are columns of $U^+(k)\tilde{I}$. We can write

$$\begin{aligned} AU - BV &= \lambda U, \\ BU - AV &= \lambda V, \end{aligned} \quad (\text{D18})$$

or, after combining both equations,

$$\begin{aligned} (A+B)(U-V) &= \lambda(U+V), \\ (A-B)(U+V) &= \lambda(U-V). \end{aligned} \quad (\text{D19})$$

Taking $(U-V)$ from the second equation and substituting in the first, we obtain

$$(A+B)(A-B)(U+V) = \lambda^2(U+V). \quad (\text{D20})$$

In the same way we can write

$$(A-B)(A+B)(U-V) = \lambda^2(U-V). \quad (\text{D21})$$

Generally A and B do not commute. Thus $U + \varepsilon V$ is an eigenvector of $P_\varepsilon = A^2 - B^2 - \varepsilon[A, B]$ with eigenvalue λ^2 ($\varepsilon = \pm 1$). (If A and B commute, U and V are common eigenvectors of A and B .) P_+ and P_- have the same eigenvalues $\{\lambda_1^2, \dots, \lambda_n^2\}$. Thus the matrix Λ defined in Eq. (D15) becomes

$$\tilde{I}\Lambda = \begin{bmatrix} \lambda_1 & & & 0 \\ & \lambda_n & & \\ & & -\lambda_1 & \\ 0 & & & -\lambda_n \end{bmatrix} \quad (\text{D22})$$

and therefore

$$\tilde{\Lambda} = \begin{bmatrix} \lambda_1 & & & 0 \\ & \lambda_n & & \\ & & \lambda_1 & \\ 0 & & & \lambda_n \end{bmatrix}.$$

If W_+ and W_- are, respectively, eigenvectors of P_+ and P_- with eigenvalue λ , we have

$$U + \varepsilon V = \mu_\varepsilon W_\varepsilon \quad (\varepsilon = \pm 1). \quad (\text{D23})$$

The constant μ_ε are determined so that U and V must solve Eq. (D18) or (D19) and are normalized by the condition obtained from the diagonal elements of Eq. (D12):

$${}^t U^* U = {}^t V^* V = 1. \quad (\text{D24})$$

We thus proceed as follows:

- (i) find the common eigenvalues and eigenvectors W_+ and W_- of P_+ and P_- ;
- (ii) determine U and V from the above conditions and Eq. (D23).

Since

$$\begin{bmatrix} U \\ V \end{bmatrix}$$

form a column of the matrix $U^+(k)\tilde{I}$, we may easily construct the relation between the spin-wave operators

$$\begin{bmatrix} e^+(-k) \\ e^+(k) \end{bmatrix}$$

and the single sublattice operators

$$\begin{bmatrix} \alpha(t) \\ \alpha^+(-k) \end{bmatrix}.$$

2. The uudd phase

a. Spin-wave Hamiltonian

The respective magnetizations of the four sublattices are shown in Fig. 34(a). The crystal axes x, y, z are such that z is perpendicular to the ferromagnetic planes. The quantization axis OZ is parallel to the magnetization of the four sublattices. Thus for each sublattice the spin vectors in the molecular field are in the reference frame XYZ :

$$\begin{aligned} \mathbf{S}_1 &= \begin{bmatrix} 0 \\ 0 \\ \frac{1}{2} \end{bmatrix}, & \mathbf{S}_2 &= \begin{bmatrix} 0 \\ 0 \\ \frac{1}{2} \end{bmatrix}, \\ \mathbf{S}_3 &= \begin{bmatrix} 0 \\ 0 \\ -\frac{1}{2} \end{bmatrix}, & \mathbf{S}_4 &= \begin{bmatrix} 0 \\ 0 \\ -\frac{1}{2} \end{bmatrix}, \end{aligned}$$

and the spin deviations are

$$\begin{aligned}
 \delta\mathbf{S}_{1,i} &= \begin{bmatrix} \frac{1}{2}(\alpha_{1,i}^+ + \alpha_{1,i}) \\ \frac{i}{2}(\alpha_{1,i}^+ - \alpha_{1,i}) \\ -\alpha_{1,i}^+ \alpha_{1,i} \end{bmatrix}, \\
 \delta\mathbf{S}_{2,j} &= \begin{bmatrix} \frac{1}{2}(\alpha_{2,j}^+ + \alpha_{2,j}) \\ \frac{i}{2}(\alpha_{2,j}^+ - \alpha_{2,j}) \\ -\alpha_{2,j}^+ \alpha_{2,j} \end{bmatrix}, \\
 \delta\mathbf{S}_{3,k} &= \begin{bmatrix} \frac{1}{2}(\alpha_{3,k}^+ + \alpha_{3,k}) \\ -\frac{i}{2}(\alpha_{3,k}^+ - \alpha_{3,k}) \\ +\alpha_{3,k}^+ \alpha_{3,k} \end{bmatrix}, \\
 \delta\mathbf{S}_{4,l} &= \begin{bmatrix} \frac{1}{2}(\alpha_{4,l}^+ + \alpha_{4,l}) \\ -\frac{i}{2}(\alpha_{4,l}^+ - \alpha_{4,l}) \\ +\alpha_{4,l}^+ \alpha_{4,l} \end{bmatrix}.
 \end{aligned} \tag{D25}$$

(Note that for sublattices 3,4, the operators change S_i^Z from $-\frac{1}{2}$ to $\frac{1}{2}$ in the frame XYZ .)

We begin with Eq. (5.10) of the Hamiltonian, including two-, three- and four-spin cyclic exchanges. We expand the Hamiltonian to second order in $\delta\mathbf{S}_{\lambda,i}$ according to the method presented above (see Sec. 1.b). Using Eq. (D25), we express the $\delta\mathbf{S}_{\lambda,i}$ in terms of the $\alpha_{\lambda,i}, \alpha_{\lambda,i}^+$ and finally apply the Fourier transform defined by Eq. (D6).

After tedious calculations we obtain as a final result

$$\begin{aligned}
 \mathcal{H} = E_0 + \sum_{k \in \mathcal{B}_1} \left[\omega(k) \sum_{l=1}^4 \alpha_l^+(k) \alpha_l(k) + \gamma(k) [\alpha_1^+(k) \alpha_3^+(-k) + \alpha_1(k) \alpha_3(-k) + \alpha_2^+(k) \alpha_4^+(-k) + \alpha_2(k) \alpha_4(-k)] \right. \\
 + \nu(k) [\alpha_1(k) \alpha_4(-k) + \alpha_2^+(k) \alpha_3^+(-k)] + \nu^*(k) [\alpha_1^+(k) \alpha_4^+(-k) + \alpha_2(k) \alpha_3(-k)] \\
 \left. + \eta(k) [\alpha_1^+(k) \alpha_2(k) + \alpha_3^+(k) \alpha_4(-k)] + \eta^*(k) [\alpha_1(k) \alpha_2^+(k) + \alpha_3(k) \alpha_4^+(k)] \right].
 \end{aligned} \tag{D26}$$

E_0 is the molecular-field energy, and the coefficients $\omega, \gamma, \nu, \eta$ are c -numbers, ω and γ being also real. In the frame (x, y, z) determined by the crystal axes (see Fig. 34),

$$\begin{aligned}
 \omega(k) &= +2J_2 - 4J_3 - 4K_F - 12K_P - 2(J_2 + K_P)(\cos ak_x + \cos ak_y) - 4 \left[J_3 + \frac{K_P}{2} \right] \cos ak_x \cos ak_y, \\
 \gamma(k) &= 2 \cos ak_z [-J_2 + 2K_F + K_P + (-2J_3 + K_P)(\cos ak_x + \cos ak_y)], \\
 \nu(k) &= |\nu| e^{i\varphi} = (-J_1 - K_F - 3K_P) 4 \cos \frac{ak_x}{2} \cos \frac{ak_y}{2} e^{i(ak_z/2)}, \\
 \eta(k) &= |\eta| e^{i\varphi} = (-J_1 + K_F + 3K_P) 4 \cos \frac{ak_x}{2} \cos \frac{ak_y}{2} e^{i(ak_z/2)}.
 \end{aligned} \tag{D27}$$

Note that ν and η have the same phase: $\varphi = ak_z/2$. The details of this calculation are presented in Roger (1980), Appendix 6.

Using the general notation of Eq. (D8), we can write

$$\mathcal{H} = E_0 + \sum_k \left[\frac{1}{2} [\alpha^+(k), \alpha(-k)] \begin{bmatrix} A & B \\ B & A \end{bmatrix} \begin{bmatrix} \alpha(k) \\ \alpha^+(-k) \end{bmatrix} - \frac{1}{2} \text{tr} A \right] \tag{D28}$$

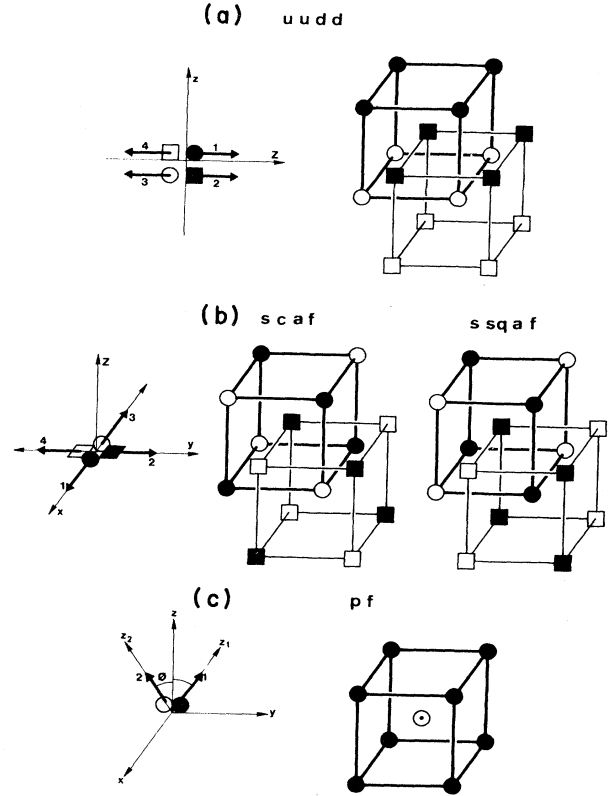


FIG. 34. Mean-field ground-state spin orientation and sublattice numbering for calculation of spin waves in the (a) uudd, (b) scaf and ssqaf; and (c) pf structures.

with

$$A = \begin{bmatrix} \Omega & 0 \\ 0 & \Omega \end{bmatrix}, \quad B = \begin{bmatrix} 0 & \Gamma \\ \Gamma & 0 \end{bmatrix},$$

Ω and Γ being the 2×2 matrices defined by

$$\Omega = \begin{bmatrix} \omega & \eta \\ \eta^* & \omega \end{bmatrix} \quad \text{and} \quad \Gamma = \begin{bmatrix} \gamma & \nu^* \\ \nu & \gamma \end{bmatrix}.$$

The constant term $-\frac{1}{2}\text{tr}A = -2\sum_k \omega(k)$ arises from the commutator:

$$\alpha_l(k)\alpha_l^\dagger(k) = 1 + \alpha_l^\dagger(k)\alpha_l(k).$$

Because of this term, the net effect is for the energy to be lowered below the mean-field energy E_0 .

b. Diagonalization of the Hamiltonian

In the uudd phase, the operators $\alpha_1(k), \alpha_2(k)$ being coupled only to $\alpha_1^\dagger(k), \alpha_2^\dagger(k)$ and $\alpha_3(-k), \alpha_4(-k)$, the general expression (D28) of the Hamiltonian can be simplified as

$$\mathcal{H} = E_0 + \sum_k \left[\alpha_1^\dagger(k), \alpha_2^\dagger(k), \alpha_3(-k), \alpha_4(-k) \right] \begin{bmatrix} \Omega & \Gamma \\ \Gamma & \Omega \end{bmatrix} \begin{bmatrix} \alpha_1(k) \\ \alpha_2(k) \\ \alpha_3^\dagger(-k) \\ \alpha_4^\dagger(-k) \end{bmatrix} - \text{Tr}\Omega. \quad (\text{D29})$$

We use the linear transformation $T(k)$:

$$\begin{bmatrix} e_1(k) \\ e_2(k) \\ e_3^\dagger(-k) \\ e_4^\dagger(-k) \end{bmatrix} = T(k) \begin{bmatrix} \alpha_1(k) \\ \alpha_2(k) \\ \alpha_3^\dagger(-k) \\ \alpha_4^\dagger(-k) \end{bmatrix}. \quad (\text{D30})$$

As shown for U in Sec. 1.c, Eq. (D13), the conservation of the commutation relations for the new boson operators e_i , e_i^\dagger also requires that

$$T^{-1}(k) = \tilde{T}T(k)\tilde{T}, \quad (\text{D31})$$

and we are led to diagonalize the matrix

$$M'I = \begin{bmatrix} \Omega & \Gamma \\ \Gamma & \Omega \end{bmatrix} \tilde{T} = \begin{bmatrix} \Omega & -\Gamma \\ \Gamma & -\Omega \end{bmatrix}. \quad (\text{D32})$$

As shown in Eqs. (D20) and (D21), if $\mathcal{V} = \begin{pmatrix} U \\ V \end{pmatrix}$ is an eigenvector of $M'I$ with eigenvalue λ , $U + \varepsilon V$ is an eigenvector of the 2×2 matrix $P_\varepsilon = \Omega^2 - \Gamma^2 - \varepsilon[\Omega, \Gamma]$ with eigenvalue λ^2 . P_ε has the form

$$P_\varepsilon = \begin{bmatrix} u - \varepsilon ic & v^* \\ v & u + \varepsilon ic \end{bmatrix},$$

with

$$\begin{aligned} c &= -i(\eta\nu - \eta^*\nu^*) = 2|\eta||\nu|\sin 2\varphi, \\ u &= \omega^2 - \gamma^2 + |\eta|^2 - |\nu|^2, \\ v &= 2(\omega\eta^* - \gamma\nu) = 2(\omega|\eta|e^{-i\varphi} - \gamma|\nu|e^{i\varphi}). \end{aligned} \quad (\text{D33})$$

P_+ and P_- have the same eigenvalues

$$\lambda_\varepsilon^2 = u + \varepsilon'(|v|^2 - c^2)^{1/2}, \quad \varepsilon' = \pm 1 \quad (\text{D34})$$

(which are independent of the subscript on P but which have the parametrization ε' coming from the solutions of the quadratic characteristic equation). If

$$\mathcal{W}_\varepsilon^{\varepsilon'} = \begin{bmatrix} x_\varepsilon^{\varepsilon'} \\ y_\varepsilon^{\varepsilon'} \end{bmatrix}$$

is an eigenvector of P_ε with eigenvalue λ_ε^2 ,

$$P_\varepsilon \mathcal{W}_\varepsilon^{\varepsilon'} = \lambda_\varepsilon^2 \mathcal{W}_\varepsilon^{\varepsilon'},$$

we have, using Eq. (D34),

$$\begin{aligned} v^* y_\varepsilon^{\varepsilon'} &= D_\varepsilon^{\varepsilon'} x_\varepsilon^{\varepsilon'}, \\ u x_\varepsilon^{\varepsilon'} &= D_\varepsilon^{\varepsilon'} y_\varepsilon^{\varepsilon'}, \end{aligned} \quad (\text{D35})$$

with $D_\varepsilon^{\varepsilon'} = \varepsilon'(|v|^2 - c^2)^{1/2} + \varepsilon ic$. From Eq. (D35) and the identity $|D_\varepsilon^{\varepsilon'}| = |v|$ we deduce

$$|x_\varepsilon^{\varepsilon'}| = |y_\varepsilon^{\varepsilon'}|.$$

Defining ϕ and t by the relations

$$\begin{aligned} v^* &= |v| e^{2i\phi}, \\ (|v|^2 - c^2)^{1/2} + ic &= |v| e^{2it}, \end{aligned} \quad (\text{D36})$$

we define the symmetrized eigenvector

$$\mathcal{W}_\varepsilon^{\varepsilon'} = \begin{bmatrix} x_\varepsilon^{\varepsilon'} \\ y_\varepsilon^{\varepsilon'} \end{bmatrix} = \begin{bmatrix} e^{i(\phi - \varepsilon\varepsilon't)} \\ \varepsilon' e^{-i(\phi - \varepsilon\varepsilon't)} \end{bmatrix}. \quad (\text{D37})$$

The eigenvector $\begin{pmatrix} U \\ V \end{pmatrix}$ of $M'I$ is such that

$$U + \varepsilon V = \mu_\varepsilon^{\varepsilon'} \mathcal{W}_\varepsilon^{\varepsilon'}, \quad (\text{D38})$$

or

$$\begin{aligned} U &= \frac{1}{2}(\mu_+^{\varepsilon'} W_+^{\varepsilon'} + \mu_-^{\varepsilon'} W_-^{\varepsilon'}), \\ V &= \frac{1}{2}(\mu_+^{\varepsilon'} W_+^{\varepsilon'} - \mu_-^{\varepsilon'} W_-^{\varepsilon'}). \end{aligned} \quad (\text{D39})$$

U and V must also satisfy relations analogous to Eqs. (D20) and (D21); for example,

$$(\Omega + \varepsilon\Gamma)(U - \varepsilon V) = \lambda_{\varepsilon'}(U + \varepsilon V). \quad (\text{D40})$$

Using the definition of Ω and Γ [Eqs. (D28) and (D37)–(D39)], this relation gives explicitly

$$\begin{aligned} \mu_{-\varepsilon}^{\varepsilon'} A_{\varepsilon}^{\varepsilon'} &= \mu_{\varepsilon}^{\varepsilon'} \lambda_{\varepsilon'}, \\ \mu_{-\varepsilon}^{\varepsilon'} A_{\varepsilon}^{\varepsilon'*} &= \mu_{\varepsilon}^{\varepsilon'} \lambda_{\varepsilon'}, \end{aligned} \quad (\text{D41})$$

where

$$A_{\varepsilon}^{\varepsilon'} = (\omega + \varepsilon\gamma)e^{2i\varepsilon\varepsilon't} + (\eta + \varepsilon\nu^*)\varepsilon'e^{-2i\phi}.$$

Substituting Eq. (D36) in (D40), we find after some rearrangements that $A_{\varepsilon}^{\varepsilon'}$ is real:

$$A_{\varepsilon}^{\varepsilon'} = \{(\omega + \varepsilon\gamma)(|v|^2 - c^2)^{1/2} + \varepsilon'\text{Re}[v(\eta + \varepsilon\nu^*)]\} / |v|.$$

We thus obtain

$$\begin{aligned} \mu_{-\varepsilon}^{\varepsilon'} A_{\varepsilon}^{\varepsilon'} &= \mu_{\varepsilon}^{\varepsilon'} \lambda_{\varepsilon'}, \\ \mu_{\varepsilon}^{\varepsilon'} A_{\varepsilon}^{\varepsilon'} &= \mu_{-\varepsilon}^{\varepsilon'} \lambda_{\varepsilon'}. \end{aligned} \quad (\text{D42})$$

[The eigenvalue $\lambda_{\varepsilon'}$ given by Eq. (D34) also verifies

$$\lambda_{\varepsilon'}^2 = A_{\varepsilon}^{\varepsilon'} A_{\varepsilon}^{\varepsilon'}$$

Thus Eq. (D41) has a solution different from zero.] The coefficients $\mu_{\varepsilon}^{\varepsilon'}$ have the same sign for the positive eigenvalue $+(A_{\varepsilon}^{\varepsilon'} A_{\varepsilon}^{\varepsilon'})^{1/2}$ and opposite signs for the negative eigenvalue $-(A_{\varepsilon}^{\varepsilon'} A_{\varepsilon}^{\varepsilon'})^{1/2}$. Their absolute values are

$$\mu_{\varepsilon}^{\varepsilon'} = C_{\varepsilon'} \left[A_{\varepsilon}^{\varepsilon'} \right]^{1/2}. \quad (\text{D43})$$

The constant $C_{\varepsilon'}$ is determined by the normalization condition (D24), which gives with Eq. (D38)

$$\text{Re}[\mu_+^{\varepsilon'} \mu_-^{\varepsilon'} (W_+^{\varepsilon'})^* W_-^{\varepsilon'}] = 1 \quad (\text{D44})$$

or

$$\mu_+^{\varepsilon'} \mu_-^{\varepsilon'} (e^{2it} + e^{-2it}) = 1.$$

Using Eqs. (D37)–(D43), we obtain

$$2C_{\varepsilon'}^2 \lambda_{\varepsilon'} (|v|^2 - c^2)^{1/2} / |v| = 1. \quad (\text{D45})$$

Finally,

$$\mu_{\varepsilon}^{\varepsilon'} = \left[\frac{B_{\varepsilon}^{\varepsilon'}}{2\lambda_{\varepsilon'}} \right]^{1/2}, \quad (\text{D46})$$

with

$$\begin{aligned} B_{\varepsilon}^{\varepsilon'} &= \frac{A_{\varepsilon}^{\varepsilon'} |v|}{(|v|^2 - c^2)^{1/2}} \\ &= \omega + \varepsilon\gamma + \frac{\varepsilon'\text{Re}[v(\eta + \varepsilon\nu^*)]}{(|v|^2 - c^2)^{1/2}}. \end{aligned}$$

The eigenvectors $(\underline{U}_\nu^{\varepsilon'})$ are thus determined by Eqs. (D39), (D37), and (D46). As shown by Eq. (D16), the eigenvectors $(\underline{U}_\nu^{\varepsilon'})$ are columns of the matrix $T^+(k)I$. We thus deduce the matrix $T(k)$:

$$T(k) = \begin{bmatrix} R^+ & R^- \\ R^- & R^+ \end{bmatrix}, \quad (\text{D47a})$$

$R^{\varepsilon''}$ ($\varepsilon'' = \pm 1$) being the 2×2 matrix

$$R^{\varepsilon''} = \begin{bmatrix} r_{\varepsilon''}^* & r_{\varepsilon''} \\ s_{\varepsilon''}^* & -s_{\varepsilon''} \end{bmatrix}$$

with

$$\begin{aligned} r_{\varepsilon''} &= \frac{1}{2}e^{i\phi}[\mu_+^{\varepsilon''} e^{-it} + \varepsilon'' \mu_-^{\varepsilon''} e^{it}], \\ s_{\varepsilon''} &= \frac{1}{2}e^{i\phi}[\mu_-^{\varepsilon''} e^{it} + \varepsilon'' \mu_+^{\varepsilon''} e^{-it}]. \end{aligned} \quad (\text{D47b})$$

[We recall that $\mu_{\varepsilon}^{\varepsilon'}$ is given by Eq. (D46), and the phase ϕ and t are defined by (D36).] The inverse matrix $T^{-1}(k)$, giving the $\alpha_i(k)$ in terms of the $e_i(k)$, is obtained by the transformation (D31).

3. scaf and ssqaf phases

a. Hamiltonian

Both phases have four sublattices with orthogonal magnetization. The scaf phase has been treated by Utsumi and Izuyama (1977). We choose the reference frame represented in Fig. 34(b). The spin vectors of each sublattice in the molecular field are thus

$$\begin{aligned} \mathbf{S}_1^0 &= \begin{bmatrix} \frac{1}{2} \\ 0 \\ 0 \end{bmatrix}, \quad \mathbf{S}_2^0 = \begin{bmatrix} 0 \\ \frac{1}{2} \\ 0 \end{bmatrix}, \\ \mathbf{S}_3^0 &= \begin{bmatrix} -\frac{1}{2} \\ 0 \\ 0 \end{bmatrix}, \quad \mathbf{S}_4^0 = \begin{bmatrix} 0 \\ -\frac{1}{2} \\ 0 \end{bmatrix}, \end{aligned}$$

and the spin deviations are

$$\begin{aligned} \delta\mathbf{S}_{1,i} &= \begin{bmatrix} -\alpha_{1,i}^+ \alpha_{1,i} \\ \frac{i}{2}(\alpha_{1,i}^+ - \alpha_{1,i}) \\ \frac{1}{2}(\alpha_{1,i}^+ + \alpha_{1,i}) \end{bmatrix}, \\ \delta\mathbf{S}_{2,j} &= \begin{bmatrix} -\frac{i}{2}(\alpha_{2,j}^+ - \alpha_{2,j}) \\ -\alpha_{2,j}^+ \alpha_{2,j} \\ \frac{1}{2}(\alpha_{2,j}^+ + \alpha_{2,j}) \end{bmatrix}, \\ \delta\mathbf{S}_{3,k} &= \begin{bmatrix} +\alpha_{3,k}^+ \alpha_{3,k} \\ -\frac{i}{2}(\alpha_{3,k}^+ - \alpha_{3,k}) \\ \frac{1}{2}(\alpha_{3,k}^+ + \alpha_{3,k}) \end{bmatrix}, \\ \delta\mathbf{S}_{4,l} &= \begin{bmatrix} \frac{i}{2}(\alpha_{4,l}^+ - \alpha_{4,l}) \\ +\alpha_{4,l}^+ \alpha_{4,l} \\ \frac{1}{2}(\alpha_{4,l}^+ + \alpha_{4,l}) \end{bmatrix}. \end{aligned} \quad (\text{D48})$$

Note that for each sublattice the operator α_i^+ change S_i^Z

from $+\frac{1}{2}$ to $-\frac{1}{2}$, the quantization axis OZ_α being taken along S_α^0 .

The procedure for expressing the Hamiltonian (5.10) in terms of $\alpha_{\lambda,i}, \alpha_{\lambda,i}^\dagger$ and, after Fourier transforming (D6), in

$$\mathcal{H} = E_0 + \sum_k \left[\frac{1}{2} \alpha^+(k), \alpha^+(-k) \right] \begin{pmatrix} A & B \\ B & A \end{pmatrix} \begin{pmatrix} \alpha(k) \\ \alpha^+(-k) \end{pmatrix} - \frac{1}{2} \text{tr} A \right], \quad (49a)$$

with

$$A = \begin{pmatrix} \omega & \eta & \delta & \eta'^* \\ \eta^* & \omega & \eta' & \delta \\ \delta & \eta'^* & \omega & \eta \\ \eta' & \delta & \eta^* & \omega \end{pmatrix}, \quad (D49b)$$

$$B = \begin{pmatrix} \varepsilon & \nu & \gamma & \nu'^* \\ \nu^* & \varepsilon & \nu' & \gamma \\ \gamma & \nu'^* & \varepsilon & \nu \\ \nu' & \gamma & \nu^* & \varepsilon \end{pmatrix},$$

and, for the scaf phase,

$$\begin{aligned} \omega(k) &= -6(J_2 - 2J_3) - 12(K_F - K_P) - J_3 g_3(k), \\ \gamma(k) &= -J_2 g_2(k); \delta(k) = -(2K_F - K_P) g_2(k), \\ \varepsilon(k) &= -\frac{K_P}{2} g_3(k), \\ \nu(k) &= \nu'(k) = -\frac{1}{2} [J_1 + 3(K_F - K_P)] f_1(k), \\ \eta(k) &= \eta'(k) = -\frac{1}{2} [J_1 - 3(K_F - K_P)] f_1(k), \\ f_1(k) &= 4 \left[\cos \frac{ak_x}{2} \cos \frac{ak_y}{2} \cos \frac{ak_z}{2} \right. \\ &\quad \left. + i \sin \frac{ak_x}{2} \sin \frac{ak_y}{2} \sin \frac{ak_z}{2} \right], \\ g_n(k) &= \sum_j^{(n)} e^{ik(R_i - R_j)}. \end{aligned} \quad (D50)$$

where \sum is over the n th neighbors of i . For the ssqaf phase,

$$\begin{aligned} \omega(k) &= -2(J_2 + 2J_3) + 4K_F - 12K_P \\ &\quad - 2J_2 \cos ak_z - 4J_3 \cos ak_x \cos ak_y, \\ \gamma(k) &= -2(J_2 + 2J_3 \cos ak_z) (\cos ak_x + \cos ak_y), \\ \delta(k) &= -2K_P (\cos ak_x + \cos ak_y) (1 + \cos ak_z), \\ \varepsilon(k) &= (-4K_F + 2K_P) \cos ak_z + 2K_P \cos ak_x \cos ak_y, \\ \nu(k) &= -2(J_1 - K_F + 3K_P) \cos \frac{ak_z}{2} \cos \frac{a}{2} (k_x + k_y), \\ \nu'(k) &= -2(J_1 - K_F + 3K_P) \cos \frac{ak_z}{2} \cos \frac{a}{2} (k_x - k_y), \\ \eta(k) &= -2(J_1 + K_F - 3K_P) \cos \frac{ak_z}{2} \cos \frac{a}{2} (k_x + k_y), \\ \eta'(k) &= -2(J_1 + K_F - 3K_P) \cos \frac{ak_z}{2} \cos \frac{a}{2} (k_x - k_y). \end{aligned} \quad (D51)$$

terms of $\alpha_\lambda(k), \alpha_\lambda^\dagger(k)$ is exactly the same as that used for the uudd phase. We give here the results. The details of this tedious calculation are described in Roger (1980), Appendix 6. We obtain

b. Diagonalization of the Hamiltonian

In the scaf phase [see Eq. (D52)], $\nu = \nu'$ and $\eta = \eta'$; hence the lines of each matrix A or B [Eq. (D49)]; deduce from one another by cyclic permutation. Such matrices have four eigenvectors V^m with respective components

$$V_n^m = e^{im\pi/2}.$$

Thus A and B have the same eigenvectors V^m ; the corresponding eigenvalues are, for A ,

$$\mathcal{A}_m = \omega + \eta e^{im(\pi/2)} + \delta e^{im\pi} + \eta^* e^{-im(\pi/2)}, \quad (D52a)$$

and, for B ,

$$\mathcal{B}_m = \varepsilon + \nu e^{im(\pi/2)} + \gamma e^{im\pi} + \nu^* e^{-im(\pi/2)}.$$

It is clear that $P_+ = P_- = A^2 - B^2$ has the same eigenvector V^m with eigenvalues

$$\lambda_m^2 = \mathcal{A}_m^2 - \mathcal{B}_m^2. \quad (D52b)$$

The eigenvectors \mathcal{Y}^m of

$$M\tilde{I} = \begin{pmatrix} A & -B \\ B & -A \end{pmatrix}$$

are

$$\mathcal{Y}^m = \begin{pmatrix} r_m V^m \\ s_m V^m \end{pmatrix}. \quad (D53a)$$

The constants r_m and s_m are determined by

$$(i) \quad M\tilde{I}\mathcal{Y}^m = \lambda_m \mathcal{Y}^m \text{ giving}$$

$$(\mathcal{A}_m - \lambda_m) r_m - \mathcal{B}_m s_m = 0,$$

$$\mathcal{B}_m r_m - (\mathcal{A}_m + \lambda_m) s_m = 0,$$

with the compatibility equation (D52b).

(ii) The normalization condition (D24), giving

$$4(r_m^2 - s_m^2) = 1.$$

We obtain

$$r_m = \frac{1}{2\sqrt{2}} \left[\frac{\mathcal{A}_m}{\lambda_m} + 1 \right]^{1/2}$$

and

$$s_m = \frac{1}{2\sqrt{2}} \left[\frac{\mathcal{A}_m}{\lambda_m} - 1 \right]^{1/2}. \quad (D53b)$$

Associated with the eigenvalues

$$\lambda_m = +(\mathcal{A}_m^2 - \mathcal{B}_m^2)^{1/2}$$

are the eigenvectors

$$e_m(k) = \frac{1}{2\sqrt{2}} \sum_n \left[\left[\frac{\mathcal{A}_m}{\lambda_m} + 1 \right]^{1/2} e^{imn(\pi/2)} \alpha_n(k) + \left[\frac{\mathcal{A}_m}{\lambda_m} - 1 \right]^{1/2} e^{imn(\pi/2)} \alpha_n^+(-k) \right]. \quad (\text{D54})$$

$[\lambda_m = -(\mathcal{A}_m^2 - \mathcal{B}_m^2)^{1/2}$ is associated with $e_m^+(-k)$.] From Eq. (D13) we obtain the α_n in terms of the e_n :

$$\alpha_n(k) = \frac{1}{2\sqrt{2}} \sum_m \left[\left[\frac{\mathcal{A}_m}{\lambda_m} + 1 \right]^{1/2} e^{-imn(\pi/2)} e_m(k) - \left[\frac{\mathcal{A}_m}{\lambda_m} - 1 \right]^{1/2} e^{-imn(\pi/2)} e_m^+(-k) \right]. \quad (\text{D55})$$

This agrees with the result given previously at $k=0$ by Utsumi and Izuyama (1977).

In the ssqaf phase, the coefficients of the matrices A

and B are real: $v=v^*$, $v'=v'^*$; $\eta=\eta^*$, $\eta'=\eta'^*$ [see Eq. (D51)]. We note that for each matrix (D49b), the coefficients of the second, third, and fourth line are deduced from the first line by the respective permutations $(P_{12}P_{34})$, $(P_{31}P_{24})$, $(P_{14}P_{23})$. We can easily prove that the four eigenvectors are

$$V^{\mu,\mu'} = \begin{bmatrix} 1 \\ \mu \\ \mu' \\ \mu\mu' \end{bmatrix}$$

with $\mu = \pm 1$, $\mu' = \pm 1$. The corresponding eigenvalues for A and B are, respectively,

$$\mathcal{A}_{\mu,\mu'} = \omega(k) + \mu\eta(k) + \mu'\delta(k) + \mu\mu'\eta'(k), \quad (\text{D56})$$

$$\mathcal{B}_{\mu,\mu'} = \varepsilon(k) + \mu\nu(k) + \mu'\gamma(k) + \mu\mu'\nu'(k).$$

Following the same scheme as for the scf phase, we obtain the eigenmodes of the Hamiltonian

$$\lambda_{\mu,\mu'} = (\mathcal{A}_{\mu,\mu'}^2 - \mathcal{B}_{\mu,\mu'}^2)^{1/2} \quad (\text{D57})$$

and the associated eigenvectors

$$e_{\mu,\mu'}(k) = \frac{1}{2\sqrt{2}} \left[\left[\frac{\mathcal{A}_{\mu,\mu'}}{\lambda_{\mu,\mu'}} + 1 \right]^{1/2} [\alpha_1(k) + \mu\alpha_2(k) + \mu'\alpha_3(k) + \mu\mu'\alpha_4(k)] + \left[\frac{\mathcal{A}_{\mu,\mu'}}{\lambda_{\mu,\mu'}} - 1 \right]^{1/2} [\alpha_1^+(-k) + \mu\alpha_2^+(-k) + \mu'\alpha_3^+(-k) + \mu\mu'\alpha_4^+(-k)] \right]. \quad (\text{D58})$$

Both the scf and the ssqaf phases give three acoustic modes and one optical mode, each being doubly degenerate.

4. pf phase, the spin-flop naf phase

a. Spin-wave operators

As shown in Fig. 34(c), the magnetic field is directed along the z axis. In the molecular field the magnetizations M_1 and M_2 of each sublattice are symmetric with respect to z . The angle between M_1 and z , or z and M_2 , is ϕ . In the (X_1, Y_1, Z_1) frame related to M_1 ($Z_1 \parallel M_1$), the spin operators are

$$\mathbf{S}_i^1 = \mathbf{S}_0 + \delta\mathbf{S}_i = \begin{bmatrix} 0 \\ 0 \\ \frac{1}{2} \end{bmatrix} + \begin{bmatrix} \frac{1}{2}(\alpha_{1,i}^+ + \alpha_{1,i}) \\ \frac{i}{2}(\alpha_{1,i}^+ - \alpha_{1,i}) \\ -\alpha_{1,i}^+ \alpha_{1,i} \end{bmatrix}. \quad (\text{D59})$$

We write a similar relation for the spins of the other sublattice in the (X_2, Y_2, Z_2) reference frame with $Z_2 \parallel M_2$.

b. Hamiltonian

The Hamiltonian (5.10) is transformed using the method described above for the other phases. We obtain as our final result

$$\mathcal{H} = E_0 + \sum \left[\frac{1}{2} [{}^t\alpha^+(k), {}^t\alpha(-k)] \times \begin{bmatrix} A & B \\ B & A \end{bmatrix} \begin{bmatrix} \alpha(k) \\ \alpha(-k) \end{bmatrix} - \frac{1}{2} \text{tr}A \right] \quad (\text{D60a})$$

where

$$A = \begin{bmatrix} \omega & \delta \\ \delta & \omega \end{bmatrix}, \quad B = \begin{bmatrix} \varepsilon & \gamma \\ \gamma & \varepsilon \end{bmatrix},$$

and where

$$\begin{aligned} \omega(\mathbf{k}) &= 8J_1 \cos 2\phi + 6J_2 + 12J_3 \\ &+ 12(K_F + K_P)(2 \cos^2 2\phi - 1) \\ &+ g_2(\mathbf{k})[-J_2 + (2K_F + K_P) \cos^2 2\phi] \\ &+ g_3(\mathbf{k}) \left[-J_3 + \frac{K_P}{2} \cos^2 2\phi \right] + \gamma H \cos \phi, \end{aligned} \quad (\text{D60b})$$

$$\varepsilon(\mathbf{k}) = g_2(\mathbf{k})[2K_F + K_P]\sin^2 2\phi + g_3(\mathbf{k})\frac{K_P}{2}\sin^2 2\phi, \quad (\text{D60c})$$

$$\gamma(\mathbf{k}) = \frac{1}{2}g_1(\mathbf{k})[-J_1(1 - \cos 2\phi) - 3(K_F + K_P)(\cos 2\phi - \cos 4\phi)], \quad (\text{D60d})$$

$$\delta(\mathbf{k}) = \frac{1}{2}g_1(\mathbf{k})[-J_1(1 + \cos 2\phi) - 3(K_F + K_P)(\cos 2\phi + \cos 4\phi)], \quad (\text{D60e})$$

Here [see Eq. (7.10b)]

$$g_n(\mathbf{k}) = \sum_j^{(n)} e^{i\mathbf{k} \cdot (\mathbf{R}_j - \mathbf{R}_0)},$$

where j runs over the n th neighbors of 0.

c. Diagonalization

The eigenvectors of A and B are simply

$$V^m = \begin{pmatrix} 1 \\ (-1)^m \end{pmatrix}, \quad m = 1, 2.$$

The corresponding eigenvalues for A and B are, respectively,

$$\mathcal{A}_m = \omega + (-1)^m \delta, \quad \mathcal{B}_m = \varepsilon + (-1)^m \gamma. \quad (\text{D61a})$$

Following the same method used for the scf and ssqf phases, we find the eigenmodes

$$\lambda_m = (\mathcal{A}_m^2 - \mathcal{B}_m^2)^{1/2} \quad (\text{D61b})$$

and the eigenvectors

$$e^m(k) = \frac{1}{2} \left[\frac{\mathcal{A}_m}{\lambda_m} + 1 \right]^{1/2} [\alpha_1(k) + (-1)^m \alpha_2(k)] + \frac{1}{2} \left[\frac{\mathcal{A}_m}{\lambda_m} - 1 \right]^{1/2} [\alpha_1^+(-k) + (-1)^m \alpha_2^+(-k)]. \quad (\text{D61c})$$

d. Correction to the molecular-field energy at $T = 0$

The Hamiltonian can be written

$$\mathcal{H} = E_0 + \sum_k \left\{ \frac{1}{2} [\lambda_1(k) + \lambda_2(k) - \text{tr}A] + \lambda_1(k) e_1^+(k) e_1(k) + \lambda_2(k) e_2^+(k) e_2(k) \right\}. \quad (\text{D62})$$

The constant term $\Delta E = \sum_k \frac{1}{2} [\lambda_1(k) + \lambda_2(k) - 2\omega(k)]$ represents the correction to the molecular-field energy.

REFERENCES

- Abragam, A., and M. Goldman, 1982, *Nuclear Magnetism—Order and Disorder* (Clarendon, Oxford).
- Adams, E. D., J. M. Delrieu, and A. Landesman, 1978, *J. Phys. (Paris) Lett.* **39**, L190.
- Adams, E. D., E. A. Schubert, G. E. Hass, and D. M. Bakalyar, 1980, *Phys. Rev. Lett.* **44**, 789.
- Andreev, A. F., and I. M. Lifschitz, 1969, *Sov. Phys. JETP.* **29**, 1107.
- Andreev, A. F., V. I. Marchenko, and A. E. Meierovich, 1977, *JETP Lett.* **26**, 36.
- Avilov, V. V., and S. V. Iordansky, 1982, *J. Low Temp. Phys.* **48**, 241.
- Bak, P., and F. B. Rasmussen, 1981, *Physica B* **108**, 849 (Proceedings of the 16th International Conference on Low Temperature Physics LT-16).
- Bakalyar, D. M., E. D. Adams, Y. C. Huang, and C. V. Britton, 1977, in *Proceedings of the International Quantum Crystal Conference, Fort Collins, Col.*, edited by James R. Sites (Colorado State University Ft. Collins, Colorado).
- Banks, T., C. M. Bender, and T. T. Wu, 1973, *Phys. Rev. D* **8**, 3346.
- Béal-Monod, M. T., 1977, *Commun. on Phys.* **2**, 199.
- Béal-Monod, M. T., and D. L. Mills, 1978, *J. Phys. (Paris) Colloq.* **39**, C6-290.
- Bean, C. P., and D. S. Rodbell, 1962, *Phys. Rev.* **126**, 104.
- Benoit, A., J. Flouquet, P. Rufin, and T. Schweizer, 1982, *J. Phys. (Paris) Lett* **43**, L-431.
- Bernardes, N., and H. Primakoff, 1960, *Phys. Rev.* **119**, 968.
- Bernier, M., and J. M. Delrieu, 1977, *Phys. Lett. A* **60**, 156.
- Brandow, B. H., 1971, *Phys. Rev. A* **4**, 422.
- Brandow, B. H., 1972, *Ann. Phys.* **74**, 112.
- Castles, S. H., and E. D. Adams, 1973, *Phys. Rev. Lett.* **30**, 1125.
- Ceperley, D. M., and M. H. Kalos, 1979, in *Monte Carlo Methods in Statistical Physics*, edited by K. Binder (Springer, Berlin), Topics in Current Physics, Vol. 7, p. 145.
- Cohen, M. H., and F. Keffer, 1955, *Phys. Rev.* **99**, 1129.
- Cooper, B. R., 1960, *Phys. Rev.* **118**, 135.
- Courant, R., and D. Hilbert, 1937, *Methoden der Mathematischen Physik* (Springer, Berlin).
- Delrieu, J. M., and M. Roger, 1978, *J. Phys. (Paris) Colloq.* **39**, C6-123.
- Delrieu, J. M., M. Roger, and J. H. Hetherington, 1980a, *J. Low Temp. Phys.* **40**, 71.
- Delrieu, J. M., M. Roger, and J. H. Hetherington, 1980b, in *Spin Polarized Quantum Systems, Aussois, France*, *J. Phys. (Paris) Colloq.* **41**, C7-231.
- Delrieu, J. M., and N. S. Sullivan, 1981, *Phys. Rev. B* **23**, 3197.
- Dirac, P. A. M., *The Principles of Quantum Mechanics*, 1947, (Clarendon, Oxford), Chap. IX.
- Dundon, J. M., and J. M. Goodkind, 1974, *Phys. Rev. Lett.* **32**, 1343.
- Dundon, J. M., and J. M. Goodkind, 1975, *J. Low. Temp. Phys.* **18**, 315.
- Erdelyi, A., W. Magnus, F. Oberhettinger, and F. G. Tricomi, 1953, *Higher Transcendental Functions* (McGraw-Hill, New York), Vol. 2, Chap. VIII, Harry Bateman Manuscript.
- Falk, Harold, 1964, *Phys. Rev.* **133**, 1382A.
- Feenberg, Eugene, 1969, *Theory of Quantum Fluids* (Academic, New York).
- Garwin, R. L., and A. Landesman, 1964, *Phys. Rev.* **133**, 1502A.
- Garwin, R. L., and H. A. Reich, 1964, *Phys. Rev. Lett.* **12**, 354.

- Gervais, J. L., and B. Sakita, 1977, *Phys. Rev. D* **16**, 3507.
- Godfrin, H., 1981, Ph.D. thesis (Grenoble University).
- Godfrin, H., G. Frossati, A. Greenberg, B. Hebral, and D. Thoulouze, 1980, *Phys. Rev. Lett.* **44**, 1695.
- Graham, R., and H. Pleiner, 1975, *Phys. Rev. Lett.* **34**, 792.
- Greywall, D. S., 1977, *Phys. Rev. B* **15**, 2604.
- Guyer, R. A., 1974, *Phys. Rev. A* **9**, 1452.
- Guyer, R. A., 1978, *J. Low Temp. Phys.* **30**, 1.
- Guyer, R. A., and P. Kumar, 1982, *J. Low Temp. Phys.* **47**, 321.
- Guyer, R. A., W. J. Mullin, and A. K. McMahan, 1975, *Phys. Rev. B* **11**, 1045.
- Guyer, R. A., R. C. Richardson, and L. I. Zane, 1971, *Rev. Mod. Phys.* **43**, 532.
- Guyer, R. A., and L. I. Zane, 1969, *Phys. Rev.* **188**, 445.
- Halperin, W. P., 1979, *J. Phys. (Paris) Lett.* **40**, L373.
- Halperin, W. P., C. N. Archie, F. B. Rasmussen, R. A. Buhrman, and R. C. Richardson, 1974, *Phys. Rev. Lett.* **32**, 927.
- Halperin, W. P., C. N. Archie, F. B. Rasmussen, and R. C. Richardson, 1975, *Phys. Rev. Lett.* **34**, 718.
- Halperin, W. P., F. B. Rasmussen, C. N. Archie, and R. C. Richardson, 1978, *J. Low Temp. Phys.* **31**, 617.
- Hammersley, J. M., and D. C. Handscomb, 1964, *Monte Carlo Methods, Monographs on Applied Probability and Statistics* (Chapman and Hall, New York).
- Hansen, J. P., D. Levesque, and D. Schiff, 1971, *Phys. Rev. A* **3**, 776.
- Harris, A. B., 1971, *Solid State Commun.* **9**, 2255.
- Hebral, B., G. Frossati, H. Godfrin, G. Schumacher, and D. Thoulouze, 1979, *J. Phys. Lett.* **40**, L41.
- Heritier, M., and P. Lederer, 1977, *J. Phys. (Paris) Lett.* **38**, L109.
- Heritier, M., and P. Lederer, 1978, *J. Phys. (Paris) Colloq.* **39**, C6-130.
- Herpin, A., 1968, *Theorie du Magnetisme* (Presse Universitaires de France, Paris).
- Herring, C., 1962, *Rev. Mod. Phys.* **34**, 631.
- Herring, C., 1966, in *Magnetism*, edited by C. I. Rado and H. Shul (Academic, London), Vol. IIB, Chap. 1.
- Hetherington, J. H., 1978, *J. Phys. (Paris) C* **6**, 126.
- Hetherington, J. H., 1981, *Physica B* **108**, 855.
- Hetherington, J. H., W. J. Mullin, and L. H. Nosanow, 1967, *Phys. Rev.* **154**, 175.
- Hetherington, J. H., and F. D. C. Willard, 1975, *Phys. Rev. Lett.* **35**, 1442.
- Holstein, T., and H. Primakoff, 1940, *Phys. Rev.* **58**, 1098.
- Hunt, E. R., Y. Morii, and E. D. Adams, 1981, *Physica B* **107**, 197.
- Iwahashi, K., and Y. Masuda, 1981, *J. Phys. Soc. Jpn.* **50**, 2508.
- Izuyama, T., 1980, *J. Phys. Soc. Japan Lett.* **49**, 2077.
- Jongh, J. de, and A. R. Miedma, 1974 *Experiments on Simple Magnetic Model Systems*, Monographs on Physics No. 7 (Taylor and Francis, London).
- Kalos, M. H., 1970, *Phys. Rev. A* **2**, 250.
- Kalos, M. H., D. Levesque, and L. Verlet, 1974, *Phys. Rev. A* **9**, 2178.
- Kirk, W. P., and E. D. Adams, 1971, *Phys. Rev. Lett.* **27**, 392.
- Kirk, W. P., E. B. Osgood, and L. Garber, 1969, *Phys. Rev. Lett.* **23**, 833.
- Kummer, R. B., E. D. Adams, W. P. Kirk, A. S. Greenberg, R. M. Mueller, C. V. Britton, and D. H. Lee, 1975, *Phys. Rev. Lett.* **34**, 517.
- Kummer, R. B., R. M. Mueller, and E. D. Adams, 1977, *J. Low Temp. Phys.* **27**, 319.
- Landau, E., and F. Lifschitz, 1958a, *Classical Mechanics* (Pergamon, New York).
- Landau, E., and F. Lifschitz, 1958b, *Statistical Physics* (Pergamon, New York).
- Landesman, A., 1973-74, *Ann. Phys. (Paris)* **8**, 53.
- Landesman, A., 1978, *J. Phys. (Paris) Colloq.* **39**, C6-1305.
- Levesque, D., 1980, *Phys. Rev. B* **21**, 5159.
- London, F., 1954, *Superfluids* (Wiley, New York), Vol. II, Sec. 56, pp. 29-31.
- Luttinger, J. H., and L. Tisza, 1946, *Phys. Rev.* **70**, 954.
- Mamiya, T., A. Sawada, H. Fukuyama, Y. Hiro, and Y. Masuda, 1981, *Phys. Rev. Lett.* **47**, 1304.
- McMahan, A. K., 1972a, *J. Low Temp. Phys.* **8**, 115.
- McMahan, A. K., 1972b, *J. Low Temp. Phys.* **8**, 159.
- McMahan, A. K., and R. A. Guyer, 1973, *Phys. Rev. A* **7**, 1105.
- McMahan, A. K., and J. W. Wilkins, 1975, *Phys. Rev. Lett.* **35**, 376.
- Montambaux, G., M. Heritier, and P. Lederer, 1982, *J. Low Temp. Phys.* **47**, 39.
- Morii, Y., K. Ichikawa, T. Hata, C. Kanamori, H. Okamoto, T. Kodama, and T. Shigi, 1978, in *Physics at Ultralow Temperatures*, edited by T. Sugawara (The Physical Society of Japan, Kyoto), p. 196.
- Mullin, W. J., 1975, *Phys. Rev. B* **12**, 3718.
- Mullin, W. J., L. H. Nosanow, and P. M. Steinbeck, 1969, *Phys. Rev.* **188**, 410.
- Nagaoka, Y., 1965, *Solid State Commun.* **3**, 409.
- Nagaoka, Y., 1966, *Phys. Rev.* **147**, 392.
- Nosanow, L. H., 1964, *Phys. Rev. Lett.* **13**, 270.
- Nosanow, L. H., and W. J. Mullin, 1965, *Phys. Rev. Lett.* **14**, 133.
- Nosanow, L. H., and C. M. Varma, 1968, *Phys. Rev. Lett.* **20**, 912.
- Nosanow, L. H., and C. M. Varma, 1969, *Phys. Rev.* **187**, 660.
- Onn, D. G., H. Meyer, and J. P. Remeika, 1967, *Phys. Rev.* **156**, 663.
- Osheroff, D. D., 1972, Ph.D. thesis (Cornell University).
- Osheroff, D. D., 1982, *Physica B + C* **109-110**, 1461 (Proceedings of the 16th International Conference on Low Temperature Physics LT-16).
- Osheroff, D. D., M. C. Cross, and D. S. Fisher, 1980, *Phys. Rev. Lett.* **44**, 792.
- Osheroff, D. D., R. C. Richardson, and D. M. Lee, 1972, *Phys. Rev. Lett.* **28**, 885.
- Osheroff, D. D., and C. Yu, 1980, *Phys. Lett. A* **77**, 458.
- Østgaard, E., 1972, *J. Low Temp. Phys.* **7**, 471.
- Panczyk, M. F., and E. D. Adams, 1970, *Phys. Rev. A* **1**, 1356.
- Pandorf, R. C., and D. O. Edwards, 1968, *Phys. Rev.* **169**, 222.
- Papoular, M., 1977, *Solid State Commun.* **24**, 113.
- Papoular, M., 1978, *J. Low Temp. Phys.* **31**, 595.
- Prewitt, T. C., and J. M. Goodkind, 1977, *Phys. Rev. Lett.* **39**, 1283.
- Prewitt, T. C., and J. M. Goodkind, 1980, *Phys. Rev. Lett.* **44**, 1699.
- Reich, H. A., 1963, *Phys. Rev.* **129**, 630.
- Roger, M., 1980, Ph.D. thesis (University of Paris-Sud, Centre d'Orsay), No. 2297.
- Roger, M., and J. M. Delrieu, 1977, *Phys. Lett. A* **63**, 309.
- Roger, M., J. M. Delrieu, and J. H. Hetherington, 1980a, *J. Phys. (Paris) Lett.* **41**, L139.
- Roger, M., J. M. Delrieu, and J. H. Hetherington, 1980b, in *Spin Polarized Quantum Systems, Aussois, France*, *J. Phys. (Paris) Colloq.* **41**, C7-241.

- Roger, M., J. M. Delrieu, and J. H. Hetherington, 1980c, *Phys. Rev. Lett.* **45**, 137.
- Roger, M., J. M. Delrieu, and A. Landesman, 1977, *Phys. Lett. A* **62**, 449.
- Rushbrooke, G. S., G. A. Baker, and P. J. Wood, 1974, in *Phase Transitions and Critical Phenomena*, edited by C. Domb and M. Green (Academic, New York), Vol. 3, p. 245.
- Sample, H. H., and C. A. Swenson, 1967, *Phys. Rev.* **158**, 188.
- Schuberth, E. A., D. M. Bakalyar, and E. D. Adams, 1979, *Phys. Rev. Lett.* **42**, 101.
- Sokoloff, J. B., and A. Widom, 1975a, *Phys. Lett.* **35**, 673.
- Sokoloff, J. B., and A. Widom, 1975b, *J. Low Temp. Phys.* **21**, 463.
- Thouless, D. J., 1965a, *Proc. Phys. Soc. London* **86**, 893.
- Thouless, D. J., 1965b, *Proc. Phys. Soc. London* **86**, 905.
- Trickey, S. B., W. P. Kirk, and E. D. Adams, 1972, *Rev. Mod. Phys.* **44**, 668.
- Utsumi, K., and T. Izuyama, 1977, *Prog. Theor. Phys.* **58**, 44.
- VanDegriфт, C. T., W. J. Bowers, Jr., P. B. Pipes, and D. F. McQueeney, 1982, *Phys. Rev. Lett.* **49**, 149.
- Varma, C. M., and L. H. Nosanow, 1970, *Phys. Rev. A* **1**, 133.
- Villain, J., 1959, *J. Phys. Chem. Solids* **11**, 303.
- Willard, F. D. C., 1980, *La Recherche* **11**, 972.
- Yu, C., and P. W. Anderson, 1979, *Phys. Lett. A* **74**, 236.
- Zane, L. I., 1972, *J. Low Temp. Phys.* **9**, 219.
- Zane, L. I., R. J. Krantz, and J. R. Sites, 1977, *Phys. Rev. B* **15**, 1343.